Hybrid Cognitive Phased and Frequency Diverse Array Radar

By

Abdul Basit

Reg. No. 32-FET/PHDEE/S10

A dissertation submitted to I.I.U. in partial fulfillment of the requirements for the degree of

DOCTOR OF PHILOSOPHY

Department of Electronic Engineering
Faculty of Engineering and Technology
INTERNATIONAL ISLAMIC UNIVERSITY
ISLAMABAD
2016

DEDICATED TO

My Teachers,

Parents,

Wife,

Sister and Brothers

CERTIFICATE OF APPROVAL

Title of Thesis: Hybrid Cognitive Phased and Frequency Diverse Array Radar

Name of Student: Abdul Basit

Registration No: 32-FET/PHDEE/S10

Accepted by the Department of Electronic Engineering, Faculty of Engineering and Technology, International Islamic University, Islamabad, in partial fulfillment of the requirements for the Doctor of Philosophy degree in Electronic Engineering.

Viva Voce Committee

Prof. Dr. Aqdas Naveed Malik _____

Dean, Faculty of Engineering & Technology,
International Islamic University, Islamabad.

Prof. Dr. Muhammad Amir (Internal Examiner) _____

Chairman, Department of Electronic Engineering,
International Islamic University, Islamabad.

Prof. Dr. Tanweer Ahmed Cheema (External Examiner-1) _____
Professor, HoD School of Engineering and Applied Science
ISRA University, Islamabad campus.

Dr. Hafiz Muhammad Faisal Zafar (External Examiner-2) _____
Principal Scientist, PAEC, Nilore, Islamabad.

Prof. Dr. Ijaz Mansoor Qureshi (Supervisor) _____
Department of Electrical Engineering
Air University, Islamabad

Dr. Ihsanul Haq (Co-supervisor) _____

Assistant Professor, DEE, FET, IIUI

Tuesday, 21st Jun, 2016

ABSTRACT

Hybrid designs in modern radar technology have drawn significant consideration of research community. They have got numerous advantages over stand-alone models. The prominent stand-alone radar models include phased array radar (PAR), frequency diverse array radar (FDA) and cognitive radar (CR). The PAR generates an energy focused beam pattern towards desired direction and has an ability to suppress interferences. An FDA radar provides additional degrees-of-freedom and generates a 3-D range-angle dependent beam pattern. Similarly, a CR adjusts the design parameters on- the-fly using situational awareness ability.

The work presented in this dissertation include the hybrid designs of CR with PAR and FDA that combines the benefits of either sides. The work is primarily divided into two parts. First part contains a novel hybrid design of CR with PAR i.e., hybrid cognitive phased array radar (HCPAR). This radar model contains the benefits of both sides. A low probability of intercept (LPI) property with transmit beamforming is also incorporated in the proposed design. The performance of proposed model is analyzed on the basis of situational awareness, which is proved to be an important parameter. The proposed hybrid design shows better signal to interference and noise ratio (SINR) and detection probability as compared to conventional stand-alone PAR model. Moreover, this design is energy efficient compared to previous models due to the reason that it illuminates only the region in vicinity of target predicted position received as feedback.

In second part of the work, a novel hybrid model of CR with FDA is presented i.e., hybrid cognitive frequency diverse array (HCFDA) radar. The objective is to combine the benefits of both sided for improved target localization and tracking performance. This hybrid design is further divided into two categories. In first category, the HCFDA design with uniform frequency offset is analyzed. In this case, a uniform frequency offset for an FDA transmitter is computed based on the receiver feedback. Situational awareness of the proposed design helps to improve SINR, detection probability and energy efficiency as compared to conventional stand-alone designs. In second category, the HCFDA design is proposed with non-uniform frequency offsets. The non-uniform frequency offsets are computed based on the receiver feedback using

four different methods i.e., i) mu-law companding formulae based offsets, ii) Hamming window based tapering offsets, iii) Genetic algorithm (GA) based fractional offsets and iv) non-uniform but integer frequency offsets. To analyze the performance of proposed designs, the situational awareness along with the non-uniform offsets, computed using various methods, have proved to be an important basis. The proposed designs achieve better SINR, detection probability, energy efficiency and improved Cramer Rao lower bound (CRLB) on range and angle estimations as compared to conventional stand-alone FDA design. The proposed designs also provide improved transmit energy focusing towards target position, which results in improved range and angle resolution as compared to the existing designs.

The proposed hybrid designs provide a strong base for the development of modern radar generations with intelligent target steering ability in space. At present, the proposed schemes are investigated only for linear array, yet they can be extended to planar arrays and other topologies according to the requirement.

LIST OF PUBLICATIONS AND SUBMISSIONS

[1]. Basit A, Qureshi I M, Khan W, A N Malik, "Cognitive Frequency Diverse Array Radar with Symmetric Non-uniform Frequency Offset," *Science china information sciences* (accepted) (ISI indexed & IF 0.89) 2016.

[2]. Basit, A., Qureshi, I. M., Khan, W., & Malik, A. N. Range–Angle-Dependent Beamforming for Cognitive Antenna Array Radar with Frequency Diversity. *Cognitive Computation*, 8, 204-216, 2016. (ISI indexed & IF 1.4)

[3]. Basit, A., Qureshi, I. M., Khan, W., Ulhaq, I., & Khan, S. U. (2014). Hybridization of Cognitive Radar and Phased Array Radar Having Low Probability of Intercept Transmit Beamforming. *International Journal of Antennas and Propagation, 2014.* Article ID 129172. (ISI indexed & IF 0.6)

[4]. Basit A, Qureshi I M, Ulhaq I, A.N Malik, Khan W, "Evolutionary Computing Based Antenna Array Beamforming with Low Probability of Intercept Property," *World Applied Sciences Journal,* 23 (11): 1570-1575, 2013.

[5]. Basit A., Qureshi I.M., Khan W, Khan W, Khan SU., "Situationally Intelligent FDA Radar with Logarithmic Frequency Offset," IEEE SAI Intelligent Systems Conference 2016. (accepted)

[6]. Basit, A.; Qureshi, I.M.; Khan, W.; Khan, S.U., "Cognitive frequency offset calculation for frequency diverse array radar," *IEEE Applied Sciences and Technology (IBCAST), 2015 12th International Bhurban Conference on* , vol., no., pp.641,645, 13-17 Jan. 2015

[7]. Basit, A.; Qureshi, I.M.; Khan, W.; Shoaib. B, " Beam Sharpening of a Range-angle-dependent pattern using Non-uniform Symmetric but integer Frequency

Offset," *IEEE* International conference on intelligent system engineering (ICISE) 2016.*(Accepted)*

[8]. Basit, A.; Qureshi, I.M.; Khan, W.; Shoaib. B, " Beam Pattern Synthesis For A Cognitive Frequency Diverse Array Radar To Localize Multiple Targets With Same Direction But Different Ranges," *IEEE Applied Sciences and Technology (IBCAST), 2016 13th International Bhurban Conference on* , Jan. 2016 *(Accepted)*

[9]. Saeed, S., Qureshi, I. M., **Basit, A**., Salman, A., & Khan, W. Cognitive null steering in frequency diverse array radars. *International Journal of Microwave and Wireless Technologies*, 1-9, 2015.(IF 0.348)

[10]. Khan, W., Qureshi, I. M., Basit, A., & Zubair, M. A Double Pulse MIMO Frequency Diverse Array Radar for Improved Range-Angle Localization of Target. *Wireless Personal Communications*, 1-15, 2015 (IF 0.6)

[11]. Wasim Khan, I.M. Qureshi, **A. Basit**, Muhammad Zubair, "Transmit/Receive Beamforming and Interferences Cancellation Using Phased MIMO Radar with Full Waveform Diversity," *World Applied Sciences Journal*, 27 (3): 392-399, 2013.

[12]. Wasim Khan, I.M. Qureshi, **A. Basit**, Muhammad Zubair, "Hybrid phased MIMO radar with Unequal Subarrays," *IEEE Antenna and Wireless Propagation Letters (AWPL) ,pp.* 1702 - 1705, Vol. 14 , 2015 (IF 1.58)

[13]. Wasim Khan, I.M. Qureshi, **A. Basit**, Waseem Khan, "Range Bins Based MIMO-Frequency Diverse Array with logarithmic offset," *IEEE Antenna and Wireless Propagation Letters (AWPL)* DOI 10.1109/LAWP.2015.2478964, (IF 1.58)

[14]. Wasim Khan, I.M. Qureshi, **A. Basit**, Bilal Shoaib , "Transmit/Received beamforming for MIMO-Log- Frequency Diverse Array radar" *IEEE IBCAST* 13-17 jan, (accepted) 2016 Islamabad Pakistan

[15]. Shafqat Ullah Khan, Qureshi I. M., Naveed A., Shoaib B., **Basit A**., "Detection of Defective Sensors in Phased array Using Compressed Sensing and Hybrid Genetic Algorithm", *Journal of Sensors*. 2015 Article Number: 6139802 Published: 2016 (IF: 1.182)

[16]. S. U. Khan, I. M. Qureshi, F. Zaman, B. Shoaib, A. Naveed, and **A. Basit**, "Correction of Faulty Sensors in Phased Array Radars Using Symmetrical Sensor Failure Technique and Cultural Algorithm with Differential Evolution," *The Scientific World Journal,* Volume 2014, Article ID 852539, 10 pages.

[17]. S. U. Khan, Qureshi I M, Zaman F, **Basit A**, Khan W, "Application of Firefly Algorithm to Fault Finding in Linear Arrays Antenna," *World Applied Sciences Journal,* 26 (2): 232-238, 2013. (ISI indexed & Science citation indexed)

[18]. Khan, S.U.; Qureshi, I.M.; Shoaib, B.; **Basit, A.**, "Correction of faulty pattern using cuckoo search algorithm and symmetrical element failure technique along with distance adjustment between the antenna array," *Applied Sciences and Technology (IBCAST), 2015 12th International Bhurban Conference on* , vol., no., pp.633,636, 13-17 Jan. 2015

[19]. B Shoaib, I.M. Qureshi , S.U. khan, **A Basit** , "A modified adaptive step size kernel least mean square algorithm for Lorenz time series prediction," *Applied Sciences and Technology (IBCAST), 2015 12th International Bhurban Conference on* (Accepted)

[20]. Wasim Khan, I.M. Qureshi, **A. Basit**, Aqdas Naveed Malik, Adnan Umar , "Performance Analysis of MIMO-Frequency diverse array radar with variable logarithmic offset" , *Progress in electromagnetic research (PIER)* (Accepted) 2016.

Submitted Papers:

[1]. Basit A, Qureshi I M, Khan W, A N Malik, "Performance Analysis of a Cognitive Phased Array Radar with Online Tracking Capability," *Wireless Personal Communication* (submitted) 2015.

[2]. Basit A, Qureshi I M, Khan W, A N Malik, "An Improved Transmit Beam Pattern Synthesis for a Symmetric Frequency Diverse Array Radar," *IEEE Antennas and Wireless Propagation Letters* (submitted) 2015.

[3]. Wasim Khan, I.M. Qureshi, **A. Basit**, Shafqat Ullah Khan , "MIMO-FDA with unequal subarrays for improved Range-angle beamforming" , *Wireless Personal Communications* (submitted) 2016.

The research work presented in this dissertation is based on the published and accepted papers No. 1-8 and the submitted paper No.1-2.

ACKNOWLEDGEMENTS

In the name of Allah, the Most Gracious and the Most Merciful. All praise and glory goes to Almighty Allah (Subhanahu Wa Ta'ala) who gave me the courage and patience to carry out this research work. Peace and blessings of Allah be upon His last Prophet Muhammad (Sallulah-o-Alaihihe-Wassalam) and all his Sahaba (Razi-Allah-o-Anhu) who devoted their lives for the prosperity and spread of Islam.

This dissertation would have not been written without the consistent support and encouragement from many colleagues, family members and friends that surround me. First, I would like to express my gratitude to Dr. Ijaz Mansoor Quershi, my PhD supervisor, mentor and teacher. He has been an inspiring figure and role model for me since I joined the teaching profession. It has been an absolute pleasure and honor to be the student of Dr. Aqdas Naveed Malik from whom I learned and benefited a lot. He is one of my ideal teachers. The role and support of Dr. Ihsanul Haq during my PhD course work was exceptional. His encouraging approach is always a source of motivation for me. I owe my special thanks to my foreign evaluators, Dr. Julio C. Proano and Dr. Ibrahim Devili, and in-country examiners, Dr. Tanweer Ahmed Cheema and Dr. Muhammad Faisal Zafar, for their critical review of this research work and their useful inputs and suggestions.

My sincere thanks also goes to my colleagues: Engr. Wasim Khan, Hafiz Muhammad Zaheer, Dr. Shafqatullah Khan and Engr. Sharjeel. I would like to acknowledge the support of International Islamic University Islamabad Pakistan for providing me eighteen months study leave and full fee waiver during the PhD studies. It was indeed a generous award and investment from my university.

The biggest thanks goes to my family members because of their love and prayers. I owe a lot to my devoted wife for her unending encouragement and patience.

(Abdul Basit)

TABLE OF CONTENTS

LIST OF FIGURES

LIST OF TABLES

LIST OF ABBREVIATIONS

ASR	Airport surveillance radar
ATC	Air traffic controller
AWGN	Additive White Gaussian Noise
BCR	Basic cognitive radar
BSB	Big-small-big
CKF	Cubature Kalman filter
CR	Cognitive radar
CRLB	Cramer Rao lower bound
DAR	Digital Array Radar
DE	Differential evolution
DOA	Direction of arrival
EKF	Extended Kalman Filter
ESPRIT	Estimation of signal parameters by rotational invariance techniques
EW	Electronic warfare
FDA	Frequency diverse array
FDTD	Finite difference time domain
GA	Genetic algorithm
GMTI	Ground moving target indication
HCFDA	Hybrid cognitive frequency diverse array
HCPAR	Hybrid cognitive phased array radar
HPBW	Half power beam width
KF	Kalman filter
LCMV	Linear constrained minimum variance

LFMCW	Linear frequency modulated continuous waveform
LPI	Low probability of intercept
MIMO	Multiple input multiple output
MLP	Multi-layer perceptron
MSE	Mean square error
MUSIC	Multiple signal classification
MVDR	Minimum variance distortion less response
NN	Neural networks
OFDM	Orthogonal frequency division multiplexing
PAPR	Peak-to-average-power-ratio
PAR	Phased array radar
PCM	Pulse coded modulation
PS	Pattern search
PSO	Particle swarm optimization
RCS	Radar cross section
SAR	Synthetic aperture radar
SBS	Small-big-small
SINR	Signal to interference and noise ratio
SLL	Side lobe levels
SLP	Single layer perceptron
SNR	Signal to noise ratio
STAP	Space-time adaptive processing
UKF	Unscented Kalman filter
ULA	Uniform linear array

LIST OF SYMBOLS

Nomenclature for all equations is defined in the main body of the document; however, a list of commonly used symbols in this dissertation is given here.

N	Number of antenna elements in a transmit-array
M	Number of antenna elements in a receive-array
d	Inter-element distance in an array of antennas
c	Speed of light
$\mathbf{w}$	Weight vector of an array
θ	All angle w.r.t. boresight of a radar
θ_0	A specific value of θ at which radar is expecting or looking for a target
λ	Wavelength
v	Wave number
r	All range values
r_0	A specific value of r at which radar is expecting or looking for a target
P	Beam pattern
AF	Array factor
f_0	Fundamental frequency
Δf	Frequency offset
s	Transmitted waveform
t	Time
k	Discrete time instant
F	Far Field sources

T_d	Time delay
$\mathbf{x}_k$	State of the system at time k
$\mathbf{z}_k$	Observation vector at time k
$\tilde{\mathbf{F}}$	A nonlinear transition matrix
$\tilde{\mathbf{H}}$	A nonlinear measurement matrix
$\boldsymbol{n}_k$	AWGN process vector at time k
$\mathbf{v}_k$	AWGN measurement vector at time k
$\mathbf{Q}$	Process noise covariance
$\mathbf{R}$	Measurement noise covariance
$\hat{\mathbf{P}}$	State covariance matrix
φ_n	Spoiled phase shift values
$\mathbf{a}$	Transmit steering vector of an array
$\mathbf{b}$	Receive steering vector of an array
ρ	Directional gain
$\mathbf{u}$	Virtual steering vector
$\mathbf{y}$	Output of the receiving array after match filtering
$\mathbf{R}_{i+n}$	Interference plus noise covariance matrix
H_0	Hypothesis when target is not present in the surveillance region
H_1	Hypothesis when target is present in the surveillance region
p_d	Probability of detection
p_M	Probability of miss
p_{fa}	Probability of false alarm

δ Threshold for target detection

(θ_0, r_0) Target position

μ Value of the u-law companding scheme

α_n Non-uniform offset coefficients

$\mathbf{J}$ Fisher information matrix (FIM)

CHAPTER-1

INTRODUCTION

The term radar, acronym for *radio detection and ranging,* was devised in 1940 by the U.S. Navy. It uses radio waves for detecting and tracking of spacecraft, aircraft, ships, guided missiles, weather formations and motor vehicles etc. It determines range, direction, altitude, speed and velocity of objects. The theory and design of modern radars is dominated by signal processing, controls, information theory, probability theory and statistical techniques to make it powerful, robust and adaptive. The design range is extended from simple air traffic controller (ATC) to phased array radar (PAR), frequency diverse array (FDA) radar and cognitive radar (CR), achieving the ultimate goal of serving the civilian and military world in diverse ways.

In this chapter, we shall introduce the existing modern radar technologies, which will be followed by the motivation and contribution of this research and finally the organization of dissertation.

1.1. Background of modern radar technologies

Two fundamental categories of radars based on the number of antennas used are the single antenna radars and multiple antenna radars. The single antenna radar conventionally uses mechanical rotations for scanning the surveillance region in all directions. Later on, the electrical beam steering was introduced in PAR, developed in

Lincoln Laboratory in 1958, which was the initial form of involving multiple antenna elements in radars.

The PAR, a group of antenna elements, exploits a relative phase variation between the elements to steer the radiation pattern in a desired direction and suppress in the undesired directions. These high gain PAR beam patterns are easy to compute, allow greater frequency agility, generate multiple beams and track multiple targets with greater accuracy, which justify wider use of these arrays in modern radar applications. Electronic phase shifters have been used to achieve these objectives, which are much more expensive compared to a traditional reflector antenna used for surveillance. However, beam steering of phased array is fixed in angle for all values of range cells i.e., independent of the target range, which degrades the performance in different applications dependent on range, e.g., range-dependent interference suppression, range ambiguities suppression and directional communications etc.

To address these issues in an elegant and less expensive manner, a range-angle dependent electronic beam steering by using successive frequency offsets at array elements is a solution, which results in a frequency diverse array (FDA) radar. In an FDA, the frequency offsets enable it to generate a range, angle and time dependent beam pattern that may help to suppress range-dependent interferences. Since an FDA beam pattern is periodic in range, angle and time, it periodically illuminates a specific range- angle pair of object position.

During last decade, another modern radar design proposed by Simon Haykin, is termed as cognitive radar (CR). According to the Oxford dictionary, a thought process for gathering knowledge of the outside world is known as *cognition*, it also embodies

processing of information, applying gathered knowledge and changing preferences based on situational awareness. Similarly, the visual brain has been characterized with functions for having perception of the outside world in one part, while taking action to control the environment in a separate part of the brain. Working in this coordinated fashion is known as *perception-action* cycle.

Similarly, the CR continuously senses its environment and learns from experiences. It is intelligent enough to utilize the extracted information as feedback between the receiver and transmitter to facilitate computational intelligence. It also preserves information in an implicit way to enhance the overall performance of radar i.e., it enhances receiver's performance directly and transmitter's performance indirectly. Therefore, the feedback link is the back bone of a cognitive system.

To understand the importance of the feedback link, the echo-location system of a bat is an example. Bat acquires information about the target of interest e.g., range, relative velocity, size, azimuth and elevation angles etc., within a nominal time and consequently, makes changes in its transmit signal. It is proficient enough to utilize the previous knowledge about the surroundings in addition with the knowledge gathered through continuous interactions with the environment.

1.2. Motivation: Hybridization of cognitive radar with modern radar systems

Previously, the conventional radars were the major focus of researchers to address various problems, such as, range estimations, speed measurements, velocity measurements, direction of arrival estimations and radar cross section (RCS)

measurements etc. Moreover, there are two major objectives supposed to be performed by the radars, which are scanning of area under surveillance and tracking of single/multiple targets simultaneously.

With the availability of quick processing machines, we are now in a position to implement algorithms demanding high computational cost, such as, neural networks, heuristic computing algorithms and advanced signal processing techniques, which pave our way towards intelligent radars.

Although, a lot of research is being carried out in this direction, yet the analogy between visual brain and radar systems has not been fully exploited. Obviously, hybridization of cognitive radar with modern radar systems is a step forward towards this direction i.e., learning from a human brain. Hence, we emphasize that hybridization of cognitive radar with modern radar technologies like PAR and FDA can indeed build a more powerful generation of radar systems. To achieve this objective, we shall utilize the cognitive information processing and learning techniques in addition with the available tools in modern radar systems.

The main objective of this dissertation is to give an idea for building a new generation of intelligent radars, which may address all the problems related to radars in an efficient way by hybridizing the modern radar systems i.e., PAR and FDA with cognitive radar properties.

1.3. Objectives and Contribution of the dissertation

There are two fundamental objectives of this dissertation.

- Hybridization of CR with PAR (i.e., HCPAR) and its performance analysis

- Hybridization of CR with FDA radar (i.e., HCFDA) and its performance analysis

We are focusing to propose hybrid radar systems that may achieve improved signal to interference plus noise ratio (SINR) and detection probability with improved transmit energy focusing towards target position. It provides improved Cramer Rao lower bound (CRLB) on target position estimation and better range and angle resolution as compared to the existing modern radar technologies. The major contributions incorporated in this dissertation can be summarized below.

A hybrid cognitive PAR with transmit-receive beamforming for tracking the targets in real time is the first contribution. This versatile cognitive design has the ability to sense the environment adaptively. It selects/decides the active number of elements, sufficient for target range, at the transmitter and receiver arrays after each scan. This reduces the computational complexity and hardware cost of the system compared to a conventional fixed element PAR. Moreover, the proposed radar system avoids continuous scanning of the surveillance region. Instead, the transmitter, based on the receiver feedback, ensures maximum power towards the target future position. This results in improved SINR and detection probability. It saves a lot of energy as the transmitter only illuminates the area of interest. Another significant feature of the proposed system is its low probability of intercept (LPI) transmit beamforming ability. The transmitter generates a set of defocused beams of low power, which are difficult to be detected by interceptor. These low power beams are combined at the specific position of the target in constructive manner. Hence, overall performance of the proposed system is not compromised.

The second contribution included in the dissertation is a hybrid cognitive FDA radar with a uniformly increasing frequency offset. The proposed design has an adaptive range-

angle dependent beamforming ability for tracking of targets and ensures enhanced signal to interference and noise ratio (SINR) with improved detection performance. The improvement in SINR and detection probability is mainly due to incorporation of cognitive radar properties. The receiver of the proposed design estimates the current and future positions of target and tunnels this information to the transmitter for adjusting its beamforming parameters, adaptively. The proposed scheme includes an analytical formulation to compute the value of frequency offset based on the feedback, which helps to generate the desired range-angle dependent beam pattern. The proposed system ensures an improved target localization performance, detection probability and SINR at the receiver as compared to the conventional FDA and PAR systems. This scheme also saves a lot of power as it illuminates only the desired area from the entire surveillance region. In addition, the computational complexity and electromagnetic pollution of the environment is decreased.

The third contribution included in this dissertation is a hybrid cognitive radar with uniformly-spaced FDA having non-uniform but symmetric frequency offsets across the array elements. Unlike the conventional frequency diverse array (FDA) radars with uniform frequency offset that exhibits maxima at multiple ranges and angles, the proposed schemes achieve a single maximum towards the target position. Thus the problem of detecting the target among potential interferers is automatically eliminated. Two cases have been considered under given scenario i) non-uniform but integer values of frequency offsets ii) non-uniform and fractional values of frequency offsets. The proposed design with non-uniform but integer values of frequency offsets has low half power beam width (HPBW) compared with previous designs. i.e., the beam is more

focused in this case. The fractional offsets values result in achieving a single maximum beam pattern. These are computed in three different ways in this dissertation. In the first case, these fractional offsets are computed using well known mu-law formulae from communication theory to achieve a single maximum beam pattern at the target position for improved detection and SINR performance. In the second case, the GA has been used to calculate non-uniform fractional offsets for localizing targets with the same directions but different ranges. Finally, in the third case, the hamming window function has been used to compute these fractional offsets for improved side-lobe suppression and transmit energy focused beam pattern performance.

The proposed cognitive design improves transmit beam pattern based on the feedback, and hence achieves improved detection probability, SINR and a better Cramer- Rao lower bound (CRLB) on target angle and range estimation. The symmetric frequency offsets scheme has been observed to achieve better null depths compared to the non- symmetric scenarios.

1.4. Organization of the dissertation

The dissertation has been organized as follows.

In chapter 1, an overview of the research problems addressed in this dissertation has been mentioned. Moreover, the motivation, objectives and achievements of the presented research work have been highlighted.

In chapter 2, a brief history of radars and introduction of modern radar designs i.e., PAR, FDA radar and cognitive radar has been given. Afterwards, the latest research work on these modern radar is highlighted.

In chapter 3, the proposed hybrid cognitive phased array radar (HCPAR) design has been discussed. Additionally, an evolutionary computing based low probability of intercept (LPI) transmit beam forming technique has been discussed for the proposed HCPAR.

In chapter 4, the proposed hybrid cognitive frequency diverse array (HCFDA) radar with uniform frequency offset design has been presented. The frequency offset selection has been formulated based on the receiver feedback. The transmitter of the proposed design has been illustrated and transmit beam-pattern has been derived to illuminate the target position.

In chapter 5, the proposed HCFDA radar design with non-uniform frequency offset has been described. The non-uniform offset selection methods have been proposed for the FDA design to generate beam patterns having single maxima with sharpened half power beam width (HPBW). Additionally, a transmit beam pattern with a hamming window based tapering frequency offsets has been presented for the FDA design under consideration. This scheme ensures the focusing of transmit energy towards the target position with increased side lobe suppression outside the area of interest.

In chapter 6, we have concluded the dissertation and suggested future directions for research in this field.

CHAPTER-2

PAR radar, FDA radar, Cognitive radar and Evolutionary computing: An Overview

In this chapter, a brief history of radar followed by the fundamentals of phased array radar (PAR), frequency diverse array (FDA) radar and cognitive radar (CR) is presented. Furthermore, a detailed overview and literature review of these modern technologies is given. At the end of this chapter, the recent research challenges in this area are highlighted.

2.1. Radar history

The basic principle of radar is to detect objects in its surrounding using the reflected radio waves, which was originally used in the early twentieth century [1]. Its early applications were to detect ships in the surroundings to avoid collision. Later on, a working radar system was patented in 1935 by Sir Robert Watson-Watt [2], which had all the important characteristics of a useful radar. The capabilities of radars significantly improved during World War II, when German radars steered the beam to scan the whole surveillance region by rotating the directional antennas mechanically [3].

Most of the radar applications demand high directivity in one direction instead of mechanically rotating directional antennas. Another key requirement for radar antennas

has been the capability to scan a large volume of space. Traditionally, scanning was done by means of mechanically rotating systems, which used to rotate the antennas on a pedestal. As the applications demand more versatile systems, more delicate means of scanning were introduced, including electronically scanned phased arrays or phased arrays [4]. A radar system exploiting these phased arrays is coined as phased array radar (PAR).

An electronic beam-steering technique using an antenna array was originally investigated and employed in military and civilian radars in the late 1970s [5]. However, mechanically steered radars are still in use e.g., the airport surveillance radar ASR-9 [6] built in 1980s along with hybrid systems, which employ both mechanical and electronic scanning at the same time, e.g., the TPS-117 radar [7].

Based on the topologies, there are three major classes of arrays, i.e., the linear array [8], the planer array [9] and the circular array [10]. We have considered a uniform linear array in this dissertation due to its simple structure and mathematical model, yet this work can be extended for the planer and circular arrays as well.

2.2. Phased array radar (PAR)

Phased array is a most common arrangement of radars with multiple transmit antennas. It has been used initially in late 1930s [11]. Since, phased arrays have been used in its simplest form during World War II, the attention of researchers towards their advancement started gaining attention in the 1950s and 1960s [12]. Nevertheless, the researchers are still investigating towards improvement in phased array radar technology [13]–[15].

Phased array antenna radar consists of a group of antennas, which are combined in such a manner that the relative phase among the elements is varied in a specific pattern to achieve a constructive and destructive interference at desired locations. This is meant to achieve a beam pattern having high directivity in the desired direction, while side lobes in undesired directions [16]. The high gain offered by phased arrays facilitates in detecting and tracking weak targets with small cross section, while suppressing strong interferences from other directions [17]. The relative phased between the elements is varied using electronic phase shifters. In order to control the side lobe levels (SLL), an appropriate amplitude distribution is applied across the phased array [18].

The phased array antennas radars having the properties of electronic steering, high gain and low side lobes, narrow beam width, multiple beams, variable scan rates and interference cancellation etc., have benefitted variety of radar and satellite applications [19]. These antennas have much more flexibility and advantages compared to a conventional reflector antenna. However, the high cost is one of the limiting factors [20]. A uniform linear array architecture [21] is shown in Fig-2.1.

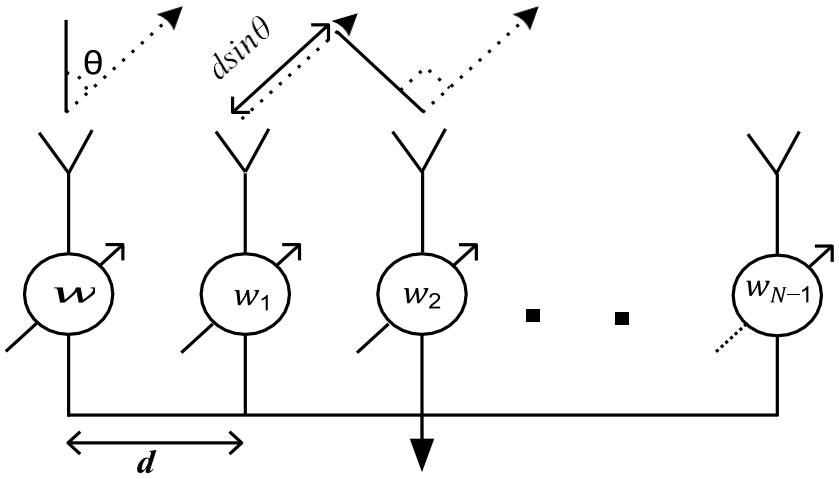

Figure-2. 1: Uniform linear phased array with *N* elements

An array of N elements is organized in a straight line with a uniform inter-element spacing d, where $w_.$ are the respective weights of each element, while θ is the direction of target.

The spacing between the elements can be non-uniform as well in many applications for achieving less complex beam forming performance [22],[23] . Moreover, the antennas can be placed in a rectangular plane area to form a planar grid of antennas according to the application requirement [24]. In any case, each element is fed with the same frequency and waveform [25]–[27]. With identical antennas, the overall electric field radiated by an array towards a point target in the surveillance region is equal to the electric field of a single antenna multiplied by an array factor, which depends upon the distance between the array elements and phase shifts [21]. The inter-element phased offset are varied, appropriately, to steer the beam pattern in the whole surveillance region, while the amplitude associated with each phase shifter controls the shape of radiation pattern quite effectively [25].

In this case, the N element array transmits single waveform towards a point target from its antennas scaled by complex weights $w_0, w_1, ..., w_{N-1}$ as shown in Fig. 2.1. The array factor of PAR is given as [28]

$$AF(\theta) = \sum_{n=0}^{N-1} w_n^* e^{jn(v d \sin\theta)} \tag{2.1}$$

where $v = 2\pi / \lambda$ represents the wave number, while λ denotes the wavelength, d is inter-element distance and θ is desired direction. The vector form of this array is given as

$$AF(\theta) = \mathbf{w}^H \mathbf{a}(\theta) \tag{2.2}$$

here $(.)^H$ is denotes the conjugate transpose of a vector, $\mathbf{w}$ is the weight vector and $\mathbf{a}(\theta)$ is the array steering vector which are given as [29]

$$\mathbf{w} = \left[w_0, w_1, ..., w_{N-1}\right]^T \tag{2.3}$$

$$\mathbf{a}(\theta) = \left[1 \; e^{jkd\sin\theta} \; e^{j2kd\sin\theta} \; \ldots \; e^{j(N-1)kd\sin\theta}\right]^T \tag{2.4}$$

here $[.]^T$ represents the transpose of a vector. With uniform weights, i.e., w_n=1, the array factor may be expressed as [30]

$$AF(\theta) = \frac{\sin\left(\frac{N}{2} kd\sin(\theta)\right)}{N\sin\left(\frac{1}{2} kd\sin(\theta)\right)} \tag{2.5}$$

The beam pattern is generally used to represent the radiation pattern of an array, which shows the space distribution of transmitted power. The beam pattern for the PAR antenna is given as [21]

$$P_{PAR}(\theta) = \left|\mathrm{AF}(\theta)\right|^2 = \left|\mathbf{w}^H \mathbf{a}(\theta)\right|^2 \tag{2.6}$$

It is apparent from (2.6) that a beam pattern towards a desired target position can be generated by applying a suitable weight vector known as beam former. It can be either adaptive to compute a weight vector adaptively for optimal performance or non-adaptive where weights are fixed to get high directivity in the desired direction. The two commonly used adaptive beam formers are minimum variance distortion less response (MVDR) and linear constrained minimum variance (LCMV) beam formers. On the other hand, non-adaptive beam formers compute weights with uniform or non-uniform amplitude distribution [31]–[33]. The non-uniform distribution includes binomial,

triangular and Dolph-Chebyshev distributions etc., while uniform weight distribution is known as conventional beam former [30].

These conventional weights are generally computed as $\mathbf{w} = \mathbf{a}(\theta_0)$, where θ_0 is the desired direction. Therefore, the beam pattern of a PAR using conventional beam former is expressed as [33]

$$P_{PAR}(\theta) = \left|\mathbf{w}^H \mathbf{a}(\theta)\right|^2 = \left|\sum_{n=0}^{N-1} e^{jn\left(vd\left(\sin\theta - \sin\theta_0\right)\right)}\right|^2 = \left|\frac{\sin\left(\frac{N}{2} vd\left(\sin\theta - \sin\theta_0\right)\right)}{\sin\left(\frac{1}{2} vd\left(\sin\theta - \sin\theta_0\right)\right)}\right|^2 \quad (2.7)$$

Fig-2.2 shows the synthesized beam pattern of a PAR using a conventional beam former weight vector. The maxima of the beam pattern is towards $\theta = \theta_0$ as apparent from (2.7) and rejects all the interferences outside the illuminated spatial sector.

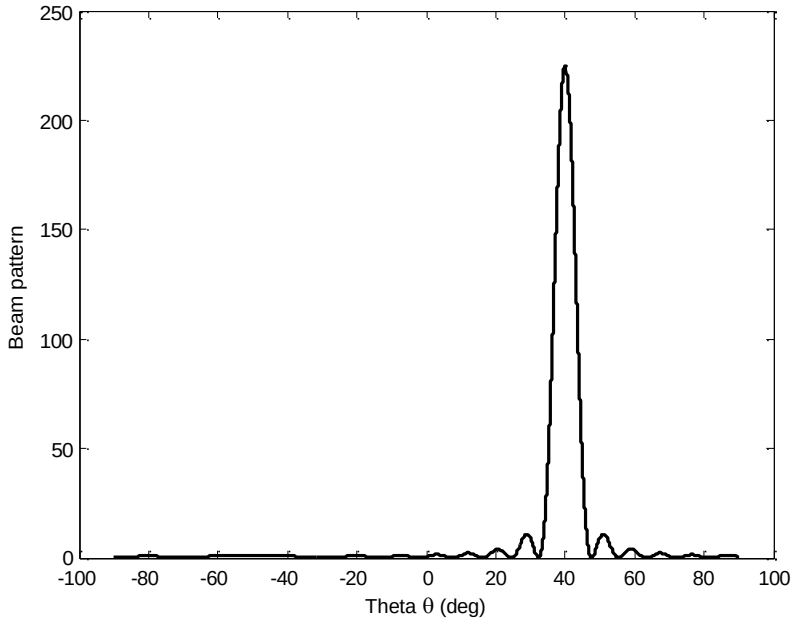

Figure-2. 2: Synthesized beam pattern using a conventional beam former $\left(N = 15, \theta_0 = 40^{\circ}, vd = \pi\right)$

If the inter-element distance exceeds $\frac{\lambda}{2}$ i.e., $d > \frac{\lambda}{2}$, the beam pattern maxima may occur at other angles causing grating lobes. To avoid this phenomenon, inter-element distance is taken less than or equal to the half wave length i.e., $d \leq \frac{\lambda}{2}$. Therefore, in this case we have considered $\nu d = \pi$, where $d = \frac{\lambda}{2}$. The PAR beam pattern helps to localize targets in the angle dimension with great success.

2.2.1. Advantages of PAR

Phased array antennas allow beam agility, multi-function radar operations, beam thinning, beam broadening, low side lobes in desired look area and nulls placement in the undesired directions to suppress interference [34].

Adaptive beamforming is another advantage of phased array antennas, which allows the computation of complex weights to form a transmit-receive beam pattern that suppresses multiple interferences, simultaneously, for improved SINR performance [35], [36].

Phased arrays also have the ability to detect a moving target in the presence of a clutter. For this, the space-time adaptive processing (STAP) uses the space-Doppler properties of clutter to adaptively suppress clutter in real time [37].

Angle estimation of multiple targets has been performed using phased arrays quite effectively. Multiple signal classification (MUSIC) algorithm [38], [39] and estimation of signal parameters by rotational invariance techniques (ESPRIT) [40] algorithm have been

widely applied in the radar field to estimate the direction of multiple targets. Likewise, ranges of targets have also been computed effectively, using phased arrays exploiting time delay between the transmitted and received signal peaks [41].

Phased array radars have the flexibility to choose one of the beamforming array structures in real time, such as narrow and wide band array structure with the choice of amplitude taper in transmit/receive modules [42], [43]. Likewise, symmetric PARs have been used to obtain better null depth and thus improved signal to interference and noise ratio (SINR) at the receiver [44]–[46].

Phased array radar antennas have also been exploited in moving target tracking problems, which is the requirement of modern radar systems. The well-known Kalman filter (KF) [47] and its variants such as extended Kalman Filter (EKF) [48] , unscented Kalman filter(UKF) [49], cubature Kalman filter (CKF) [50] etc., have been widely applied in modern phased array radar systems to improve the target tracking and prediction performance [51]–[53].

The unequal spacing between the elements increase the aperture of array without increasing the employed number of antenna elements, this helps in thinning or broadening of beam-width and reduces the side lobe level (SLL) with a reduced number of elements [54]. A variety of algorithms have been applied in literature to suppress interferences for unequally spaced phased arrays [55], [56].

2.2.2. Disadvantages of PAR

Although phased arrays have many advantages, but we will highlight some of its drawbacks and disadvantages in many applications. One of the major disadvantage is their high cost. Depending upon the application, a more directed high gain beam with low

side lobes requires a greater number of antenna elements and so the greater number of electronic phase shifters, which are quite expensive and hence increase the cost drastically. Therefore, researchers have investigated the alternative array structures exploiting a less number of elements to reduce the cost [57].

Another disadvantage is that most of linear arrays require an equal inter-element spacing, which is not applicable for wideband applications. In phased arrays, exceeding inter-element distance beyond half wavelength results in the appearance of grating lobes in the visible regions that deteriorates the radar tracking performance [58]. Different techniques [18], [23] have been used in literature to reduce the disadvantages of non-uniform inter-element distances.

The phased array antennas with the advantage of higher gain compared to isotropic antennas, are very likely to be detected by the jammers and intruders due to the amount of energy transmitted towards the target based on conventional techniques. It is very common that intruders degrade, exploit and prevent radar operations. The competition between the radar and intruders is termed as electronic warfare (EW) [59].

To achieve a low probability of intercept (LPI) beamforming, various techniques have been proposed to ensure an effective detection range [60]–[62]. Three widely used LPI techniques include i) spreading energy in time domain by means of high duty cycle waveforms ii) spreading energy in frequency domain by means of wide-bandwidth waveforms and iii) spreading energy in spatial domain by means of broader transmit antenna beams [60], [63]. Hybridization of these techniques also helps to enhance the overall performance [62], [64]**.**

The commonly used techniques are high duty cycle, wide-bandwidth waveforms that are extensively exploited in LPI based applications [65]. Moreover, the side lobes are suppressed, effectively, to reduce the probability of being detected up to some extent [66]. In [67], a pseudo random frequency jitter for the fundamental frequency has been presented to design an LPI waveform for orthogonal frequency division multiplexing (OFDM) systems. In [68], time-energy management techniques have been presented for digital array radar (DAR) to analyze its LPI performance. Along with the waveform design, numerous other techniques using different types of antennas modifications are available in literature to improve the LPI performances. Antenna hopping technique presented in [69] uses a switch to connect two or more spaced antennas linked with a single input or output. Additionally, multiple input multiple output (MIMO) antennas have been employed in different techniques to shape the transmit beam in such a manner that restricts the radiations in undesired directions to achieve improved LPI performance [70]. Similarly in [71], a frequency hop multiple access technique is used for evaluating an LPI performance for a network, where the intruder determines whether a network is active or not, based on the received energy.

Another disadvantage is that a phased array antenna produces a power maximum at a fixed angle for all ranges. Therefore, it is very difficult to suppress range-dependent clutter and to localize multiple targets having same direction but different ranges using phased arrays. Although many techniques exist to suppress a range-dependent interferences such as STAP techniques [72], [73] but they increase the computational cost and complexity.

A major disadvantage is that an overall phased array radar system is not aware of changing characteristics of non-stationary environment in real time as the receiver is not linked with transmitter. It cannot perform intelligent signal processing at transmitter based on its learned knowledge of the environment. It cannot adjust parameters or learn about the environment changes on the fly or use the prior knowledge. It is not capable of changing beam steering pattern adaptively, while in operation. It is the need of modern time that a radar should learn from its experience to deal with diverse type of targets with diverse properties in an effective manner.

Due to range ambiguity, a phased array generated beam pattern cannot estimate the target range directly because it generates a pattern which has maximum power at a fixed direction for all ranges. Likewise, the desire for more advanced array antennas such as multitask radar [74] to radio astronomy [75] and pursuit to localize and track multiple targets in more than one dimension, have come up with a novel beam steering technique exploiting frequency diverse array (FDA) [76].

2.3. Frequency Diverse Array (FDA) radar

The frequency diversity was originally exploited to get independent measurements of radar cross section [77]. In order to do so, a single antenna was used to transmit frequency diverse pulses sequentially. In contrast, an FDA radar is multiple element radar like PAR. But it is different from a conventional phased-array antenna radar in a sense that it uses a frequency offset across the array, which help to generate a range, angle and time dependent beam pattern [78].

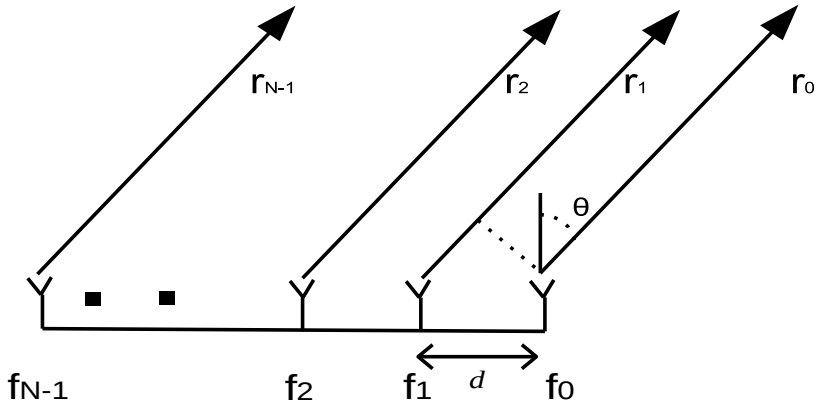

Figure-2. 3: A linear FDA structure with N antennas

An FDA uses a small frequency offset Δf compared to the fundamental frequency f_0, across the array elements [79]. Fig-2.3 shows a linear FDA structure having N antenna elements.

where the input frequency at n^{th} antenna element is given as [80],

$$f_n = f_0 + n\Delta f \;; \qquad n = 0,1,\ldots,(N-1) \tag{2.8}$$

where f_0 is a fundamental frequency and Δf is a frequency offset value. Each antenna element transmits a signal waveform $s_n(t)$ given as

$$s_n(t) = \exp(-j2\pi f_n t); \qquad n = 0,1,\ldots,(N-1) \tag{2.9}$$

The distance between the antenna elements is $d = \frac{\lambda}{2}$, where $\lambda = \frac{c}{f_{\max}}$ and $f_{max} = f_0 + (N-1)\Delta f$.

The array factor of an FDA has been derived in [81]. Therefore, adapting from (2.1) to the notations used in this dissertation, we can write

$$AF\left(t,\Delta f,r,\theta\right)=\sum_{n=0}^{N-1}w_n^*\times\frac{1}{r_n}\exp\left\{-j2\pi\left(f_n t-\frac{r_n}{\lambda_n}\right)\right\} \tag{2.10}$$

where $r_n = r_0 + ndsin(\theta)$ denotes a path difference and λ denotes wavelength. Assuming a point target in space, the generated FDA beam pattern P_{FDA} with uniform weights i.e., $w_n = 1$ can be written as [81], [82].

$$P_{FDA}(t, \Delta f, r, \theta) = \left| \sum_{n=0}^{N-1} \frac{1}{r_n} \exp\left\{ -j2\pi \left(f_n t - \frac{r_n}{\lambda_n} \right) \right\} \right|^2 \tag{2.11}$$

For a far field target i.e., $r_n \approx r_0$ and considering $f_0 \gg \Delta f$, the pattern can be approximated as [82]

$$P_{FDA}(t, \Delta f, r, \theta) \approx \left| \frac{\exp(j\gamma)}{r_0} \sum_{n=0}^{N-1} \exp\{-jn\psi\} \right|^2 \tag{2.12}$$

where $\gamma = -2\pi \left(t - \frac{r_0}{c} \right)$ and $\psi = \left(2\pi \Delta f t - \frac{2\pi \Delta f r}{c} + vdsin(\theta) \right)$.

The beam pattern can also be expressed as (adapting from (2.5))

$$P_{FDA}(t, \Delta f, r, \theta) = \left| \frac{\sin\left(\frac{N}{2} \left(2\pi \Delta f t - \frac{2\pi \Delta f r}{c} + vdsin(\theta) \right) \right)}{\sin\left(\frac{1}{2} \left(2\pi \Delta f t - \frac{2\pi \Delta f r}{c} + vdsin(\theta) \right) \right)} \right|^2 = \left| \frac{\sin\left(\frac{N}{2} \psi \right)}{\sin\left(\frac{1}{2} \psi \right)} \right|^2 \tag{2.13}$$

The FDA generated beam pattern in (2.13) is not merely a function of angle (θ) but also a function of time (t), target range (r) and frequency offset value (Δf).

From (2.13), following observations can be concluded [83]

(i): With $\Delta f = 0$, the FDA steering vector is alike a linear phased array steering vector,

(ii): With a constant Δf, an FDA beam pattern changes as a function of target range.

Additionally, with a fixed r, it becomes a function of frequency offset.

FDA is quite different from multiple input multiple output (MIMO) [84] radar as it transmits overlapped signals closely spaced in frequencies, while MIMO employs orthogonal signals from widely separated antennas over multiple independent paths to provide spatial diversity [85] or uses multiple waveforms to provide waveform diversity [86] and improved signal to noise ratio (SNR) . Likewise, it is also different from orthogonal frequency division multiplexing (OFDM) [87] as different from FDA, an OFDM technique uses orthogonal sub-carriers [88]. An FDA is also different from the conventional frequency scanning arrays [89], where each element uses the same frequency at a given time [90].

2.3.1. Advantages of FDA

Different from phased arrays, the FDA beam pattern provides a global maximum, as well as, a number of local maxima at diverse angle and ranges values [91]. This ability can be utilized for detecting multiple targets having same directions but different range values. Figs-2.4 (a) & (b) show the comparison between phased array and FDA beam patterns. It is noteworthy that several maxima are generated in the range dimension only. Using (2.13), the magnitude of maxima can be achieved as

$$\psi = 2\pi m \;\; ; \; m = 0, \pm 1, \pm 2, \ldots \tag{2.14}$$

$$i.e., \left(2\pi \Delta f t - \frac{2\pi \Delta f r}{c} + v d \sin(\theta) \right) = 2\pi m \;\; ; \; m = 0, \pm 1, \pm 2, \ldots \tag{2.15}$$

where $v = 2\pi / \lambda$.

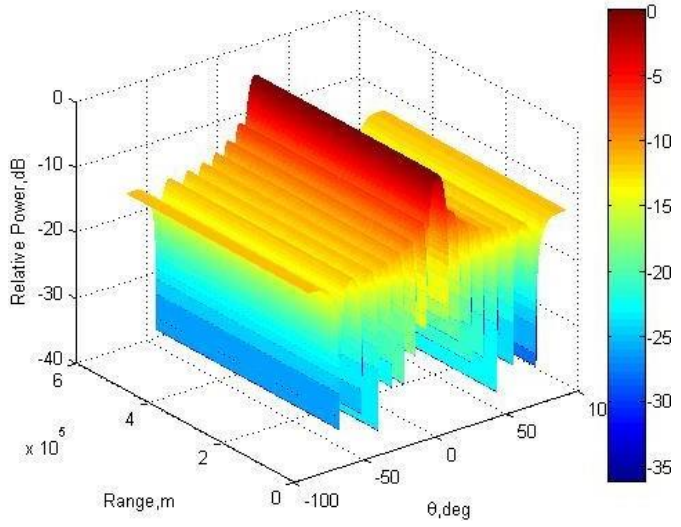

(a)

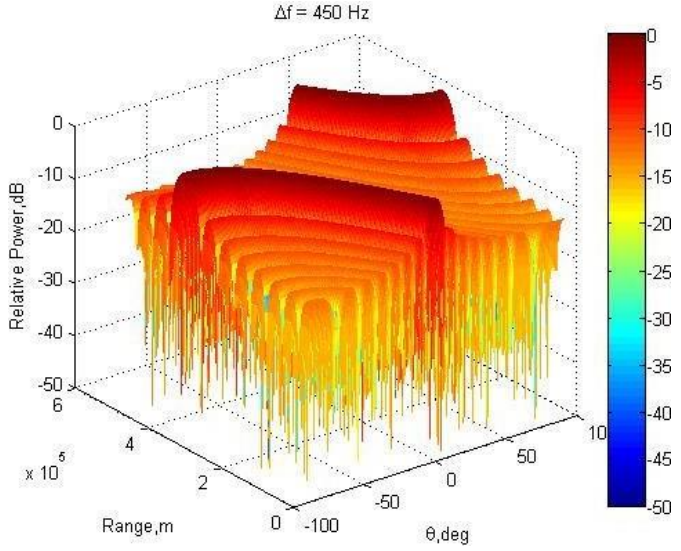

(b)

Figure-2. 4: (a) PAR generated beam pattern ($d = \lambda/2$, $N = 15$, $f_0 = 10GHz$)
(b) FDA generated beam pattern ($d = \lambda/2$, $N = 15$, $f_0 = 10GHz$, $\Delta f = 450Hz$)

We can see from (2.15) that there exist enormously many pairs of range and angle values for a fixed time $t = t_0$, which cause multiple peaks in the range dimension. Similarly, keeping two parameters fixed changes the FDA pattern into a periodic function of third parameter [81]. Figs-2.5 (a) -(c) show the periodicity of an FDA beam pattern.

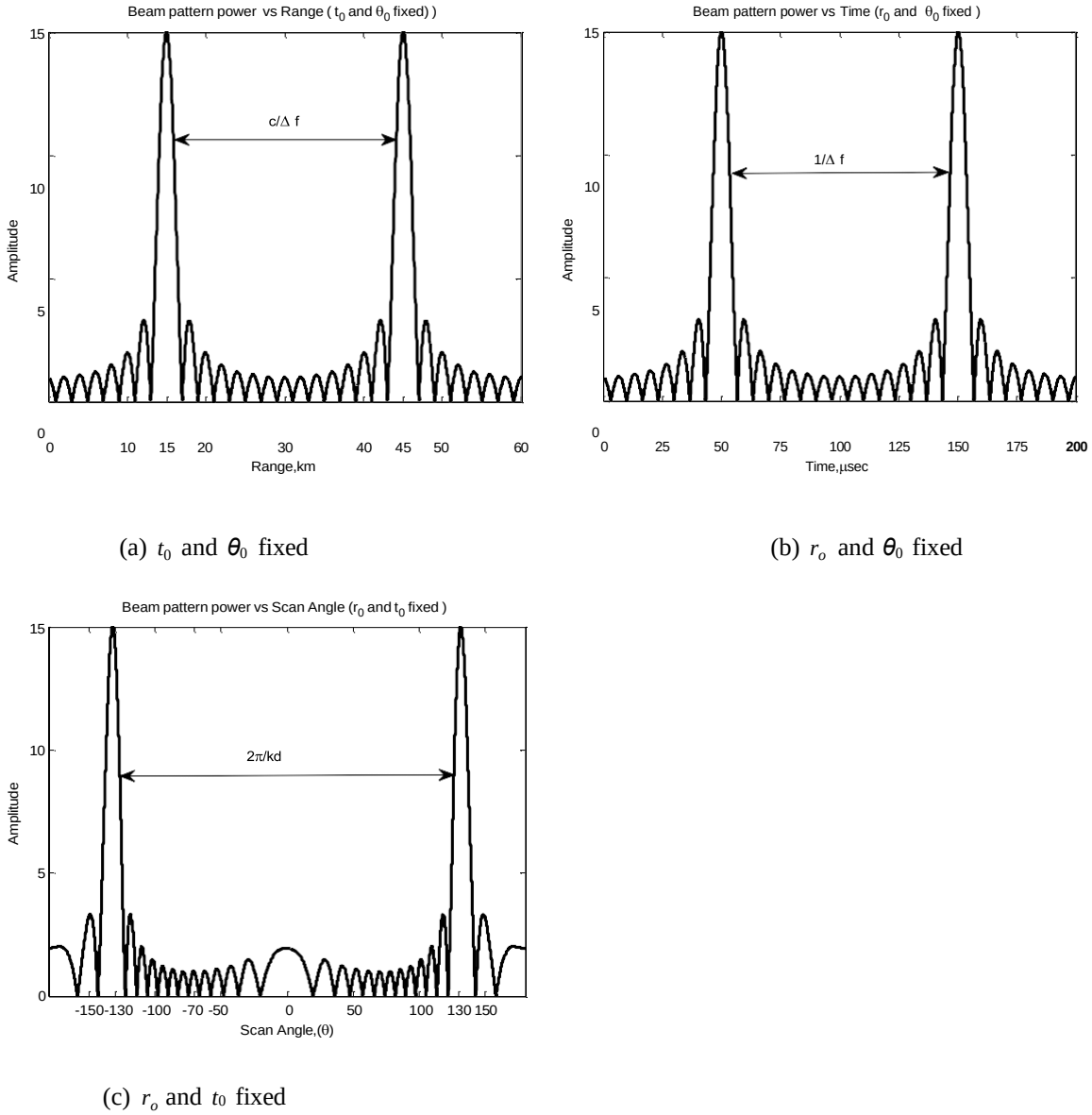

(a) t_0 and θ_0 fixed

(b) r_o and θ_0 fixed

(c) r_o and t_0 fixed

Figure-2. 5: Periodicity of FDA generated beam-pattern in a) range dimension b) time dimension and c) angle dimension having parameters $(d = \lambda/2,\ N = 15,\ f_0 = 10GHz,\ \Delta f = 10kHz)$

The fundamental periods of the FDA pattern w.r.t the range, time and angle are $\frac{c}{\Delta f}$, $\frac{1}{\Delta f}$ and $\frac{2\pi}{vd}$, respectively [81]. Therefore, the periodicity property of an FDA pattern can be utilized to generate power maxima at desired range-angle position pairs by controlling Δf across the array antenna elements.

The apparent scan angle of an FDA beam pattern is different from the nominal scan angle [76] and its array factor is dependent upon on both the range and angle [92]. Therefore, precise beam steering alike phased arrays is not sufficient. Moreover, its apparent scan angle can be outside of the real beam space that provides additional degrees of freedom to perform multiple operations simultaneously [93].

The frequency offset plays a vital role to improve the performance of FDA radar therefore, researchers have shown their keen interest to investigate different ways for its proper selection. Consequently, FDA radars with small inter-element frequency offset [94], [95] has been used to generate range dependent pattern. On the contrary, large frequency offset [82], [92], [96] has been exploited to achieve independent echoes from the target for improved localization performance. Similarly, an FDA with an adaptive frequency offset selection scheme was proposed in [97] to improve localization performance. Likewise, in [98] an FDA with a time dependent frequency offset was proposed to get improved beam pattern for a given range and direction. Moreover, the characteristics of an FDA beam pattern by changing frequency offset, inter-element spacing and array number have been investigated in [99] using the finite difference time domain (FDTD) method.

The range-angle dependent FDA beam pattern allows the radar system to illuminate a desired spatial sector, while suppressing the range-dependent clutter and

interferences [91]; thus resulting in improved SINR. On the other hand, this range angle coupling may degrade the range and angle estimation performance of an FDA, therefore, in [100] a range-angle coupled beam pattern for improved performance has been explored with frequency diverse chirp signals. Likewise an FDA structure for bi-static radars has been introduced in [101], [102] for improved estimation performance . Furthermore, an FDA design with transmit sub-apertures has been proposed in [103] for improved range angle estimation of targets. Some useful investigations about application of frequency offset across an FDA have been made in for improved range- angle localization performance [104], [105].

An FDA design for forward looking ground moving target indication (GMTI) benefits has been analyzed in [106], while multipath characteristics of FDA over a ground plane have been examined in [107]. The usage of a linear frequency modulated continuous waveform (LFMCW) for FDA and its mathematical design have been proposed in [108]. Different frequency diverse array receiver structures have been proposed in [109] , while planer FDA receiver architectures have been proposed in [110]. The FDA concept has also been applied towards synthetic aperture radar (SAR) systems for achieving high resolution imaging of targets [111],[112]. Furthermore, two patents [113], [114] have been issued vitalizing the range-dependent characteristics of an FDA.

2.3.2. Disadvantages of FDA

Frequency diverse array (FDA) radar with uniform inter-element frequency offset generates a range-angle dependent beam pattern, which exhibits maxima at multiple range and angle values [76]. It also causes broadening of half power beam width

(HPBW). Certainly, this multiple maxima property and broadening of the main beam are undesirable due to the facts that it allows the interferers located at any of the maxima to affect the target- returns. Moreover, it decreases the maximum reachable range and does not facilitate to distinguish between targets that are very close in range. It is also unable to localize the targets and interferences having same direction but different ranges. Therefore, it results in weak signal to interference noise ratio (SINR), which degrades the probability of detection and parameter estimation performance.

Therefore, researchers are finding different methods to mitigate these disadvantages. Consequently, in [82], an FDA with non-uniform frequency offsets has been proposed and hence simulations are carried out to indicate the modified shape of beam pattern in terms of null depths and placements. Likewise, the inter-element spacing of FDA, proportional to the wavelength was investigated in [105] for improved localization performance. Uniform linear array with logarithmically increasing inter- element frequency offset has been presented in [115], which generates a single-maximum beam pattern for an arbitrary value of frequency offset and also suppresses interferences.

Since, the current radar designs are often confined to adaptive receivers, they are unable to sense the environment through transmitters. Therefore, researchers' pursuit to develop an intelligent radar system, adaptive in both the receiver and the transmitter, paved a way for an intelligent radar system known as cognitive radar (CR).

2.4. Cognitive Radar (CR)

The research towards an intelligent radar, which can adapt itself to the statistical changes of environment and unknown time varying scenarios, has been one of the dynamic research areas since last decade [116]. To address this issue, modern radar

design technologies have been dominated not only by signal processing and control techniques alone, but also with the hybridization of both to meet numerous milestones [117]. These advancements in the field of radar design have addressed diverse radar problems, such as range estimation, radar cross section (RCS) measurement, speed estimation, and direction estimation [118],[119] etc., quite effectively to enhance the radar detection and tracking performance. But there is always room for optimum solutions of these problems.

For the first time, an adaptive waveform transmission [120], [121] was considered by Delong and Hofstetter, where they studied adjustable pulse amplitude and phases with limited dynamic range to suppress clutter. Similarly, information theory was considered for radar waveform designs for the first time by Bell, where he assumed a random extended target to generate a desired waveform [122].

Since a radar can be used for detection and tracking, an optimal design of waveforms is task dependent because for a detection task; a waveform should put maximum energy in the largest mode of target to get better SNR. On the other hand, for estimation and filtering task; a waveform should allocate energy towards different modes of target to enhance mutual information between target signature and received signal [123]. A radar with an optimal waveform design, which can give more information about a target rather than just detecting it, is far better than that of a simple radar. Likewise, an intelligent dynamic system like a human brain that can have the properties of problem solving, decision making, memory, learning and perception etc., may outperform all the conventional system. Therefore, the idea of *cognitive radar* was firstly coined by Simon Haykin in [124].

In [124], the emphasis is made on the four essential points of cognitive radar i.e., Bayesian filtering in the receiver, dynamic programming at the transmitter, memory and global feedback, which acts a facilitator of intelligence. A basic cognitive radar should have following properties [124]:

i) It should be continuously sensing its environment and should be intelligent enough to utilize the extracted information effectively.

ii) It should be embedded with a feedback to facilitate computational intelligence for radar systems.

iii) It should be able to preserve information in an implicit way to enhance the overall performance of radar system i.e., extracted information that enhances the receiver's performance directly and the transmitter's performance indirectly.

Fig-2.6 shows the difference between a basic cognitive and a monostatic radar structures [125], [126]. These structures show that a radar interfaces the environment, having potential targets, while the transmitter is connected with receiver through a feedback link in a cognitive structure, which is missing in a monostatic radar structure.

The basic cognitive cycle of this structure begins with the transmitter illuminating the radar environment. Echoes contain the information about the targets/interceptors in the space.

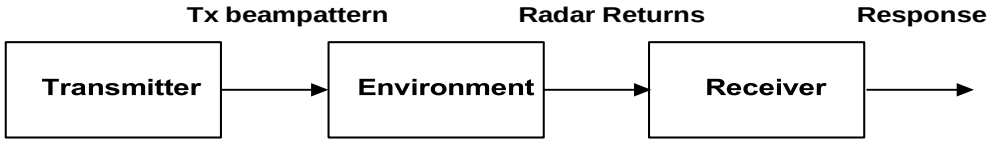

(a)

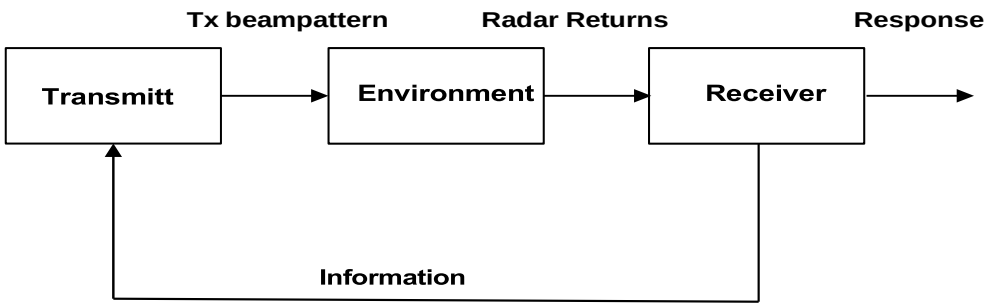

(b)

Figure-2. 6: a) Block diagram of monostatic radar (b) Block diagram of a cognitive radar

The receiver senses the radar environment by continuously interacting with it to get the necessary information regarding targets/interceptors. This information is sent as a feedback from the receiver to the transmitter. The transmitter of cognitive radar contains the intelligent signal processing block which allows to change its properties for transmitting an appropriate beam pattern in accordance with the statistical variations in the environment. This cycle is known as *perception- action cycle* and keeps on repeating itself for improved performance [126]–[129].

To utilize the benefits of a feedback, a cognitive tracking radar was proposed for the first time in [130], where the cubature Kalman filter (CKF) was used for estimation in the receiver instead of Bayesian filtering, while dynamic programming was used for waveform selection in the transmitter and global feedback embodied transmitter, receiver and the radar environment.

For surveillance applications, the situational awareness is of great interest. A radar is connected with its surrounding environments through an electromagnetic link to sense it. It strongly depends upon the echoes form one scan to the next for identifying targets on unknown locations in the surveillance region [131], [132].

Usage of a recursive state- space model is essential to represent estimates of certain varying parameters of the non-stationary radar environment. Since, the current radar designs are often confined to adaptive receivers [133], they are unable to sense the environment through transmitters. In concrete terms, a feedback [134]–[136] that connects the receiver to the transmitter is very essential for improved radar performance. A cognitive FDA radar with situational awareness has been proposed in [137], where frequency offset is selected based on the receiver feedback [134]–[136] to improve the received SINR and direction of arrival (DOA) estimation performance.

A radar should have an ability to perform intelligent signal processing at both the transmitter and receiver based on the preserved or acquired knowledge of the environment in real time [138]. Moreover, it should learn from its experience to tackle different types of targets in diverse environments [127]. A CR continues to learn from the environment and keeps on updating its statistical variations on-the-fly [124], [126], [127].

Cognitive radar utilizing adaptive waveforms and machine learning techniques has been considered in [139],[140] where it was used to achieve improved performance for sensor scheduling, scene analysis and target recognition. In [141] , a cognitive radar system has been proposed that can exploit and mitigate various interference sources. A cognitive radar network for extended target recognition was proposed in [142], likewise scheduling and power allocation for multiple target tracking using a cognitive radar network has been proposed in [140].

A cognitive single-tone waveform design for target recognition in cognitive radar has been proposed in [143], while optimal waveform design for improved performance in cognitive MIMO radars was presented in [144]. Diverse waveform designs for a

cognitive radar in the presence of signal dependent interferences and clutters have been investigated in[145], [146]. Moreover, to sense a radar environment and exploit the useful information for improved detection performance, a passive coherent location as cognitive radar has been proposed in [147], [148]. An investigation has been made in [149] for a cognitive beamforming considering multiple secondary data stream having constraints on individual SNR of each secondary data stream.

Additionally, various cognitive radars working in parallel, improve the overall system performance as compared to a single cognitive radar and it has been investigated in [150], [151]. Extensive investigation on cognitive radar networks and its application has been made in [152].

2.5. Biologically and nature inspired evolutionary computing based algorithms

The biologically and nature-inspired techniques, i.e., genetic algorithm (GA) [153] , particle swarm optimization (PSO) [154], differential evolution (DE) [155] , Neural networks (NN) [156]–[159] etc., offer near optimum solutions with affordable computational costs [160]. The heuristic techniques have a vital advantage of avoiding the local minima along with the best performance in low SNR scenarios [161]. With these tools, diverse engineering problems have been addressed effectively [162]. Researchers have also been applying these techniques in the fields of radars [163]–[165].

Genetic algorithm, one of the most useful biologically inspired techniques, was developed by Holland [166], where he presented an easy solution to natural selection. A GA based nature-inspired technique has been exploited in [153] to optimize the search

problems that are computationally complex to solve. In [167], some new methods are proposed for achieving interaction of mutation rate, selection and self-adaptation for GA.

GA presents an iterative method to reach the optimum solution, which starts with a fixed number of random possible solutions called population. Population contains a number of individual solutions that represent the length of a chromosome. Each randomly generated chromosome contains a specific number of genes [168]. After a population is generated, the best solution is chosen based on selection operator during each generation. This process creates a set of chromosomes known as parents. These parent chromosomes contribute to find the best solution using the process of crossover, mutation, and elitism etc. The outcome is a new set of chromosomes, which are known as the offspring. This process keeps on searching the best chromosome until the termination criterion is met[161], [162]. The pseudo steps for GA are given below [162], [164].

Algorithm. 2.1: Genetic Algorithm

Step 1: Generate a random chromosome set ensuring an appropriate upper and lower bounds. Also define No. of generations, fitness limit, crossover fraction, elite count, number of cycles etc.

Step 2: Calculate a fitness values for each chromosome and sort results by keeping the highest fitness value on top and lowest on the bottom. .

Step 3: Terminate the GA, if best available fitness value is achieved or the maximum number of cycles is reached.

Else go to step 4

Step 4: Select the parents based on their best chances to survive in the next generation.

Step 5: To improve the fitness, reproduce a new generation using crossover and mutation functions.

Crossovers: This process exchanges the information among the chromosomes to find different ways to create offspring.

Mutation: This process randomly changes the gene in a chromosome when the fitness function does not improve for a long time.

Step 6: Select the offspring to generate a new generation of chromosomes using elitism or generation replacement etc., methods.

The pattern search (PS) algorithm is used as a local optimizer to optimize the performance of a system. Hooke and Jeeves developed this algorithm for the first time in [169] , which was used to find the solutions of numerical and statistical problems. The PS attempts to find a sequence of points in each step, known as mesh, around the previous step to reach optimal results [170]. Although, PS solution search performance is not as good as a GA or other evolutionary algorithms, but its hybridization with these global optimizers can facilitate to reach more accurate results [171].

We have chosen GA in this dissertation for estimating directions of arrival (DoA) of sources' signals impinging on an array [172], [173] due to its ability of autonomous learning and satisfactory performance in low SNR scenarios. Additionally, an appropriate fitness function selection has always been an open area of discussion. Mostly in radar applications, mean square error (MSE) between the desired and estimated DoAs is taken as a fitness function [172], [173].

2.6. Conclusion

In this chapter, an overview of PAR, FDA radar and Cognitive radar has been mentioned, which are directly linked to the work presented in this dissertation. Although, all these radars have their own advantages, yet hybridization of these modern technologies can indeed build a new generation of radar that can outperform the existing radar systems.

For example, a cognitive radar may be hybridized with a LPI based phased array radar. Similarly, an FDA radar is novel radar technology, which may be hybridized with CR properties for improved detection and tracking performance.

CHAPTER-3

Hybrid Cognitive Phased Array Radar (HCPAR)

In this chapter, an idea of a hybrid cognitive phased array radar design is presented, which uses cognitive radar (CR) properties hybridized with phased array radar (PAR). This new design improved the overall radar performance. The chapter starts with a brief introduction of CR and PAR followed by the hybrid cognitive phased array radar (HCPAR) design. Afterwards, each block of the proposed HCPAR design is discussed in detail. Moreover, an LPI transmit beamforming technique is also presented for the given HCPAR system, which protects the transmitter from being detected by interceptors. At the end of the chapter the simulation results are provided, which show improved detection, SINR and target tracking performance of the proposed design. The results are compared to the conventional phased array radar.

3.1. Introduction

The echo-location system of a bat is the motivation of an important concept of linking the receiver to transmitter [124] . A bat acquires information about the target of interest e.g., range, relative velocity, size, azimuth and elevation angles etc., within a nominal time and consequently, makes changes in its transmit signal. It is proficient enough to utilize previous knowledge (i.e., memory) about the surrounding environment, as well as, to learn through continuous interactions with the environment [127].

Accordingly, a cognitive radar (CR) has three essential elements, which include feedback, memory and signal processing in the receiver and transmitter [125]. A feedback link embodying the transmitter, radar environment and receiver acts as a tunnel for information delivery and acts as a facilitator of intelligence [124]. These three essential properties of CR are combined with high gain and interference suppression properties of PAR for improved target tracking, detection and SINR performance.

The receiver of the proposed design estimates the directions of arrival (DOA) of target and interferences using genetic algorithm (GA). It also calculates ranges of the target and interferences using conventional range calculation formula. An appropriate number of array elements has been selected for the phased array antenna block to generate nulls in accordance with the sensed number of interferences. Moreover, the well-known minimum variance distortion-less response (MVDR) beam-former is used to generate distortion-less response towards the estimated target direction and minimum variance towards the interference directions for improved SINR.

Consequently, the target position, i.e., the direction along with target range value are supplied to an extended Kalman filter (EKF) predictor block, which estimates the target next position. This predicted estimation position is sent to the transmitter as a feedback. An appropriate number of active elements of the transmitter array has been chosen on the basis of the predicted range value. A conventional beam-former computes a transmitter weight vector to direct a beam towards the target predicted direction at each scan.

Moreover, most of the targets/interceptors are equipped with modern warfare technologies, in the recent era, to detect the direction of transmitter from which they are receiving bursts of energy. Therefore, due to the high gain generated by PAR towards the

target position, it is very likely to be detected by an interceptor, which may affect the PAR performance. Since, the aim is "to see but not to be seen", we have proposed an evolutionary computing based low probability of intercept (LPI) beamforming technique for this transmitter without affecting the overall system performance.

3.2. Proposed HCPAR System Design

The block diagram of the proposed design is discussed in this section. Fig-3.1 demonstrates the working principle of the proposed hybrid cognitive phased array radar (HCPAR) at time k.

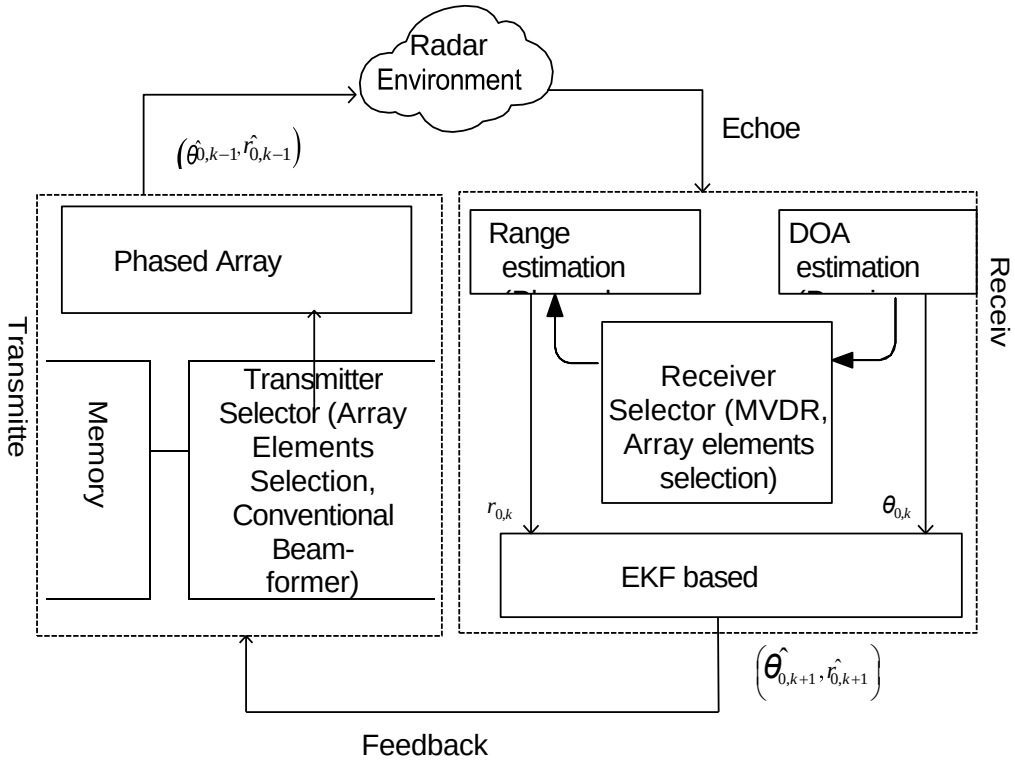

Figure-3. 1: Block diagram of the proposed HCPAR radar

As seen in Fig. 3.1, the transmitter contains three sub-blocks that are phased array antenna, transmitter selector and memory. Similarly, the receiver contains four sub- blocks that are DOA estimation block, range estimation block, predictor block and a receiver selector. The feedback link tunnels the target predicted position from the receiver to transmitter. The phased array antenna block, illuminates the surrounding environment at time $(k-1)$. The radar-returns are received by two receiver sub-blocks; the DoA estimation and range estimation blocks. In DoA estimation, GA is used to compute the directions of target $(\theta_{0,k})$ and interferences $(\theta_{1:p,k})$, where p is the number of interferences.

The receiver selector selects an appropriate number of receiver array elements (M), while the minimum variance distortion less response (MVDR) adaptive beam former calculates the weight vector $(\mathbf{w}_R)$ for the selected array elements. This weight vector is used to place nulls in the estimated interferences directions to improve SINR. In parallel, the range estimation block computes the target range $(r_{0,k})$ using the conventional range estimation formula. Consequently, the computed target position estimates i.e., $(\theta_{0,k}, r_{0,k})$ at k^{th} time instant, are sent to the predictor to get the estimate of the next position $(\hat{\theta}_{0,k+1}, \hat{r}_{0,k+1})$. An extended Kalman filter [50] is used to predict the future position of target, which is delivered as feedback.

The transmitter selector examines the target predicted range $(\hat{r}_{0,k+1})$ and decides an appropriate number of elements (N) of the transmit phased array using a predefined lookup table kept in the memory. It also updates the conventional beam former weights

$(\mathbf{w}_T)$ to direct the maximum power towards the target predicted direction. This perception-action cycle keeps on repeating itself for improved performance. Each block of the proposed system design has been discussed in detail.

3.2.1. Receiver

The receiver in the proposed design consists of four sub-blocks detailed as below.

3.2.1.1. DOA estimation

The DOAs of targets are estimated using GA [162], [172], [173]. The MSE between the actual and estimated DoAs of the signals impinging on receiver array defines the fitness function. Several sources (F) signals are impinging on a passive array from different directions.

Fig-3.2 shows a uniform linear receiving array having M elements with inter-element distance d. The output of m^{th} element o_m, provided $F \le M$, is given as [173]

$$o_m = \sum_{l=1}^{F} A_l e^{(-jkd(m-1)\sin(\theta_l))} + n_m \;; m = 1, 2, \ldots, M \tag{3.1}$$

here n_m is additive white Gaussian noise added for m^{th} element and A_l is an amplitude of l^{th} far field source.

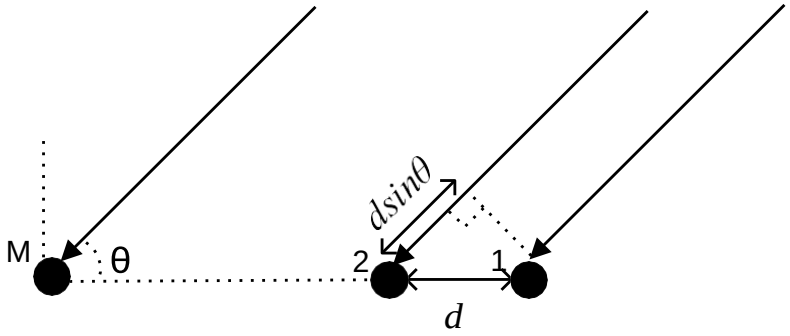

Figure-3. 2: A linear receiver array having M elements for HCPAR design

The MSE between desired and estimated response is computed using the following fitness function.

$$MSE_m = \frac{1}{M}\sum_{m=1}^{M} \left| o_m - \hat{o}_m \right|^2; \quad m = 1, 2, \ldots, M \tag{3.2}$$

The desired response is given by equation (3.1), while estimated response is given as:

$$\hat{o}_m = \sum_{l=1}^{s} e^{(-jkd(m-1)\sin(\theta_{l+1}))} \tag{3.3}$$

The basic steps of a GA based estimation are given in the introduction of the dissertation.

3.2.1.2. Range Estimation block

This block computes the range of a far field target by measuring the time delay (T_d) between the peaks of the transmitted and received signals given as [174]

$$r_0 = \frac{c}{2} T_d \tag{3.4}$$

where r_0 is the target range and c is the velocity of light.

3.2.1.3. Receiver Selector

This block decides the number of array elements (M) for the receiving phased array. The decision is based on the required number of nulls to be placed in the direction of interferences. The number of array elements must be greater than the number of interferences [31].

3.2.1.4. EKF based predictor

Kalman filter (KF) provides a recursive solution to the linear filtering problem of stationary, as well as, non-stationary linear dynamical systems [47]. However, KF cannot be applied to nonlinear systems. Therefore, some variants of KF such as extended Kalman filter (EKF) [48] and unscented Kalman filter (UKF) [49] have been presented in literature to solve this problem. We have used EKF based predictor for the proposed system. All these algorithms necessitate the knowledge of transition and measurement functions [48]–[50]. Therefore, with a known transition matrix and learned measurement function, the position of target is estimated for the next step. For an extended Kalman filter, the process equation of a nonlinear dynamical model is given as [48]

$$\mathbf{x}_{k+1} = \tilde{\mathbf{F}}\mathbf{x}_k + \mathbf{n}_k \tag{3.5}$$

where $\mathbf{x}_k$ represents the system state at time k, $\tilde{\mathbf{F}}$ is a non-linear transition matrix; $\boldsymbol{n}_k$ is a zero mean Gaussian process noise with covariance matrix $\mathbf{Q}$ as

$$\boldsymbol{E}\left[\mathbf{n}_k \mathbf{n}_l^T\right] = \begin{cases} \boldsymbol{Q}_k & for\ k = l \\ 0 & for\ k \neq l \end{cases} \tag{3.6}$$

where superscript T denotes transpose of a vector. The measurement equation is given as

$$\mathbf{z}_k = \tilde{\mathbf{H}}\mathbf{x}_k + \mathbf{v}_k \tag{3.7}$$

where $\tilde{\mathbf{H}}$ is a nonlinear measurement matrix, $\mathbf{z}_k$ denotes an observation vector at time k and $\mathbf{v}_k$ is zero mean Gaussian measurement noise with covariance matrix $\mathbf{R}$ given as

$$E\left[\mathbf{v}_k \mathbf{v}_l^T\right] = \begin{cases} \mathbf{R}_k & for\ k = l \\ 0 & for\ k \neq l \end{cases} \tag{3.8}$$

Moreover, the process noise $\mathbf{n}_k$ is uncorrelated with the measurement noise $\mathbf{v}_k$.

In an EKF algorithm, first order Taylor series approximation has been used to linearize $\tilde{\mathbf{F}}$ and $\tilde{\mathbf{H}}$ functions, then a standard Kalman filter is applied for estimation and filtering [48], [50]. The approximation of $\tilde{\mathbf{H}}$ is as follows

$$H_k(\mathbf{x}_k) = H_k(\hat{\mathbf{x}}_{k-1}) + \frac{\partial H_k}{\partial \hat{\mathbf{x}}_{k-1}}(\mathbf{x}_k - \hat{\mathbf{x}}_{k-1}) \tag{3.9}$$

The updated state $\mathbf{x}_k$ is estimated as the linear combination of previous states and a new measurement $\mathbf{z}_k$. Therefore, the conditional mean and covariance is given as [50]

$$\hat{\mathbf{x}}_{k/k} = E\left[\mathbf{x}_k \mid \mathbf{z}_1^k\right] \tag{3.10}$$

$$\hat{\mathbf{x}}_{k+1/k} = E\left[\mathbf{x}_{k+1} \mid \mathbf{z}_1^k\right] \tag{3.11}$$

The filtered $\hat{\mathbf{P}}_{k/k}$ and predicted covariance $\hat{\mathbf{P}}_{k+1/k}$ matrices are given as [50]

$$\hat{\mathbf{P}}_{k/k} = E\left[(\mathbf{x}_k - \hat{\mathbf{x}}_{k/k})(\mathbf{x}_k - \hat{\mathbf{x}}_{k/k})^T \mid \mathbf{z}_1^k\right] \tag{3.12}$$

$$\hat{\mathbf{P}}_{k+1/k} = E\left[(\mathbf{x}_{k+1} - \hat{\mathbf{x}}_{k+1/k})(\mathbf{x}_{k+1} - \hat{\mathbf{x}}_{k+1/k})^T \mid \mathbf{z}_1^k\right] \tag{3.13}$$

The prediction error is defined as

$$\mathbf{x}_{k+1/k} = \mathbf{x}_{k+1} - \hat{\mathbf{x}}_{k+1/k} \tag{3.14}$$

where $\hat{\mathbf{x}}_{k+1/k} = \tilde{\mathbf{F}}\hat{\mathbf{x}}_{k/k}$ and $\tilde{\mathbf{F}}$ is known. In the same way, we define the prediction measurement error vector as

$$\mathbf{z}_{k+1/k} = \mathbf{z}_{k+1} - \hat{\mathbf{z}}_{k+1/k} \tag{3.15}$$

where $\hat{\mathbf{z}}_{k+1/k} = \tilde{\mathbf{H}}_{k+1}\hat{\mathbf{x}}_{k+1/k}$

These errors are meant to be minimized to improve the overall performance of the system. In this case, the target direction and range has been predicted using this EKF block. The predicted target position $\left(\hat{\theta}_0, \hat{r_0}\right)$ is sent as feedback to the transmitter.

3.2.2. Transmitter

For the given HCPAR design, we have proposed two different types of transmitter blocks. One has a transmitter antenna with high power gain, while second type of transmitter antenna block has low probability of intercept (LPI) beamforming property. Both of the transmitter blocks have been discussed below in detail.

3.2.2.1. Transmitter with high power gain

The transmitter selector, a sub-block of the transmitter, selects an appropriate number of elements *N* for the transmit array. The decision is based on the target predicted range $\hat{r_0}$ and direction $\hat{\theta_0}$ received as feedback. This feedback is like a one bit feedback

used in [134]–[136]. The memory, residing in transmitter, maintains a predetermined lookup table of the number of elements vs. range values. A basic feed forward neural network (NN) [158] is selected for implementation of memory as shown in Fig-3.3.

In a feed forward NN, the information moves in a forward direction only, i.e., from input nodes, through any available hidden nodes and then to the output node. There are further two types of NN based on the hidden layers, i.e., single layer perceptron (SLP) and multi-layer perceptron (MLP) [156]. For the precision of the output, the MLP with 5

hidden layers is used to implement memory in this case, while the back propagation algorithm has been applied for offline training [157], [159]. The chosen neural network takes the predicted range $\hat{r_0}$ as single value input and gives out the corresponding appropriate number of elements (N).

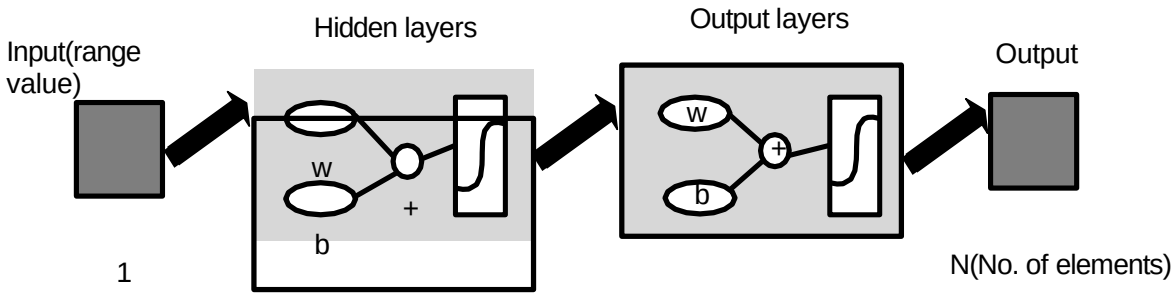

Figure-3. 3: Neural Network block diagram (Memory)

As each antenna element is connected with a weight, therefore, the weight vector is $\mathbf{w}_T = [w_0, w_1, ..., w_{N-1}]$. Hence, the steering vector $\mathbf{a}(\theta)$ for this antenna array is given as

$$\mathbf{a}(\theta) = [1 \; e^{jvd(\sin\theta - \sin\hat{\theta}_0)} \; e^{j2vd(\sin\theta - \sin\hat{\theta}_0)} \cdots e^{j(N-1)vd(\sin\theta - \sin\hat{\theta}_0)}]^T \tag{3.16}$$

here $v = 2\pi/\lambda$ is the wave number, λ is the wavelength, θ is the target direction and d is inter-element distance.

The phased array antenna structure is given in Fig. 3.4, where the transmit weight vector $\mathbf{w}_T$ is computed using a conventional beamformer for this antenna [33]

$$\mathbf{w}_T = \frac{\mathbf{a}(\hat{\theta}_0)}{\|\mathbf{a}(\hat{\theta}_0)\|} \tag{3.17}$$

Using these weights, the phased array antenna steers the maximum power towards the target predicted direction $\hat{\theta}_0$, received as feedback. The beam pattern is given as

$$P_{PAR}\left(\hat{\theta}_0, k\right) = \left| \left[\mathbf{w}_T^H \mathbf{a}\left(\hat{\theta}_0\right) \right] \times s(k) \right|^2 \tag{3.18}$$

where $s(k)$ is the transmitted waveform at any time k.

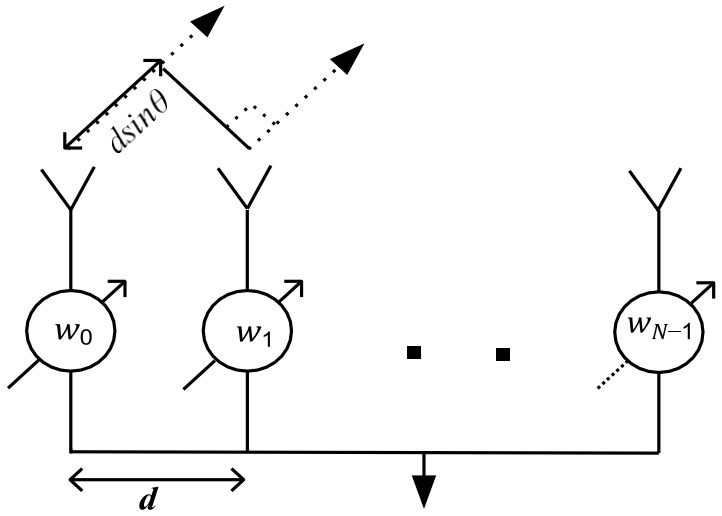

Figure-3. 4: Uniform linear transmit array with N elements for HCPAR design

3.2.2.2. Transmitter having LPI beamforming property

The second type of proposed transmitter design is based on LPI beamforming property. Once the target predicted position i.e., predicted DOA and range of target is received as feedback, the transmitter of the proposed design generates a beam pattern having low probability of intercept property without affecting the system performance.

One of the methods presented in recent past for achieving LPI beamforming is presented in [62]. In this method, high-gain scanned beam patterns have been spoiled into a series of low-gain basis patterns. This has been achieved by applying an additional phase shift across the array elements. Afterwards, complex weight vector has been computed to coherently combine these spoiled beam patterns to generate a high gain pattern in desired direction. Since the total incident energy on the target remains same,

the detection performance of radar is not affected. The spoiled patterns with reduced peak power in any direction ensure the reduced probability of being detected. Using the approach of [62], we have proposed a transmitter with GA based LPI beamforming property. Fig-3.5 shows the block diagram of HCPAR having LPI beamforming property.

The receiver is same as of HCPAR with a high gain but the transmitter side contains four different sub-blocks. The phased array antenna, memory, set of phase shifts to spoil beam and transmitter selector blocks. The phased array antenna in the transmitter block, with a predetermined extra phase shifter value for each element, has been designed to get spoiled/low gain basis pattern to ensure the LPI property. In order to maintain its detection performance, a suitable set of complex weights is needed to linearly combine these spoiled pattern to synthesized high gain beam pattern towards the desired direction.

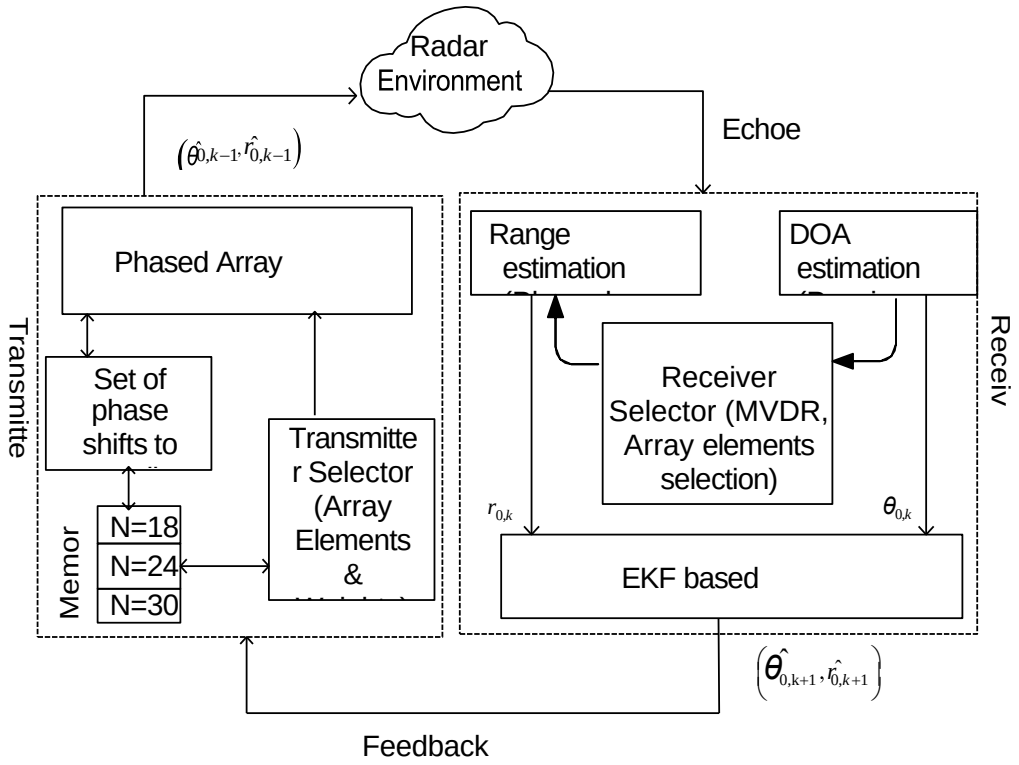

Figure-3. 5: Block diagram of a HCPAR with LPI beamforming

Unlike the method used in [62], we have used GA based evolutionary computing block to calculate these complex weights with a vital advantage of avoiding the inversion of a matrix. Here, these offline GA based calculated weights for three different number of array elements are kept in the corresponding memory block of the transmitter. The memory block consists of a feed forward neural network (NN) with a back propagation algorithm for training [158], [159].

Since a maximum value of gain towards a desired direction equals the array antenna elements [31], the higher target range requires more number of transmit array elements to achieve improved detection performance. Consequently, the selector block of transmitter examines the predicted range to select a suitable number of array elements using a predetermined look up table. It also interacts with the memory block to set corresponding phase shifts to spoil beam. Moreover, it gets an appropriate weight vector from memory to synthesize a high gain beam pattern towards the desired direction using these low gains basis patterns.

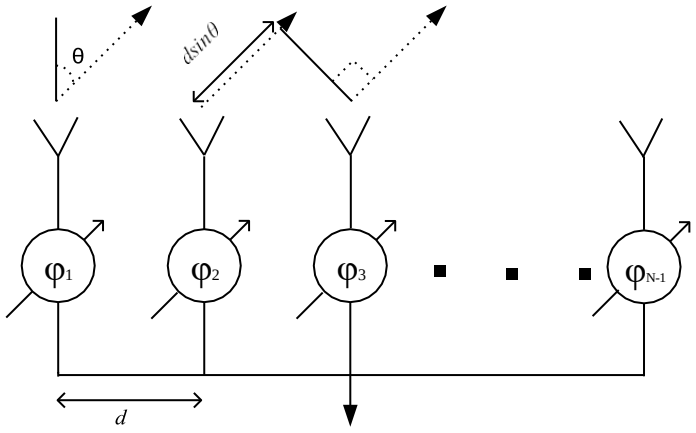

Figure-3. 6: N-element phased array antenna. φ_n represents the phase shift values for spoiling beam

The fitness function for this GA algorithm is mean square error between the desired and synthesized beam pattern using these complex weights. The proposed algorithm is simulated for environment containing Additive White Gaussian Noise (AWGN). A uniform linear array (ULA) with LPI property having inter-element distance d is shown in Fig-3.6

We start with the output of a ULA, given as

$$h(\psi_0) = 1 + e^{j\psi_0} + e^{j2\psi_0} + ... + e^{j(N-1)\psi_0} \tag{3.19}$$

(3.19) may be written as

$$h(\psi_0) = \sum_{n=0}^{N-1} e^{jn\psi_0} \tag{3.20}$$

where $\psi_0 = vd\left(\sin\theta - \sin\hat{\theta}_0\right)$ and $v = 2\pi/\lambda$ is the wave number. This pattern generates a high-gain towards the predicted target direction $\hat{\theta}_0$. The high gain beam pattern scans the surveillance region using a linearly applied progressive phase shift across the array.

The fundamental scan phase shift can be defined as $\gamma = 2\pi/N$, where N is the number of transmitter array elements. Therefore, we can define $\psi_b = \psi_0 + b\gamma$; $b = 0,1,...,(N-1)$. The remaining set of $N-1$ scanned pattern except the fundamental pattern throughout the surveillance region can be obtained as

$$h(\psi_b) = \sum_{n=0}^{N-1} e^{jn\psi_b}; b = 1,2,...,(N-1) \tag{3.21}$$

To achieve a LPI property, the high gain scanned beam pattern have been spoiled in a specific manner to reduce their peak power in any specific direction significantly. In [62], quadratic phase variance technique has been presented to compute a set of phase shifts (φ_n

) for defocusing the high gain beam patterns. The corresponding phase shift values

from the set φ_n are applied to each element of array antenna respectively as shown in Fig.3.6. These N spoiled or basis patterns $l(\Psi_b)$; $b = 0,1,...,(N-1)$ can be expressed as:

$$\begin{aligned} l(\psi_0) &= 1 + e^{j\varphi_1} e^{j\psi_0} + e^{j\varphi_2} e^{j2\psi_0} + ... + e^{j\varphi_{N-1}} e^{j(N-1)\psi_0} \\ l(\psi_1) &= 1 + e^{j\varphi_1} e^{j\psi_1} + e^{j\varphi_2} e^{j2\psi_1} + ... + e^{j\varphi_{N-1}} e^{j(N-1)\psi_1} \\ &\vdots \\ l(\psi_{N-1}) &= 1 + e^{j\varphi_1} e^{j\psi_{N-1}} + e^{j\varphi_2} e^{j2\psi_{N-1}} + ... + e^{j\varphi_{N-1}} e^{j(N-1)\psi_{N-1}} \end{aligned} \tag{3.22}$$

These scanned patterns are assumed to be linearly independent. It is a requirement to synthesize a high gain beam pattern using the linear combination of these spoiled beam patterns $l(\Psi_b)$, such that $\hat{h}(\psi_b)$ is the closest to $h(\psi_b)$ in the mean square error sense.

This can be written as

$$\begin{bmatrix} \hat{h}(\psi_0) \\ \hat{h}(\psi_1) \\ \vdots \\ \hat{h}(\psi_{N-1}) \end{bmatrix} = \begin{bmatrix} w_{0,0} & w_{0,1} & \cdots & w_{0,N-1} \\ w_{1,0} & w_{1,1} & \cdots & w_{1,N-1} \\ \vdots & \vdots & \ddots & \vdots \\ w_{N-1,0} & w_{N-1,0} & \cdots & w_{N-1,N-1} \end{bmatrix} \begin{bmatrix} l(\psi_0) \\ l(\psi_1) \\ \vdots \\ l(\psi_{N-1}) \end{bmatrix} \tag{3.23}$$

The vector forms of $l(\psi_b)$ $\hat{h}(\psi_b)$ and complex weight matrix are given as $\mathbf{l}_{N\times 1}$, $\hat{\mathbf{h}}_{N\times 1}$, and $\mathbf{W}_{N\times N}$ respectively. We can rewrite (3.23) as

$$\hat{\mathbf{h}} = \mathbf{W}\mathbf{l} \tag{3.24}$$

In this section, a GA hybridized with pattern search (PS) is used to derive these complex weights in the presence of AWGN noise. The general steps to implement a GA algorithm

are given in [162], while the fitness function for the proposed system is given as

$$MSE = \sum_{i=1}^{N} \left| h_b(i) - \hat{h}_b(i) \right|^2 ; \; b = 0,1,2,\ldots,(N-1) \tag{3.25}$$

where h_b denotes b^{th} element of the vector $\mathbf{h}$ and $\hat{h}_b = \sum_{i=0}^{N-1} \hat{\mathbf{W}}_{b,i} \; l(\psi_i)$

This procedure for computing MSE is repeated for all rows of this weight matrix. The GA is hybridized with pattern search (PS) for improved beam synthesis performance in an AWGN scenario.

3.3. SINR and Detection Analysis

The equivalent of signals received at the array can be given as [32]

$$y(k) = \rho_0 \mathbf{b}(\theta_0) s(k) + \sum_{i=1}^{P} \rho_i \mathbf{b}(\theta_i) s(k) + n(k) \tag{3.26}$$

where, $\rho_0 = \mathbf{w}_T^H \mathbf{a}(\theta_0)$, $\rho_i = \mathbf{w}_T^H \mathbf{a}(\theta_i)$ are directional gains for the target and interferences, $\mathbf{a}(\theta_0)$ is the transmit steering vector , $\mathbf{b}(\theta_0)$ is the receive steering vector, which can be of different length at each cycle. $s(k)$ is the transmitted waveform at any time k ,while $n(t)$ is zero mean additive white Gaussian noise with variance σ_n^2.

We define the virtual steering vector $\mathbf{u}_0(\theta_0) = \rho_0 \mathbf{b}(\theta_0)$ and $\mathbf{u}_i(\theta_i) = \rho_i \mathbf{b}(\theta_i)$, therefore, the array output after match filtering in vector form is given as

$$\mathbf{y} = \mathbf{u}_0(\theta_0) + \sum_i \mathbf{u}_i(\theta_i) + \mathbf{n} \tag{3.27}$$

The MVDR beam former has been used to calculate weight vector $\mathbf{w}_R$ that gives distortion less response in the target direction and maximizes SINR. The MVDR

optimization problem is stated as [32], [117]

$$\min_{\mathbf{w}_R} \mathbf{w}_R^H \mathbf{R}_{i+n} \mathbf{w}_R \tag{3.28}$$

where $\mathbf{R}_{i+n}$ is the interference plus noise covariance matrix. The solution of (3.28) is given in [30], [31] as

$$\mathbf{w}_R = \frac{\mathbf{R}_{i+n}^{-1} \mathbf{u}_0(\theta_0)}{\mathbf{u}_0(\theta_0) \mathbf{R}_{i+n}^{-1} \mathbf{u}_0(\theta_0)} \tag{3.29}$$

These are the receiver array weights, which generate distortion-less response in the target direction while minimizing the interferences. The signal to interference and noise ratio (SINR) has been evaluated as [31]

$$SINR = \frac{\left| \mathbf{w}_R \mathbf{u}_0(\theta_0) \right|^2}{\mathbf{w}_R^H \mathbf{R}_{i+n}^{-1}(\theta) \mathbf{w}_R} \tag{3.30}$$

The signal at the array after the suppression of interference is given by

$$\mathbf{y} = \mathbf{u}_0(\theta_0) + \mathbf{n} \tag{3.31}$$

where $\mathbf{u}_0(\theta_0)$ is the desired target signal and $\mathbf{n}$ is the additive white Gaussian noise.

The radar detection problem is modeled as

$$\begin{cases} H_0 : \mathbf{y} = \mathbf{n} \\ H_1 : \mathbf{y} = \mathbf{u}_0(\theta_0) + \mathbf{n} \end{cases} \tag{3.32}$$

where it is assumed that the noise process is independent and identically distributed (i.i.d) Gaussian random noise wih zero mean and σ_n^2 covariance.

The probability density function (PDF) for H_0 is given by [32]

$$p(\mathbf{y}; H_0) = \exp\left(-\frac{\|\mathbf{y}\|^2}{\sigma_n^2} \right) \tag{3.33}$$

Likewise, the PDF for H_1 is given by [32]

$$p(\mathbf{y};H_1)=\exp\left(-\frac{\|\mathbf{y}\|^2}{\sigma_n^2}\right)\times\exp\left(-\frac{\|\mathbf{u}_0(\theta_0)+\mathbf{n}\|^2}{2\sigma_n^2}\right) \tag{3.34}$$

The likelihood ratio test is given as

$$\wedge=\frac{p(\mathbf{y};H_1)}{p(\mathbf{y};H_0)}\underset{H_0}{\overset{H_1}{\gtrless}}\delta \tag{3.35}$$

where, δ is the threshold for detection.

Therefore, the probability of detection and probability of false alarm is given as

$$p_d=p(\wedge>\delta\mid H_1)=1-F_{\chi^2_{(2)}}\left(\frac{\sigma_n^2F_{\chi^2}^{-1}(1-p_{fa})}{M^2N^2+\sigma_n^2}\right) \tag{3.36}$$

$$p_{fa}=p(\wedge>\delta\mid H_0)=1-F_{\chi^2_{(2)}}\left(\frac{2\delta}{\sigma_n^2}\right) \tag{3.37}$$

where M represents the receiving array elements , while N denotes transmitting array elements. Both are adaptively selected at each scan, and play a vital role for improved detection probability. Likewise $\chi^2_{(2)}$ is chi-square distribution having 2 degrees-of-freedom and $F(.)$ is the cumulative distribution function. In this case, the proposed HCPAR achieves an improved detection probability than that of conventional phased array radar, where the array elements are kept fixed.

3.4. Performance analysis of the proposed HCPAR design

MATLAB 2012 has been used for simulations. Its *nntool* and *optimtool* toolboxes have been used for implementing the neural network and GA based estimations, respectively. The transmitter and receiver have same number of elements at the first cycle i.e., $N=M$, with half wavelength inter-element distance.

3.4.1. Energy efficiency

In both type of transmitter antenna cases, the surveillance region is in between –π/2 to π/2 as shown in Fig- 3.7 (a). The proposed system design avoids the continuous scanning of the surveillance region. Instead, it only steers the predicted target position received as feedback as shown in Fig-3.7 (b).

Therefore, the ratio of transmitted energy by the proposed transmitter to conventional one is given by

$$\eta \cong \frac{\theta_{0_{HP}}}{\pi} \times 100 \tag{3.38}$$

where $\theta_{0_{HP}}$ denotes half-power beam width (HPBW) in θ_0 direction, while we neglect the side-lobes energy effects. The proposed system design saves $(100-\eta)\%$ energy as compared to a conventional PAR. Moreover, it has the ability to sense the environment and consequently, makes changes in its attributes and parameters adaptively.

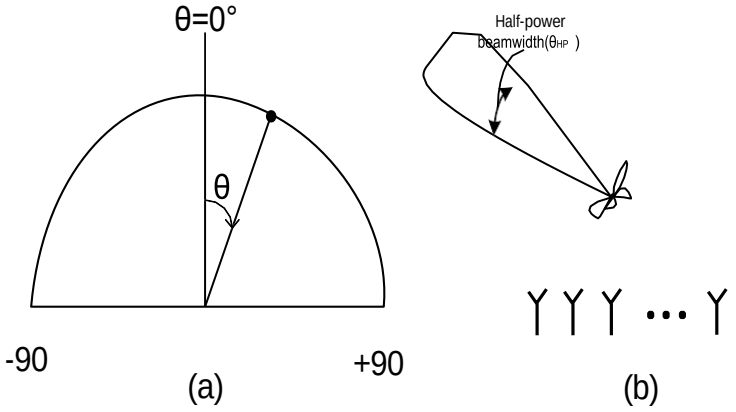

Figure-3. 7: Energy transmitted in one cycle (a) by a conventional PAR (b) by the proposed radar

3.4.2. Target range estimation performance

For range estimation, if the total time delay (T_d) (from transmitter to target and then to receiver) is calculated as 30μs using the delay estimation formula in this case. Hence, the target range value can be calculated as $\hat{r_0} = \frac{c}{2} T_d = 4500\,m$.

3.4.3. DOA estimation performance

The reflected echoes from five far field sources at any time k have been provided to the DOA estimation block with a receiving passive array having 11 elements i.e., $M = 11$ with half wavelength separation. The *optimtool* toolbox of MATLAB has been used for GA based simulation. The performance of GA for estimating the DoAs of five far field sources has been shown in Table-3.1.

Table-3. 1: Target direction estimation using the GA for HCPAR design

Estimation performance of DoA using the GA					
Desired DoA	45°	60°	75°	-30°	0°
Estimated DoA	45.003°	59.997°	75.0012°	-30.0012	0.0001°

The direction of target is already known for the first time i.e., 0°, while four interference are at -30°, 75°, 60° and 45°, respectively. Table 3.1 shows that the estimated results are quite close to the desired results, which is very essential for an efficient estimator to predict the next position.

3.4.4. Target tracking performance

The target position $\left(\hat{\theta}_{0,k}, \hat{r}_{0,k}\right)$ calculated at time k, along with all the previous position states, is given to the prediction block for estimation of predicted target position $\left(\hat{\theta}_{0,k+1}, \hat{r}_{0,k+1}\right)$ using EKF algorithm. $\mathbf{x} = \begin{bmatrix} \theta & \dot{\theta} & r & \dot{r} & \omega \end{bmatrix}^T$ is the state of a nonlinear system, while θ and $\dot{\theta}$ are the angle and velocity components of target position, r and $\dot{r}$ are the range and its velocity component and ω is the turn rate. The transition matrix is taken as

$$\tilde{F} = \begin{bmatrix} 1 & T_0 & 0 & 0 & 0 \\ 0 & 1 & 0 & 0 & 0 \\ 0 & 0 & 1 & T_0 & 0 \\ 0 & 0 & 0 & 1 & \frac{T_0^2}{2} \\ 0 & 0 & 0 & 0 & 0 \end{bmatrix}$$

where T_0 is the sample time. We assume that the process noise is zero mean Gaussian with a covariance matrix given as $\mathbf{Q} = diag[0, \sigma_1^2, 0, \sigma_2^2, \sigma_2^2]$, where $\sigma_1^2 = \sigma_2^2 = 0.10$. Likewise, the initial value of measurement function $\tilde{\mathbf{H}}$ is given as

$$\tilde{\mathbf{H}} = \begin{bmatrix} 1 & 0 & 0 & 0 & 0 \\ 0 & 0 & 1 & 0 & 0 \end{bmatrix}$$

We aslo assume that the measurement noise is zero mean Gaussian with covariance matrix given as $\mathbf{R} = diag\left([\sigma_\theta^2, \sigma_r^2]\right)$, where $\sigma_\theta^2 = 0.2$ and $\sigma_r^2 = 0.15$. These parameters are preferred to achieve the best performance. Keeping the SNR value as 10 dB, Fig. 3.8(a) show the performance of position predictor block a nonlinear trajectory using EKF without feedback loop and with feedback loop. Fig-3.8(b), (c) show the comparison of prediction

error plots of this trajectory w.r.t. range and angle.

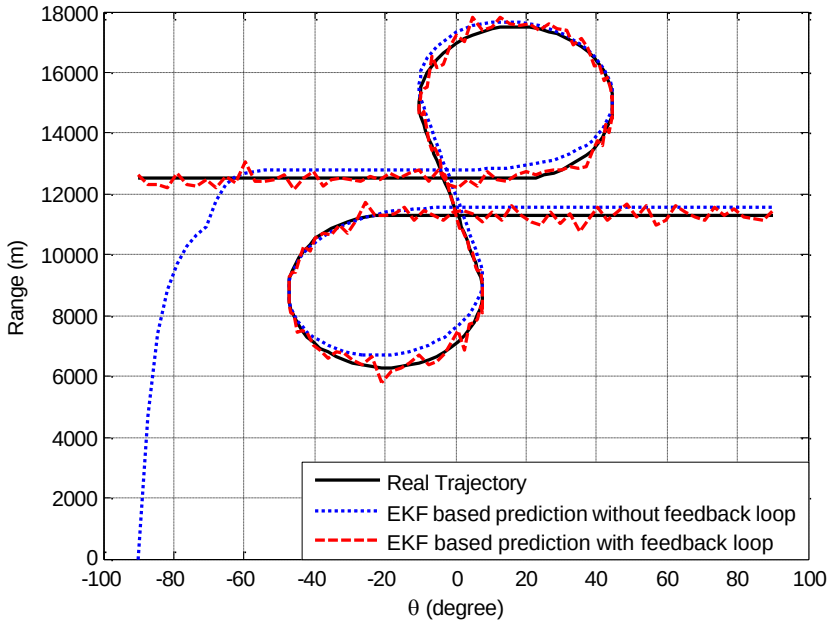

(a) True position of target and the prediction performance of target position using EKF without feedback loop and EKF with feedback loop (i.e., cognitive)

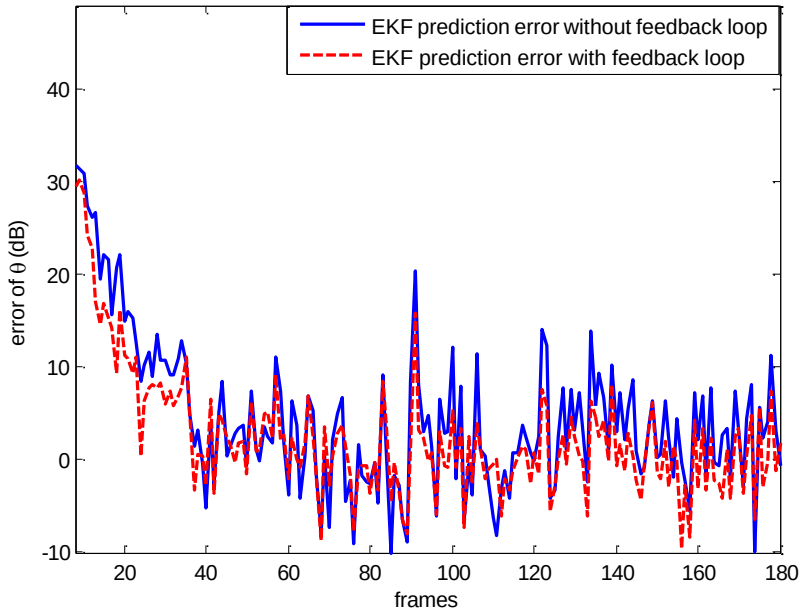

(b) Prediction error performance comparison of the EKF without feedback loop and EKF with feedback loop in angle (θ) dimension

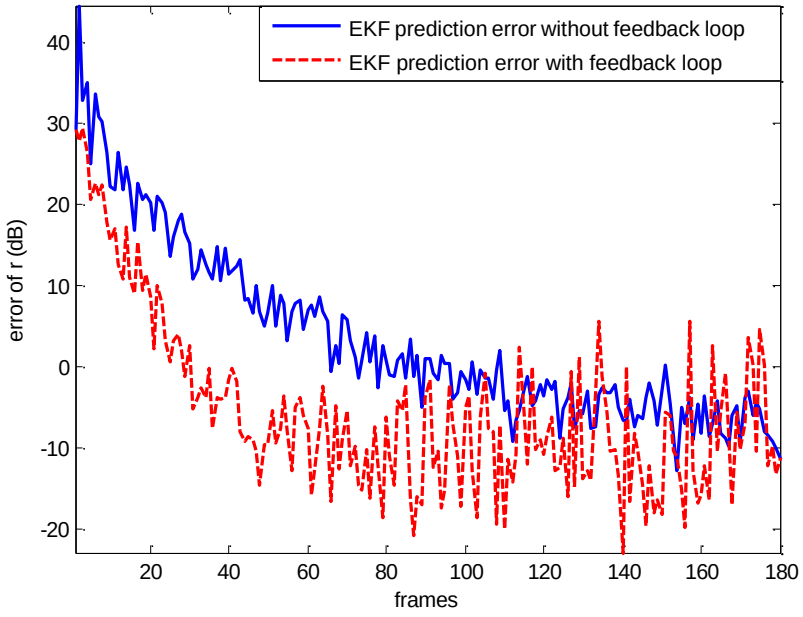

(c) Prediction error performance comparison of the EKF without feedback loop and EKF with feedback loop in range (r) dimension

Figure-3. 8: (a)-(c) Performance Analysis of the EKF for a monostatic radar and EKF for the proposed HCPAR design with comparison of their respective prediction errors

These results show that EKF algorithm for the proposed HCPAR with feedback loop has a better tracking performance than a radar without a feedback loop in predicting the true positions of a nonlinear target trajectory.

3.4.5. Adaptive beam former performance

The MVDR is used to calculate the weight vector for the selected array, which ensures the maxima in target direction and nulls in the interference directions as shown in Fig. 3.9. Consider the target direction is at 0°, while the interferences directions are taken as 45° , 75° and –30°.

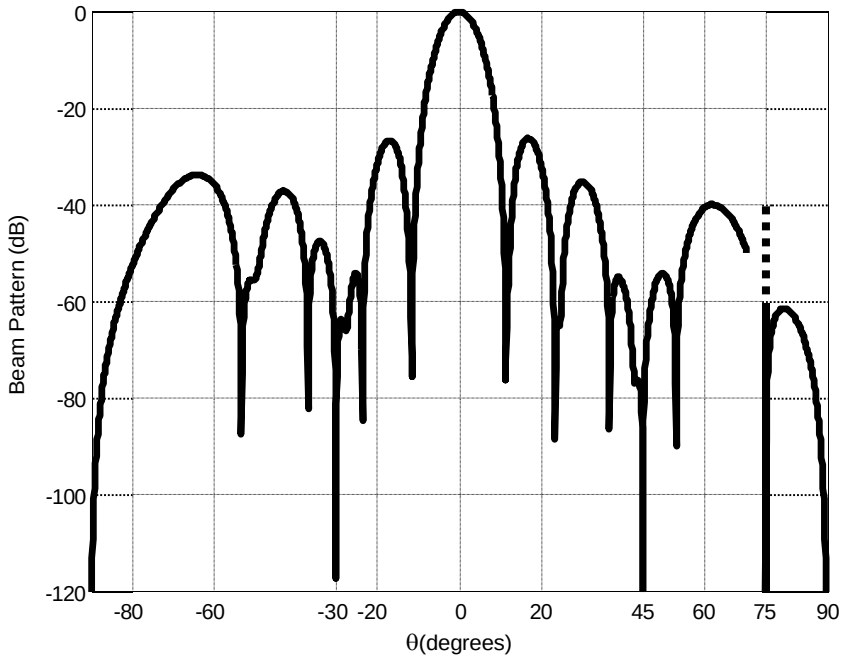

Figure-3. 9: MVDR performance for beam pattern maxima towards target at 0°whereas nulls at -30°, 45° and 75°, $f_0 = 10\,GHz, M = 11,\ d = \lambda / 2$

The MVDR beam-former technique improves the SINR at the receiver as it suppresses the interferences quite impressively.

For this design to be cognitive, the predicted target position $\left(\hat{\theta}_{0,k+1}, \hat{r}_{0,k+1}\right)$ is sent as feedback to the transmitter.

3.4.6. High gain transmitter beam forming performance

Once these predicted positions are received at the transmitter, the selector chooses an appropriate number of transmit array elements. A lookup table is maintained, which has the information about the appropriate number of array elements (N) needed for a specific range limit. Table-3.2 shows the lookup table. For simulations, the initial range value of target is taken as 1 km. Likewise, maximum 54 array elements can be taken for a

transmitting array. The predicted target positions $\left(\hat{\theta}_{0,k+1}, \hat{r}_{0,k+1}\right)$ on two different cycles are sent as feedback and are given as $\left(30^o, 2.8\,km\right)$ and $\left(0^o, 3.1km\right)$, respectively.

Table-3. 2: The predefined lookup table

Range limits vs. an appropriate number of active elements						
Range (km)	0-3	3-6	6-9	9-12	12-15	>15
N	18	24	32	40	48	54

For the first position, the range is $2.8\,km$, which yields 18 transmitter active array elements i.e., $N = 18$ using the lookup table. On the other hand, when the range is $3.1km$ in the received next position, 24 active array elements have been selected. These elements have been selected, adaptively, using a feed forward NN shown in Fig 3.3. In both cases, the transmitter array generates high gain beam patterns towards the target direction.

The corresponding beams generated towards the target directions are shown in Fig-3.10. It shows when the target range is $2.8km$, the maximum gain value in its direction using 18 array elements is $11.3dB$ but when the target range increases to $3.1km$, the transmitter gain also increases to $12.55dB$. This feature is an addition to the conventional PAs.

In the nutshell, as soon as the range of target increases/decreases, the transmitter increases/decreases the active number of transmitting elements that results in less computational complexity as compared to a fixed element transmitter without affecting the overall radar performance.

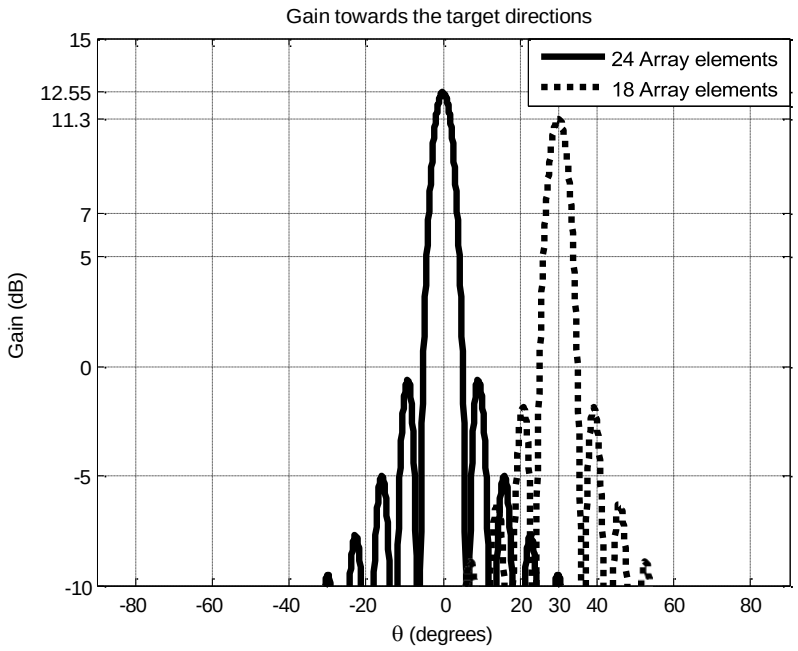

Figure-3. 10: Beam patterns generated by the HCPAR high gain transmit array

3.4.7. LPI beam forming performance of the transmitter

A high gain of PAR is undesirable in some applications, where the objective is "to see but not to be seen". Therefore, an LPI beamforming has been used to hide the radar from potential interceptors.

An array with 32 antenna elements with half wavelength inter-element distance is considered i.e.,$(N = 32)$ for performance evaluation of proposed LPI technique. The

gain value of high gain beam pattern is compared with a low gain spoiled beam pattern and is shown in Fig 3.11. The spoiled beam pattern is achieved using an additional phase shift set (i.e. set of φ_n shown in Fig.3.6) across each element of the array.

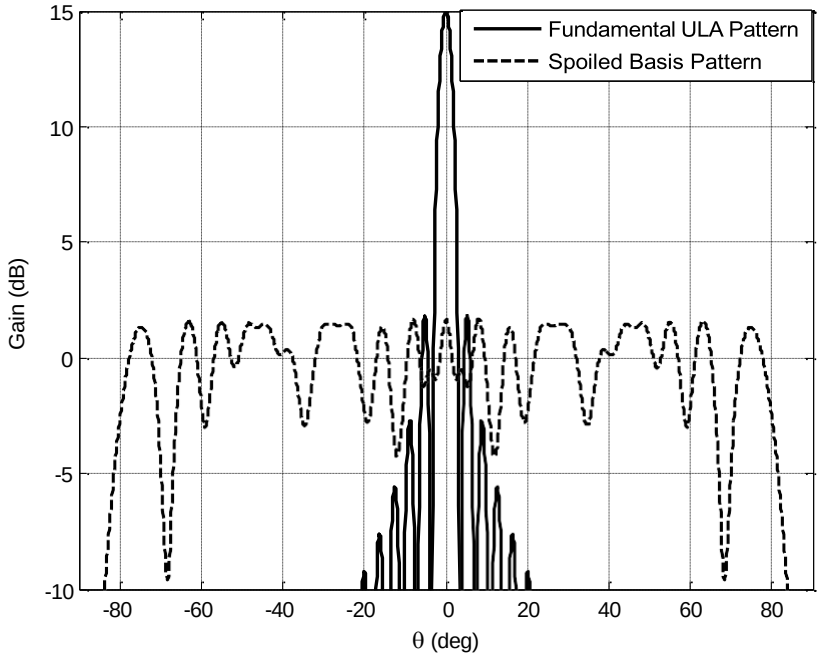

Figure-3. 11: Comparison between High gain beam pattern and spoiled beam pattern for a 32-element linear phased array, steered at 0 deg

The high gain beam pattern has 15dB gain, while spoiled beam pattern has gain of 1.7dB that is significantly low. Other scanned high-gain and low gain basis patterns can be constructed by applying a linear phase progressive phase shift to the fundamental patterns. Fig. 3.12 shows the first four spoiled patterns.

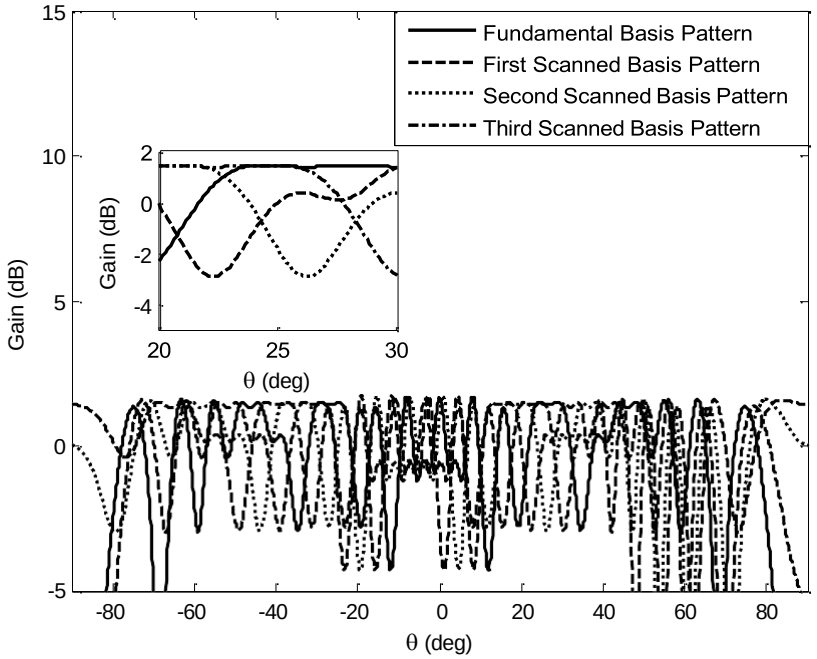

Figure-3. 12: First four spoiled beam patterns, 4 basis patterns

These spoiled basis patterns have very low-gain (less than 2dB) as compared to high gain beam patterns (15dB). With the complex weights computed using a GA, we can synthesize high-gain pattern in any desired direction using low gain spoiled beam patterns. The performance of GA based synthesized beam pattern in presence, as well as, in absence of the AWGN is discussed in the next section.

3.4.7.1. LPI beam forming with no AWGN

For the first case, we assume that no AWGN disturbs the process of spoiling high gain patterns. The complex weights computed using GA avoids the inverse of a matrix (see (3.23)) as used in [62]. Fig. 3.13 shows the genetic algorithm (GA) based synthesized high-gain patterns directed towards $0^{\circ}, 45^{\circ} and -45^{\circ}$.

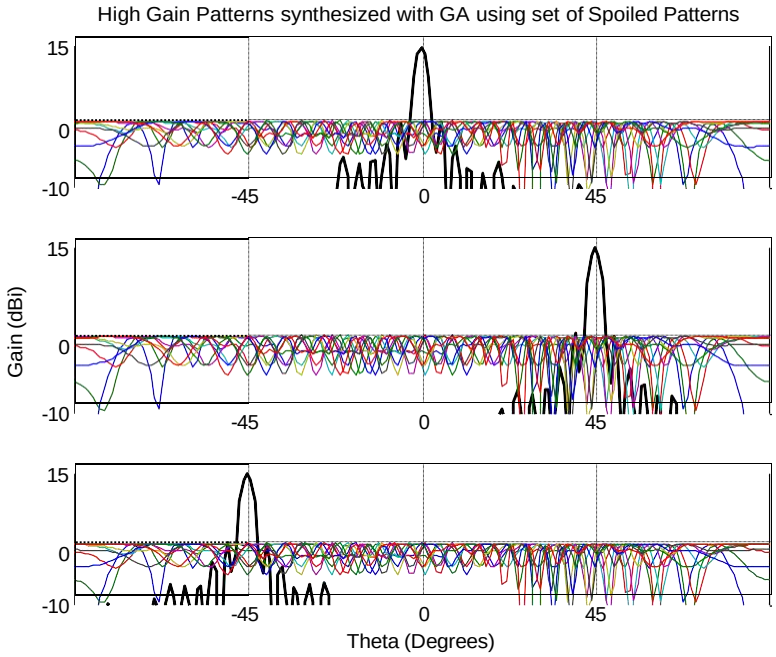

Figure-3. 13: GA based synthesized high gain beam patterns steered at 0,-45 and +45 deg respectively.

We can see from the above figure that high gain patterns have the similar gain of 15dB towards the desired direction as of conventional array antennas. It also ensures that this LPI beamforming property does not affect the overall performance of a radar.

3.4.7.2. LPI beam forming in presence of AWGN

In second case, an AWGN has been added to the spoiled patterns, while maintaining a SNR of 10 dB. Fig-3.14 shows the comparison of a GA performance alone and GA hybridized with pattern search (PS) performance for synthesizing a high gain beam towards 0°. The hybridized GA with PS algorithm shows improved performance as compared to GA alone as it has considerably low side lobes than a GA alone synthesized beam.

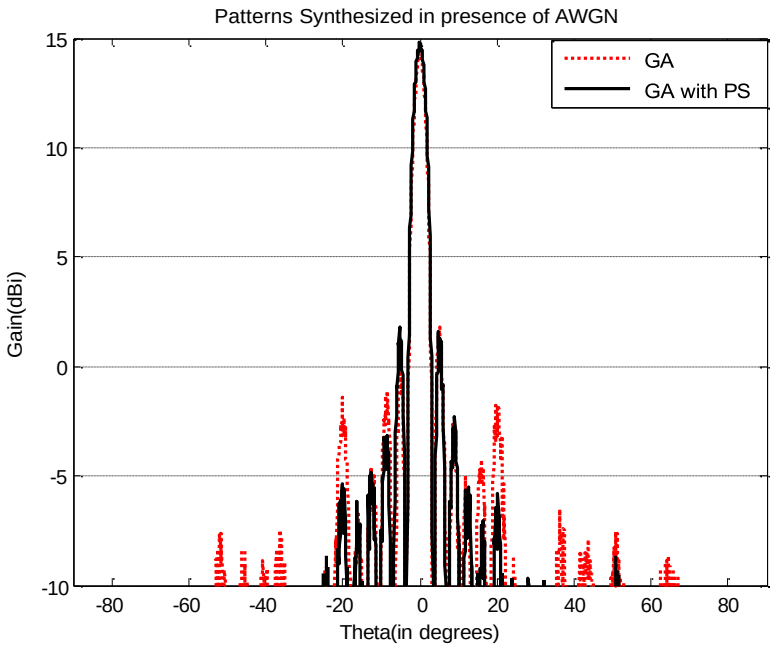

Figure-3. 14: Synthesized beam using GA alone and hybridized GA with PS in AWGN scanario

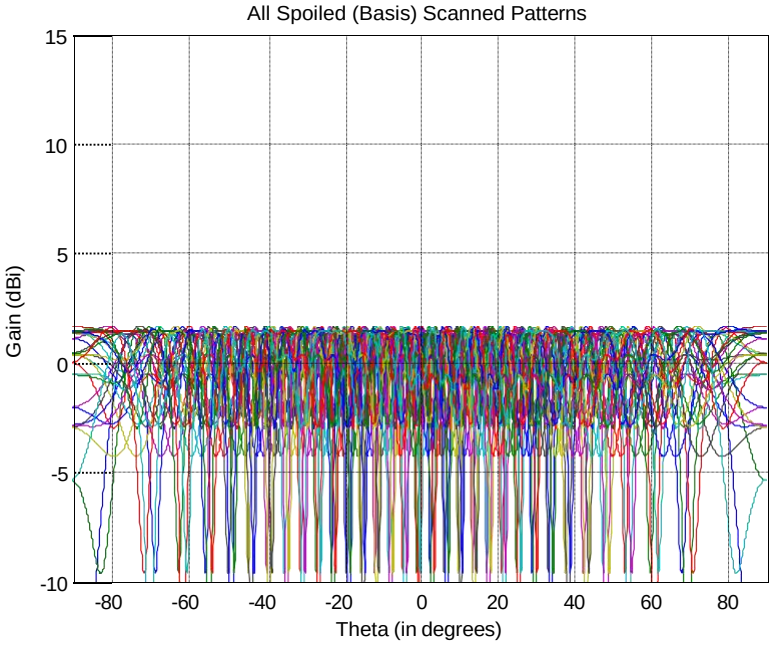

(a) All spoiled beam patterns

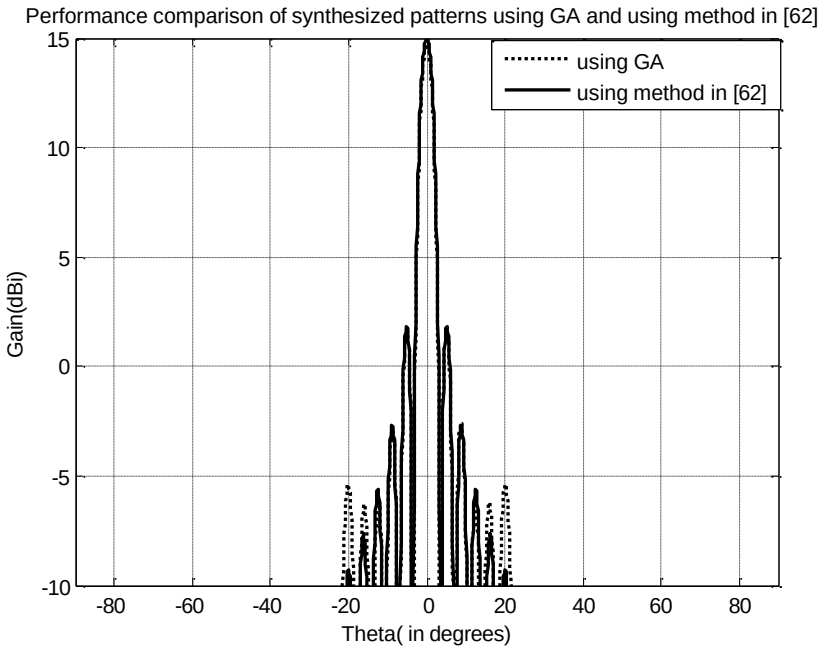

(b) Pattern synthesis performance of the GA and the author's method in[62].

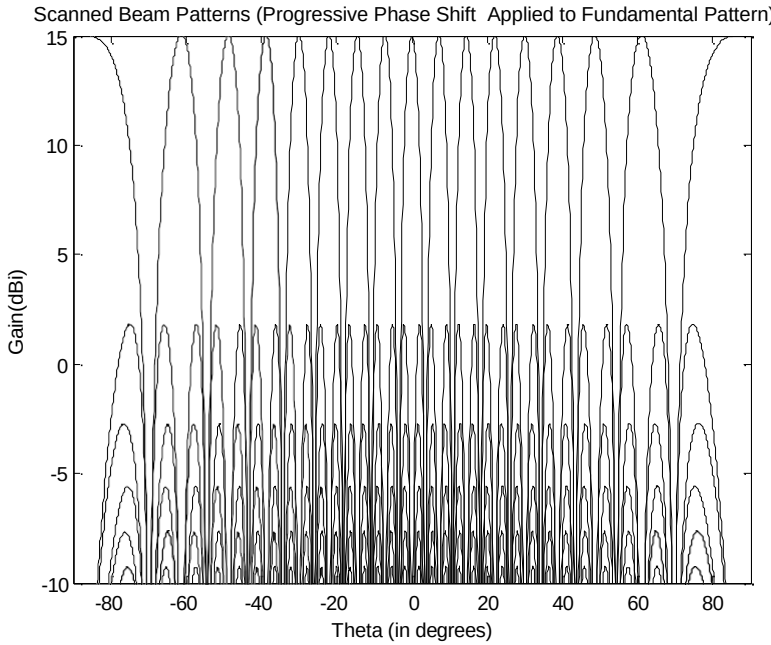

(c) Scanned high gain beam patterns

Figure-3. 15: Performance analysis comparison of the GA and already existing technique in [62]

Figs-3.15 (b) & (c) show that GA based computed weights, synthesize the high gain beam patterns using these spoiled beam pattern quite accurately. All spoiled beam patterns have low gains i.e., less than 2dB as shown in Figure 3.15 (a). Fig. 3.15 (b) gives a clearly shows that the GA method used for synthesis of a high gain beam pattern shows almost equal performance as compared to the method used in [62]. But the advantage of GA is low complexity, specifically by avoiding the matrix inversions (see (3.23)) as used in [62]. Table 3.3 gives parameter setting for the GA and PS algorithms.

Table-3. 3: Parameter settings of the used algorithms

GA		**PS**	
Parameters	**Settings**	**Parameters**	**settings**
population size	40	mesh initial size	1.0
chromosome size	64	mesh maximum size	infinity
creation function	Uniform	initial penalty	10
selection function	stochastic uniform	penalty factor	100
reproduction crossover fraction	0.6	bind tolerance	1e-3
mutation function	adaptive heuristic	mesh tolerance	1e-6
crossover function	Heuristic	max iterations	6400
migration direction	Both	function evaluation	128k
hybrid function	None	time limit	infinity
no of generations	1000	x tolerance	1e-6
function tolerance	1e-10	function tolerance	1e-6
constraint tolerance	1e-10	constraint tolerance	1e-6

For the given HCPAR scenario, the transmitter increases or decreases the number of active array elements based on the receiver feedback about the target predicted position. Fig-3.16 shows the dB gain of three synthesized beam patterns. We can see that when the target range is increasing, the gain towards the target also increases, adaptively. The high gain value is generated in the direction of target received as feedback using a conventional beam-former.

Increase in a target range value, decreases incident power on the target. The proposed hybrid cognitive PAR selects an active number of elements according to range value of target to maintain a reasonable incident power (directivity) for better detection performance. Fig-3.17 shows the comparison of incident power on the target between the proposed radar and a fixed elements uniform linear array transmitter.

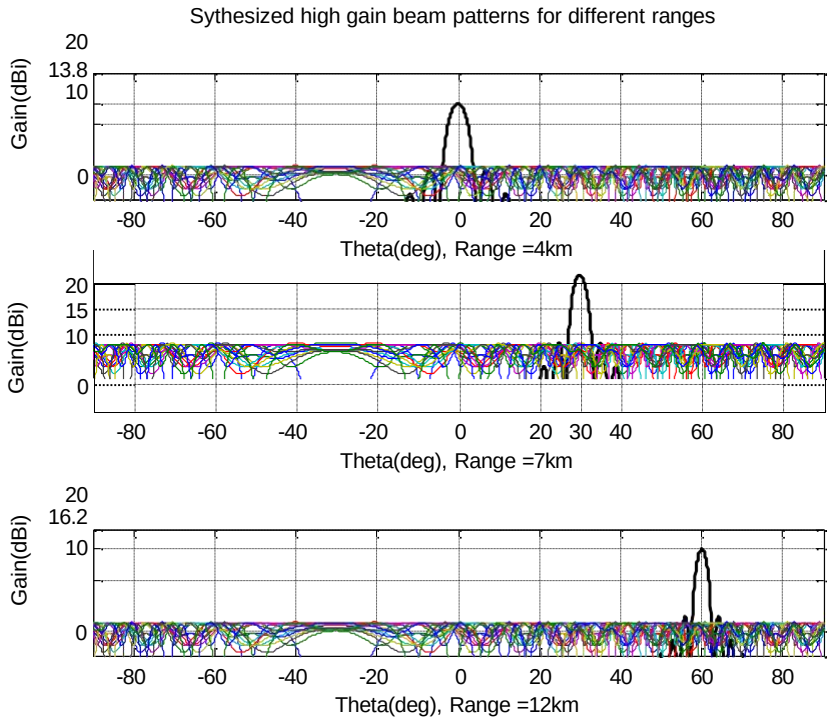

Figure-3. 16: Synthesized respective beam patterns for different target ranges and directions

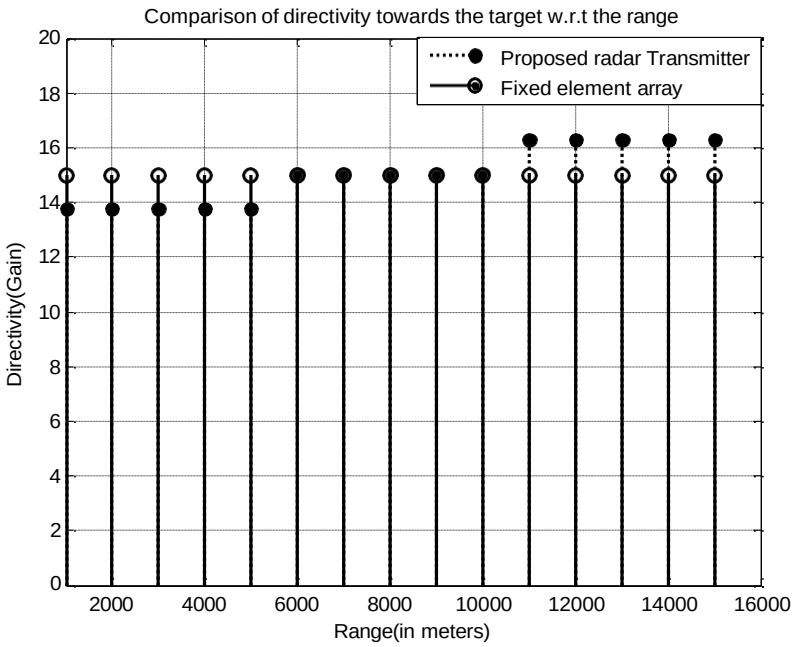

Figure-3. 17: Comparison of incident power on the target w.r.t. the range

We can see that the proposed radar increases the directivity towards the target direction as soon as the range of the target increases. On the other hand, when the range of target is low, the proposed radar uses a lesser number of elements in the transmitter array that results in a lesser size of the transmitter and target steering vectors and lesser size of the weight vector for it. Hence, the computational complexity is reduced as compared to a fixed sized transmitter array. The generation of beam pattern maxima in accordance with the target position sent as receiver feedback reduces computational complexity even more.

3.5. Overall performance of the proposed HCPAR design

The overall performance of the proposed radar design has been evaluated on SINR and detection probability performance.

3.5.1. SINR performance of the proposed HCPAR design

To evaluate the overall SINR performance, noise power is fixed to 0 dB and the interference to noise ratio (INR) is taken as 30dB . Fig-3.18 shows the SNR vs. SINR performance of the proposed system.

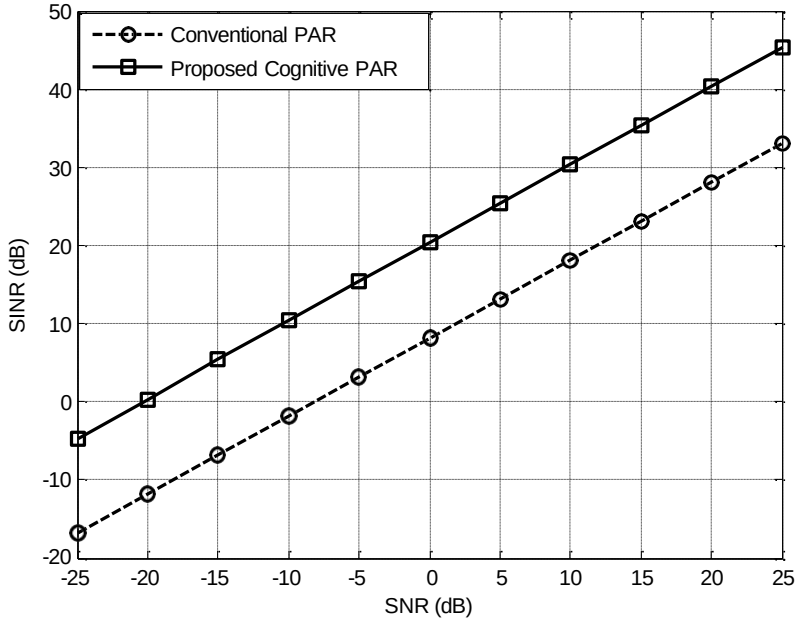

Figure-3. 18: SNR vs. SINR performance of the proposed HCPAR design

A significantly higher SINR has been achieved using the proposed cognitive PAR as compared to a conventional PAR.

3.5.2. Detection performance of the proposed HCPAR design

The detection performance of the proposed CPAR in comparison with the conventional PAR fixed array elements is shown in Fig. 3.19. SNR is maintained at 5dB, the figure shows improved detection performance of the proposed CPAR based on its cognition properties.

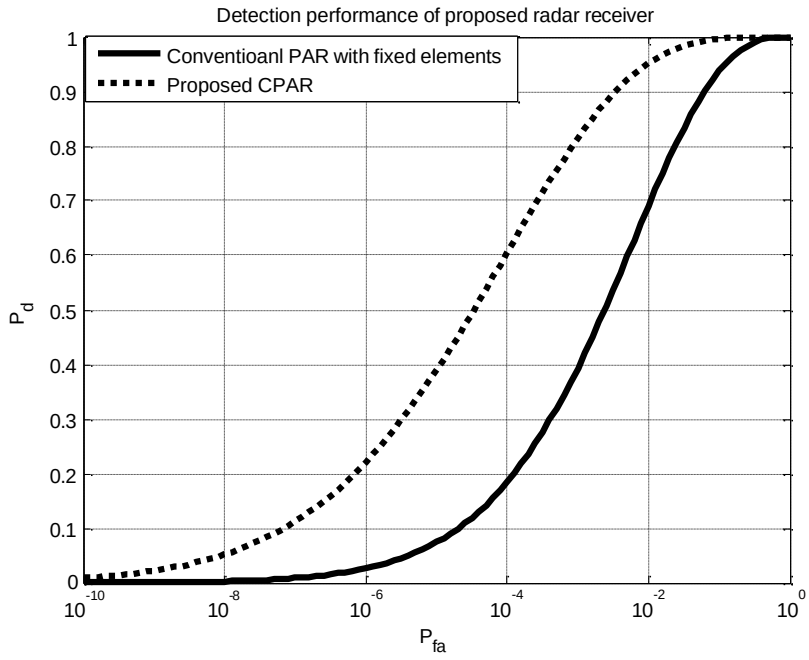

Figure-3. 19: Detection performance comparison of the proposed HCPAR and conventional PAR

3.6. Conclusion and discussion on HCPAR performance

Different from existing radar systems, the proposed radar avoids continuous scanning of the surveillance region. Instead, only the predicted regions based on the receiver feedback are scanned during next cycle. It saves a lot of power. The receiver phased array varies the number of elements to place nulls in the interferences directions, adaptively. This results in a higher signal to interference noise ratio (SINR). Moreover, it consequences in reduced computational and hardware complexity as compared to the fixed element phased array. Accordingly, the selected number of transmitting and receiving array elements, based on sensing the environment, result in improved detection probability.

The receiver and the transmitter of proposed system change the attributes after sensing the environment for improved performance.

CHAPTER-4

Hybrid Cognitive Frequency Diverse Array (HCFDA) Radar with Uniform Frequency Offset

In this chapter, we present a new design of hybrid cognitive frequency diverse array (HCFDA) radar, which combines the cognitive radar (CR) properties with range-angle-dependent beamforming property of frequency diverse array (FDA) radar. We consider an FDA having uniform frequency offset applied at the input of array. The chapter starts with brief introductions of CR and FDA with range-angle dependent beam forming ability. Afterwards, the idea of HCFDA system design with uniform frequency offset is presented in detail. A novel analytic method to calculate this frequency offset based on receiver feedback is also presented. At the end, the simulation results are provided, which show improved detection, SINR and tracking performance of the proposed radar as compared to the conventional FDA and phased array radar.

4.1. Introduction

Cognitive dynamical systems theory is an emerging discipline, which use the basic ideas of neuroscience and statistical signal processing. It paves the way for a new generation of dynamic systems, such as, cognitive radio, cognitive radar, etc.,[128]. The analogy that exists between a human brain and radar signal processing methods is the inspiration behind a basic cognitive radar (BCR) [128], [129]. BCR consists of a global

feedback, which connects the receiver, surrounding environment and the transmitter [127]. BCR equipped with memory is known as CR and its idea was originally presented in [124]. The signal processing techniques alongside with the memory and global feedback make these cognitive systems flexible for intelligence [125].

Moreover, if the environment is non-stationary, the estimation and updating of target state vector turns out to be a challenging task. To deal with this problem, recursive updating of a system state has been utilized to make the transmitter adaptive based on the statistical variation information received as feedback [127], [135]. The CR senses the surrounding environment, continuously, to improve its performance consequently [124].

Additionally, an FDA radar is quite different from a conventional phased-array radar because it generates a time, range, angle dependent beam pattern [76]. The frequency diverse array utilizes a small frequency offset, as compared to the carrier frequency, across the employed array elements to generate a range-angle dependent beam pattern. These frequency offsets can be either uniform or non-uniform.

In the proposed HCFDA design, a uniform frequency offset configuration has been considered. The receiver estimates the current along with the future target positions, which are sent as feedback to the transmitter. Since an FDA utilizes a small frequency offset for generating a range-angle dependent beam pattern, we have provided an analytical formulation to compute the offset based on the receiver feedback. The transmitter illuminates, merely, the predicted target position, which results in saving a lot of energy and ultimately decreasing the electromagnetic pollution of environment. Additionally, it reduces computational cost. The proposed system avoids continuous scanning of the surveillance region. Instead it only scans the desired area received as

feedback from the receiver. The illumination and energy focusing towards the desired target position consequences in an improved SINR and probability of detection in comparison with a conventional PAR and FDA.

4.2. Proposed HCFDA System Design

The receiver contains four sub-blocks i.e., the DOA estimation, the range estimation, memory and EKF based estimation block. In the same way, the transmitter contains two sub-blocks i.e., a frequency diverse array block and the selector. Fig. 4.1 shows the block diagram and corresponding information flow of the proposed HCFDA radar at any time k.

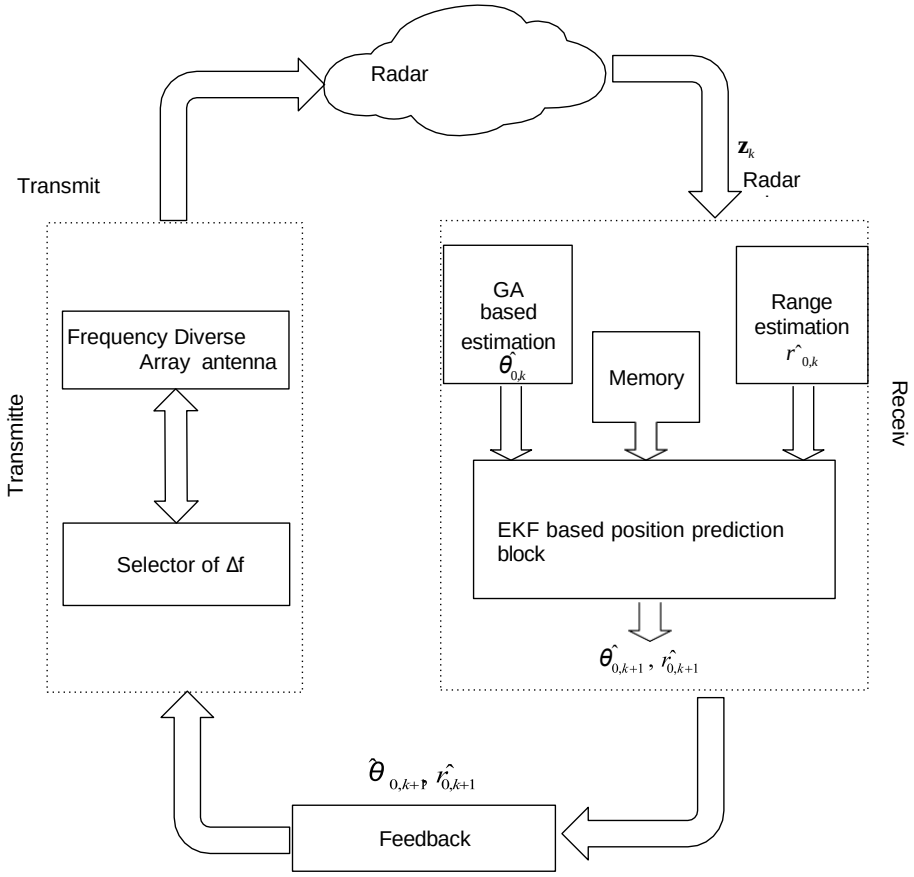

Figure- 4. 1: Block diagram of the proposed radar

The transmitter illuminates the surrounding environment consisting of many potential targets at time $k-1$. The echoes $\mathbf{z}_k$ are received, simultaneously, by two sub-blocks i.e., the range estimation and GA based DOA estimation blocks. The filtered target position pair $\left(\hat{\theta}_{0,k}, \hat{r}_{0,k}\right)$ is estimated at time k. The filtered target position, as well as, the previous target position estimates are passed into the EKF block for predicting the target future position $\left(\hat{\theta}_{0,k+1}, \hat{r}_{0,k+1}\right)$. This predicted position is sent to the transmitter block as a feedback. With the target current and predicted positions estimates i.e., $\left(\hat{\theta}_{0,k}, \hat{r}_{0,k}\right)$ and $\left(\hat{\theta}_{0,k+1}, \hat{r}_{0,k+1}\right)$, the selector, a sub-block of transmitter, calculates frequency offset value Δf_{k+1} for the new cycle. This new frequency offset ensure maximum power peaks towards the target predicted position.

This cognitive cycle keeps on repeating itself for improved radar performance. Each block of the proposed receiver, as well as, the transmitter is discussed below.

4.2.1. Receiver

The receiver has four sub-blocks. DOA estimation, range estimation, memory and EKF based estimation and prediction block.

4.2.1.1. Direction of arrival estimation

The fitness function for DoA estimation is taken as the mean square error between the desired and estimated DoA. Fig-4.2 shows the receiving passive array with M elements for the HCFDA design.

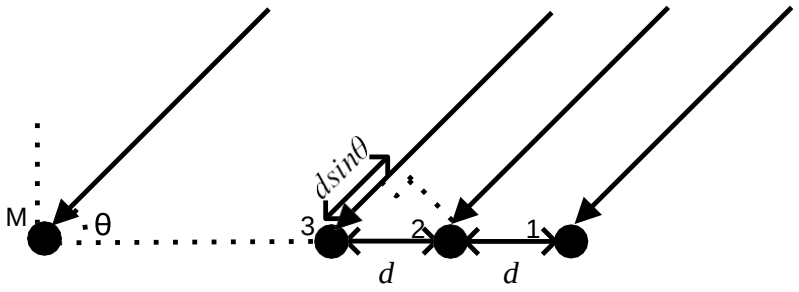

Figure- 4. 2: A receiver passive array with M elements for HCFDA design

The array has a half wavelength inter-element distance, while there are F far field source signals that imping on a passive array from diverse directions. The output of m^{th} array element is given as [160], [164]

$$o_m = \sum_{q=1}^{F} A_q e^{\left(-jvd(m-1)sin(\theta_q)\right)} + n_m \tag{4.1}$$

where $m=1,2,\ldots,M$ and $F \leq M$; A_q denotes the amplitude of q^{th} source, while n_m represents an AWGN at the output of m^{th} array element. The estimated output of m^{th} array element is given as

$$\hat{o}_m = \sum_{q=1}^{F} \hat{A}_q e^{\left(-jvd(m-1)sin(\theta_{F+q})\right)} \tag{4.2}$$

Following are the GA steps used for DOA estimation:

Step 1: Generate a set of random chromosomes with an appropriate upper and lower bounds. The lower bound for DOA is -90°, in this case, while upper bound is $+90^{\circ}$. The population size is 20, while the size of chromosome vector is F.

Step 2: The fitness value of each chromosome is computed using the following fitness function.

$$MSE_m = \frac{1}{M}\sum_{m=1}^{M} \left| \phi_m - \hat{o}_m \right|^2 \text{ where } m = 1, 2, \ldots, M \tag{4.3}$$

Step 3: Crossover operation is performed for production of offspring using a selected parent set. In this case, we have selected a 2 point heuristic crossover type, while the crossover fraction is kept 0.8.

Step 4: Generate a fresh population set.

Step 5: Mutation is performed for improved convergence rate. We have selected a adaptive feasible mutation function in this case.

Step 6: Termination criterion is analyzed after either achieving a best fitness value or maximum cycles are reached. In this case, we have used a maximum cycle length of 500 in this case.

Step 7: Otherwise jump to *step 2*.

4.2.1.2. Range estimation block

In the range estimation block, the target range is estimated using received echoes. In FDA case , the total time delay not merely depends upon the target-transceiver distance but also on the used frequency offset value Δf [81]. Consequently, the signal arrival time τ_{ar_t} from a FDA transmitter to a desired target position is given as [81]

$$\tau_{ar\_t} = \frac{r_0}{c} + \left(m - \frac{d}{\lambda} \sin(\theta_0) \right) \left(\frac{1}{\Delta f} \right) \tag{4.4}$$

where c denotes speed of light, r_0 is target range value, θ_0 represents the direction of target, Δf is the used frequency offset and m stand for an integer value, which stands for grating lobes.

The proposed transmitter and receiver are collocated, therefore, the time delay τ_{ar_r} from

the target to the proposed receiver is given as:

$$\tau_{ar\_r} = \frac{r_0}{c} \tag{4.5}$$

The complete time delay T_d is stated as:

$$T_d = \tau_{ar\_t} + \tau_{ar\_r} = \frac{2r_0}{c} + \left[m - \frac{d}{\lambda} \sin(\theta_0) \right] \left(\frac{1}{\Delta f} \right) \tag{4.6}$$

The angle information (θ_0) and time delay are already known in this case. Therefore, the target range can be found as (using (4.6))

$$r_0 = \frac{c}{2} \left| T_d - \left\{ m - \frac{d}{\lambda} \sin(\theta_0) \right\} \left(\frac{1}{\Delta f} \right) \right| \tag{4.7}$$

With the information of frequency offset, time delay and DOA, we can compute target range at each cycle.

4.2.1.3. EKF algorithm for position prediction

For a nonlinear radar environment, extended Kalman filter (EKF) has been used for implementing the prediction block [48]. The process equation of EKF state space model is described at any time l using [50]

$$\mathbf{x}_{k+1} = \tilde{\mathbf{F}}\mathbf{x}_k + \mathbf{n}_k \tag{4.8}$$

where $\mathbf{x}_k$ is system state at time k, $\tilde{\mathbf{F}}$ represents a nonlinear transition matrix and $\mathbf{n}_k$ stands for process noise which is assumed AWGN with zero mean and covariance matrix $\mathbf{Q}$ given by

$$E\left[\mathbf{n}_k \mathbf{n}_l^T\right] = \begin{cases} \mathbf{Q}_k & for\ k = l \\ 0 & for\ k \neq l \end{cases} \tag{4.9}$$

Similarly, the measurement equation is given as

$$\mathbf{z}_k = \tilde{\mathbf{H}}\mathbf{x}_k + \mathbf{v}_k \tag{4.10}$$

where $\mathbf{z}_k$ represents an observation vector at time k, $\underset{\sim}{\mathbf{H}}$ stands for a nonlinear measurement matrix and $\mathbf{v}_l$ is assumed to be zero mean AWGN with covariance matrix $\mathbf{R}$, given by

$$E\left[\mathbf{v}_k \mathbf{v}_l^T\right] = \begin{cases} \boldsymbol{R}_k & k = l \\ 0 & k \neq l \end{cases} \tag{4.11}$$

Moreover, a Gaussian distribution can be totally characterized by a state mean and covariance matrix [52]

$$\hat{\mathbf{x}}_{k/k} = E\left[\mathbf{x}_k \mid \mathbf{z}_1^k\right] \tag{4.12}$$

$$\hat{\mathbf{x}}_{k+1/k} = E\left[\mathbf{x}_{k+1} \mid \mathbf{z}_1^k\right] \tag{4.13}$$

In the same way, the filtered covariance matrix and predicted covariance matrix are given by [22]

$$\hat{\mathbf{P}}_{k/k} = E\left[\left(\mathbf{x}_k - \hat{\mathbf{x}}_{k/k}\right)\left(\mathbf{x}_k - \hat{\mathbf{x}}_{k/k}\right)^T \mid \mathbf{z}_1^k\right] \tag{4.14}$$

$$\hat{\mathbf{P}}_{k+1/k} = E\left[\left(\mathbf{x}_{k+1} - \hat{\mathbf{x}}_{k+1/k}\right)\left(\mathbf{x}_{k+1} - \hat{\mathbf{x}}_{k+1/k}\right)^T \mid \mathbf{z}_1^k\right] \tag{4.15}$$

The prediction error vector is stated as

$$\tilde{\mathbf{x}}_{k+1/k} \triangleq \mathbf{x}_{k+1} - \hat{\mathbf{x}}_{k+1/k} \tag{4.16}$$

where $\hat{\mathbf{x}}_{k+1/k} = \tilde{\mathbf{F}}\hat{\mathbf{x}}_{k/k}$

Likewise, we define the prediction measurement error vector as

$$\tilde{\mathbf{z}}_{k+1/k} \triangleq \mathbf{z}_{k+1} - \hat{\mathbf{z}}_{k+1/k} \tag{4.17}$$

where $\hat{\mathbf{z}}_{l+1/l} = \tilde{\mathbf{H}}_{l+1}\hat{\mathbf{x}}_{l+1/l}$

4.2.1.4. SINR and detection Performance Analysis

The objective is to minimize the prediction measurement error. Strong echoes from the target promise in minimizing the error.

An echo from a target position (θ_0, r_0) can be expressed as [32]

$$m(\theta_0, r_0, k) = \rho(\theta_0, r_0)\mathbf{w}_T^H \mathbf{u}(\theta_0, r_0, \Delta f)\, s(k) \tag{4.18}$$

where $\rho(\theta_0, r_0)$ represents the reflection coefficient, $\mathbf{u}(\theta_0, r_0, \Delta f)$ represents a target steering vector, $s(k)$ denotes a transmit waveform at any time k, while $\mathbf{w}_T^H$ is the weight vector computed using conventional beam-former.

We also assume that there are multiple interference sources, which are located at (θ_i, r_i), therefore echo at the receiver array is given as [117]

$$y(k) = m(\theta_0, r_0, k)\mathbf{b}(\theta_0, r_0, \Delta f) + \sum_i m(\theta_i, r_i, k)\mathbf{b}(\theta_i, r_i, \Delta f) + \mathbf{n}(k) \tag{4.19}$$

where $\mathbf{b}(\theta_0, r_0, \Delta f)$ represents receive steering vector, while $\mathbf{n}(k)$ is AWGN with zero mean and σ_n^2 variance. After match filtering, the array output can be given as

$$\mathbf{y} = \mathbf{u}_0(\theta_0, r_0, \Delta f) + \sum_i \mathbf{u}_i(\theta_i, r_i, \Delta f) + \mathbf{n} \tag{4.20}$$

where $\mathbf{u}_0(\theta_0, r_0, \Delta f) = m(\theta_0, r_0, k)\mathbf{b}(\theta_0, r_0, \Delta f)$ and $\mathbf{u}_i(\theta_i, r_i, \Delta f) = m(\theta_i, r_i, k)\mathbf{b}(\theta_i, r_i, \Delta f)$.

The receiver beamforming weight vector $\mathbf{w}_R$ is computed using MVDR beam-former. The MVDR beamforming ensures the suppression of interferences, while generating distortion-less response towards the position of target [31].

$$\mathbf{w}_R = \frac{\hat{\mathbf{R}}_{i+n}^{-1}\mathbf{u}(\theta_0, r_0, \Delta f_0)}{\mathbf{u}^H(\theta_0, r_0, \Delta f_0)\hat{\mathbf{R}}_{i+n}^{-1}\mathbf{u}(\theta_0, r_0, \Delta f_0)} \tag{4.21}$$

where, $\hat{\mathbf{R}}_{i+n}$ is interference plus noise covariance matrix. The SINR is evaluated as

$$SINR = \frac{\left|\mathbf{w}_R \mathbf{u}_0(\theta_0, r_0, \Delta f)\right|^2}{\mathbf{w}_R{}^H \hat{\mathbf{R}}_{i+n}^{-1} \mathbf{w}_R} \tag{4.22}$$

In the proposed case, an adaptive frequency offset calculation promises improved FDA radar performance, at each cycle, even more.

The signal at receiver array after suppressing interferences is given as

$$\mathbf{y} = \mathbf{u}_0(\mathrm{r}_0, \theta_0, \Delta f) + \mathbf{n} \tag{4.23}$$

$\mathbf{u}_0(\mathrm{r}_0, \theta_0, \Delta f)$ is the desired signal of target, while $\mathbf{n}$ is AWGN.

Furthermore, a hypothesis testing problem for a radar detection is modeled as:

$$\begin{cases} H_0 : \mathbf{y} = \mathbf{n} \\ H_1 : \mathbf{y} = \mathbf{u}_0(\mathrm{r}_0, \theta_0, \Delta f) + \mathbf{n} \end{cases} \tag{4.24}$$

We assume that the noise process is independent and identically distributed (i.i.d) Gaussian random noise process with zero mean and σ_n^2 variance.

The probability density function (PDF) that is basically the likelihood for this random variable $\mathbf{y}$ to achieve a value of H_0 is given as [104]

$$p(\mathbf{y}; H_0) = \exp\left(-\frac{\|\mathbf{y}\|^2}{\sigma_n^2}\right) \tag{4.25}$$

The PDF of H_1 is given by [104]

$$p(\mathbf{y}; H_1) = \exp\left(-\frac{\|\mathbf{y}\|^2}{\sigma_n^2}\right) \times \exp\left(-\frac{\left|\|\mathbf{u}_0(\mathrm{r}_0, \theta_0, \Delta f)\|^2 + n\right|^2}{2\sigma_n^2}\right) \tag{4.26}$$

The likelihood ratio test is expressed as

$$\wedge = \frac{p(\mathbf{y}; H_1)}{p(\mathbf{y}; H_0)} \underset{H_1}{\overset{H_0}{\lessgtr}} \delta \tag{4.27}$$

where δ is detection threshold.

The false alarm probability and detection probability is expressed as [104]

$$p_{fa} = p(\wedge > \delta \mid H_0) = 1 - F_{\chi^2_{(2)}}\left(\frac{2\delta}{\sigma_n^2}\right) \tag{4.28}$$

$$p_d = p(\wedge > \delta \mid H_1) = 1 - F_{\chi^2_{(2)}}\left(\frac{\sigma_n^2 F^{-1}_{\chi^2_{(2)}}(1 - p_{fa})}{M^2 N^2 + \sigma_n^2}\right) \tag{4.29}$$

where M and N represent the receiving and transmitting elements, respectively. The expression $\chi^2_{(2)}$ is the chi-square distribution having 2 degrees-of-freedom, while $F(.)$ is a cumulative distributive function. In the same way, a probability of miss detection is computed as

$$p_M = p(\wedge < \delta \mid H_1) = (1 - p_d) \tag{4.30}$$

The frequency offset is computed at every cycle in this case, which also contributes in minimizing the prediction and measurement errors. The strong echoes promise the increase in target detection probability(p_d) and at the same time ensuring decrease in probability of miss(p_M).

If the estimated range and angle values of target are not in the bounds provided, the transmitter starts scanning the surveillance region, continuously.

4.2.2. Transmitter

The proposed transmitter adjusts its parameters and properties based on the

feedback. It contains two sub-blocks that are selector and FDA antenna block. The FDA

periodicity property facilitates to compute an appropriate frequency offset value Δf that ensures FDA beam pattern maximum towards the predicted target position.

4.2.2.1. Calculation of frequency offset based on the feedback

In [81] , a formulation has be presented to compute the time delay (τ_0) of signal peak between a FDA transmitter and target position (θ_0, r_0) is given as

$$\tau_0 = \frac{r_{0,0}}{c} + \left(m - \frac{d}{\lambda} \sin(\theta_{0,0}) \right) \times \frac{1}{\Delta f_0} \tag{4.31}$$

where c represents velocity of light , m symbolizes an integer standing for grating lobes, while Δf_0 denotes an appropriate frequency offset for an FDA. $r_{0,0}$ is the range value of target and $\theta_{0,0}$ is the target direction. This τ_0 depends upon $r_{0,0}$ and Δf_0 used. As target range value is not in our control, we can choose an appropriate frequency offset to control this time delay. Similarly, we can express the time delay value for the next cycle, taken between FDA maxima and a next fixed target position $(\theta_{0,1}, r_{0,1})$ as

$$\tau_1 = \frac{r_{0,1}}{c} + \left(m - \frac{d}{\lambda} \sin(\theta_{0,1}) \right) \times \frac{1}{\Delta f_1} \tag{4.32}$$

Time delay from FDA transmitter to reach target position is kept equal for all cycles. Therefore, we equate (4.31) and (4.32) to get the following expression

$$\Delta f_1 = \frac{\left(m - \frac{d}{\lambda} \sin(\theta_{0,1}) \right)}{\frac{(r_{0,0} - r_{0,1})}{c} + \left(m - \frac{d}{\lambda} \sin(\theta_{0,0}) \right) \times \frac{1}{\Delta f_0}} \tag{4.33}$$

Therefore, a frequency offset value at time $l+1$ can be formulated in the proposed cognitive radar design scenario as

$$\Delta f_{k+1} \cong \frac{\left(m - \frac{d}{\lambda}\sin(\hat{\theta}_{0,k+1})\right)}{\frac{(r_{0,k} - \hat{r}_{0,k+1})}{c} + \left(m - \frac{d}{\lambda}\sin(\theta_{0,k})\right) \times \frac{1}{\Delta f_k}} \tag{4.34}$$

This frequency offset (Δf_{k+1}) ensures the FDA beam pattern maxima with power peaks at the predicted target position $\left(\hat{\theta}_{0,k+1}, \hat{r}_{0,k+1}\right)$.

Fig- 4.3 shows the information flow in the generic form. The system state at time k is denoted as $\mathbf{x}_k$, which contains target angle and range information at time k.

The HCFDA transmitted beam pattern results in observation vector $\mathbf{z}_k$ at time $k-1$. The complete computation sequence at k^{th} instant is stated as under

i) It finds a filtered state estimate $\mathbf{x}_k$ i.e., $\hat{\mathbf{x}}_{k/k}$,

ii) Afterwards, it calculates filtered error covariance matrix $\hat{\boldsymbol{\Gamma}}_{k/k}$ to estimate target future state.

iii) It also estimates the next state i.e., $\hat{\mathbf{x}}_{k+1/k}$

iv) It estimates the error covariance matrix i.e., $\hat{\boldsymbol{P}}_{k+1/k}$.

v) The predicted state is sent as feedback.

vi) The transmitter computes new value of frequency offset for new cycle.

vii) It generates an FDA beam pattern ensuring power peaks towards the target predicted position.

viii) The design repeats the sequences for improved performance.

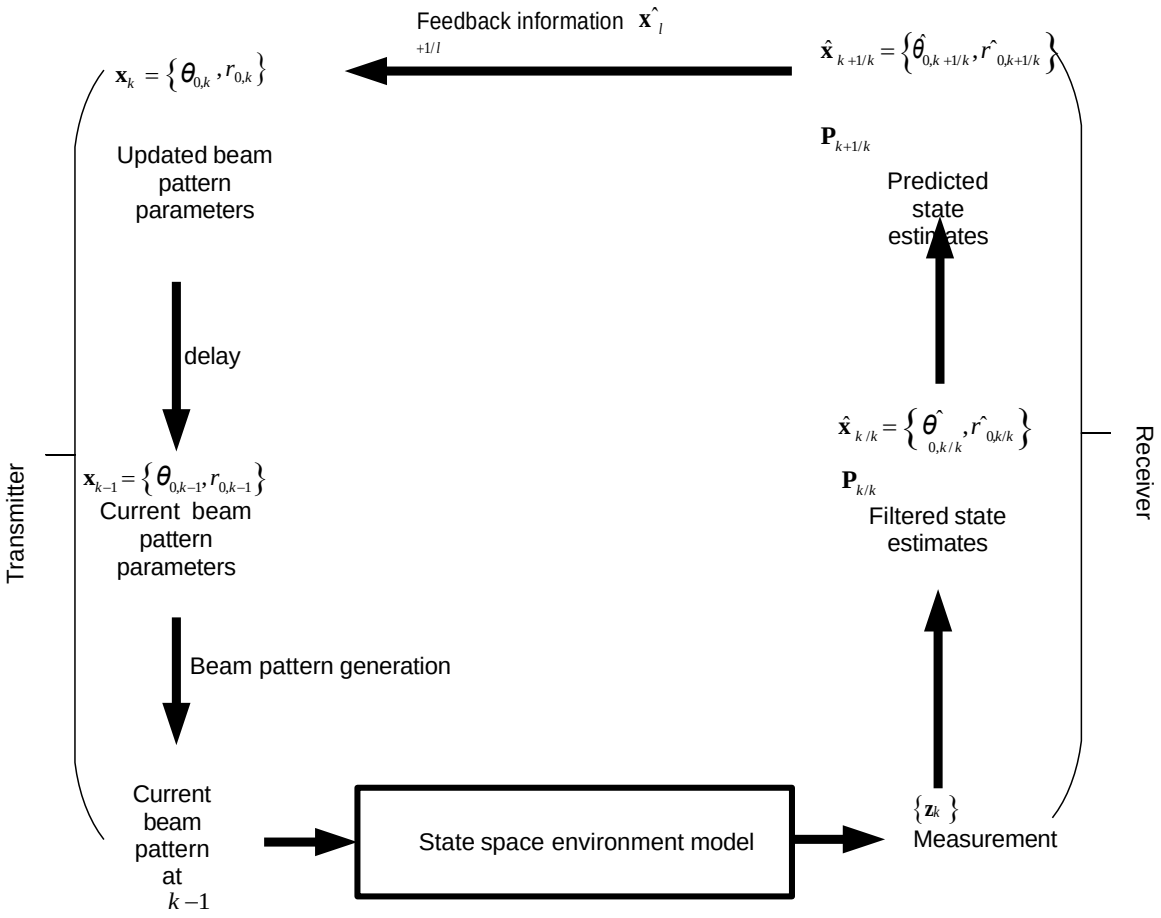

Figure- 4. 3: Information flow cycle in basic form for HCFDA design

4.3. Performance of the HCFDA radar design having uniform frequency offset

The performance analysis of the proposed HCFDA design has been given below in terms of energy efficiency, SINR and detection performance. Matlab 2012 and its toolbox *optimtool,* has been used for simulations purposes. The carrier frequency is kept 1 GHZ and we considered the receiving and transmitting arrays having 10 elements each with half wavelength inter-element distance.

4.3.1. Energy efficiency

We consider a surveillance region that lies between $-\pi/2$ to $\pi/2$ (Fig 4.4. (a)). As the proposed HCFDA transmitter merely steers the predicted target position (Fig 4.4. (b)), in contrast with a conventional FDA transmitter that steers whole surveillance region. Therefore, the ratio of energy transmitted by the proposed HCFDA transmitter to conventional FDA transmitter is given by

$$\eta \cong \frac{\theta_{0_{HP}}}{\pi} \times 100 \tag{4.35}$$

where $\theta_{0_{HP}}$ denotes the half-power beam width (HPBW) of FDA beam pattern towards θ_0 direction. We ignore the effect of side lobes on this ratio. Consequently, the proposed HCFDA design saves $(100-\eta)\%$ energy in comparison with the conventional FDA radar. Additionally, it consequences in decreased electromagnetic pollution of environment.

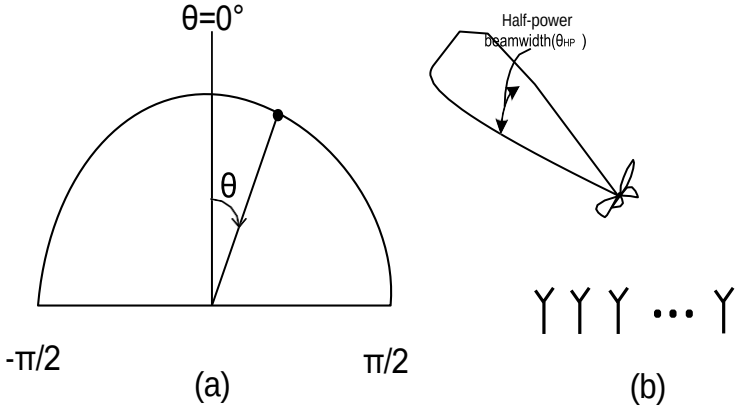

Figure- 4. 4: Comparison of the transmitted energy in one cycle by (a) a conventional FDA radar (b) the proposed HCFDA radar

4.3.2. DOA estimation performance

The radar-returns are received at the GA based DOA estimation block. The parameter settings of GA used for *optimtool toolbox* of Matlab are given in Table 4.1.

Table-4. 1: Parameters settings of the GA for HCFDA design

GA parameter settings	
Parameters	**Settings**
Population size	20
Chromosome size	1
Creation function	Uniform
Selection function	Stochastic uniform
Reproduction crossover fraction	0.8
Mutation function	Adaptive feasible
Crossover function	Heuristic
Migration direction	Both
No of generations	500
Function tolerance	1e-22
Nonlinear constraint tolerance	1e-22

We assumed a single target in the surveillance region. The following Table 4.2 shows the DOA estimation performance of proposed design.

Table-4. 2: Accuracy analysis of target direction estimation for HCFDA design

DOA estimation results using GA					
Actual DOA	0°	40°	50°	-30°	-45°
Estimated DOA	0.0001°	40.0012°	49.9841°	-30.0012	-44.9988

The estimation performance shows satisfactory results and it has been evaluated for five different discrete time instants.

4.3.3. Target range estimation performance

The total time delay is computed as 30μs for the range estimation of target. We assume that the target is at $\theta_0 = 0°$. Therefore, the computed target range is $r_0 = 4500m$.

In the same way, we can compute target ranges at different discrete time instants easily.

4.3.4. Prediction performance of the target future state using EKF

The filtered target position $\left(\hat{\theta}_{0,k}, \hat{r}_{0,k}\right)$ computed at discrete time *k* is passed to the HCFDA prediction block. An EKF predicts future position of target i.e. $\left(\hat{\theta}_{0,k+1}, \hat{r}_{0,k+1}\right)$. We can define a state of a nonlinear system as $\mathbf{x} = \begin{bmatrix} \theta & \dot{\theta} & r & \dot{r} & \xi \end{bmatrix}^T$, where θ denotes an direction or angle component of the target position, $\dot{\theta}$ represents a velocity component along angle dimension, *r* denotes a range component of target position, $\dot{r}$ represents velocity component along range dimension and ξ denotes the turn rate. We can write the nonlinear transitional matrix as

$$F = \begin{bmatrix} 0 & 1 & 0 & 0 & 0 \\ 0 & \xi & 0 & 0 & 0 \\ 0 & 0 & 0 & 1 & 0 \\ 0 & 0 & 0 & \xi & 0 \\ 0 & 0 & 0 & 0 & 0 \end{bmatrix}$$

The process noise assumed to be zero mean AWGN with covariance matrix given as $\mathbf{Q} = diag[0, \sigma_1^2, 0, \sigma_2^2, \sigma_2^2]$, where $\sigma_1^2 = \sigma_2^2 = 0.25$.

Similarly, the measurement matrix can be given as

$$\tilde{H} = \begin{bmatrix} 1 & 0 & 0 & 0 & 0 \\ 0 & 0 & 1 & 0 & 0 \end{bmatrix}$$

The measurement noise is assumed to be zero mean AWGN with covariance matrix given as $\mathbf{R} = diag([\sigma_\theta^2, \sigma_r^2])$, where $\sigma_\theta^2 = 0.01$ and $\sigma_r^2 = 0.2$. Fig. 4.5 shows the EKF tracking performance for two nonlinear trajectories..

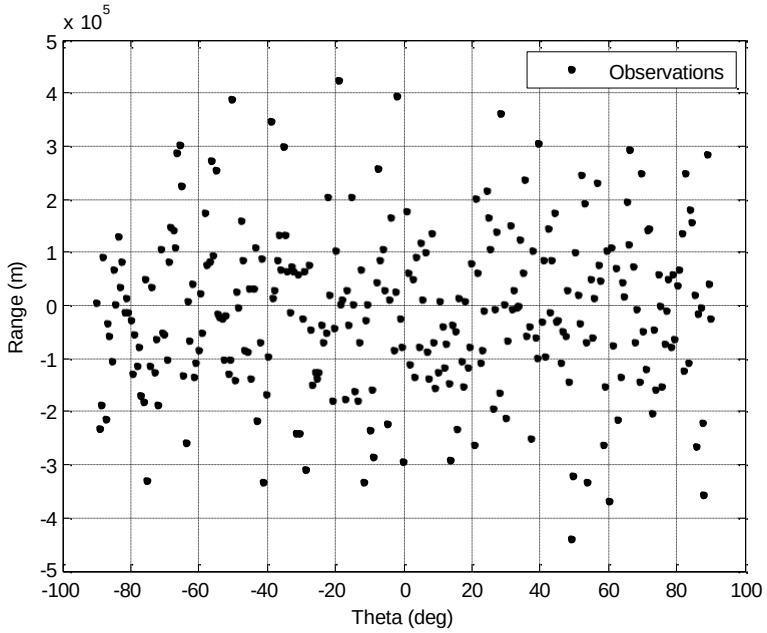

(a) Observation for trajectory 1

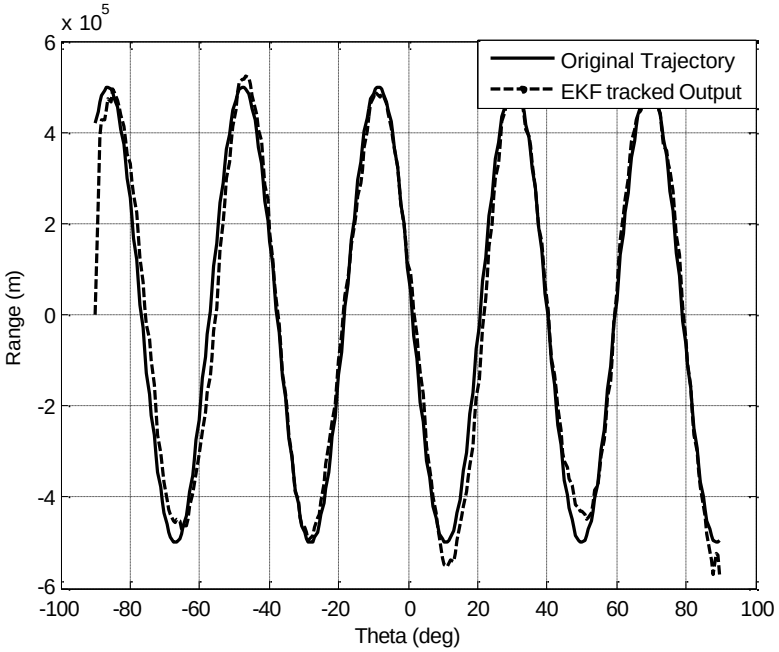

(b) prediction performance of EKF for trajectory 1

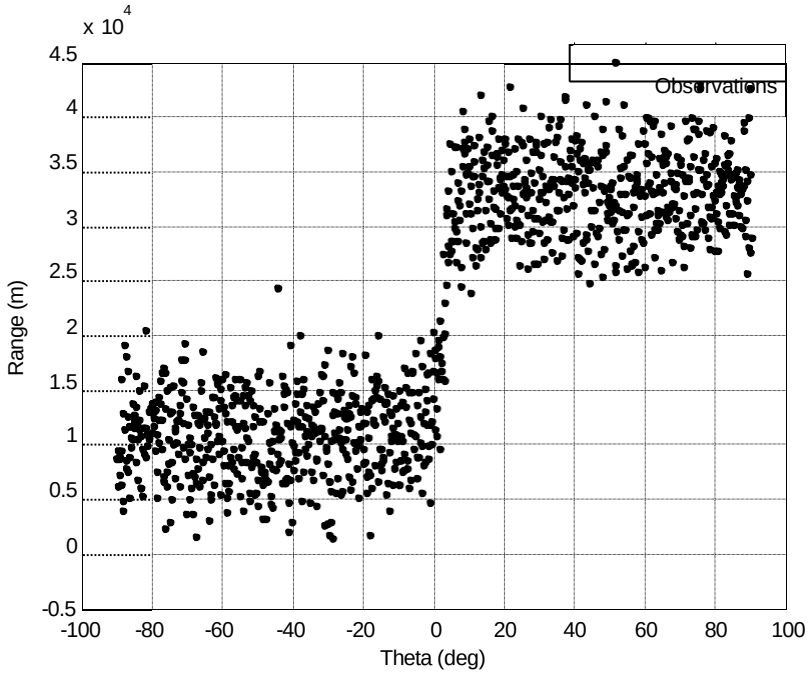

(c) Observations of trajectory2

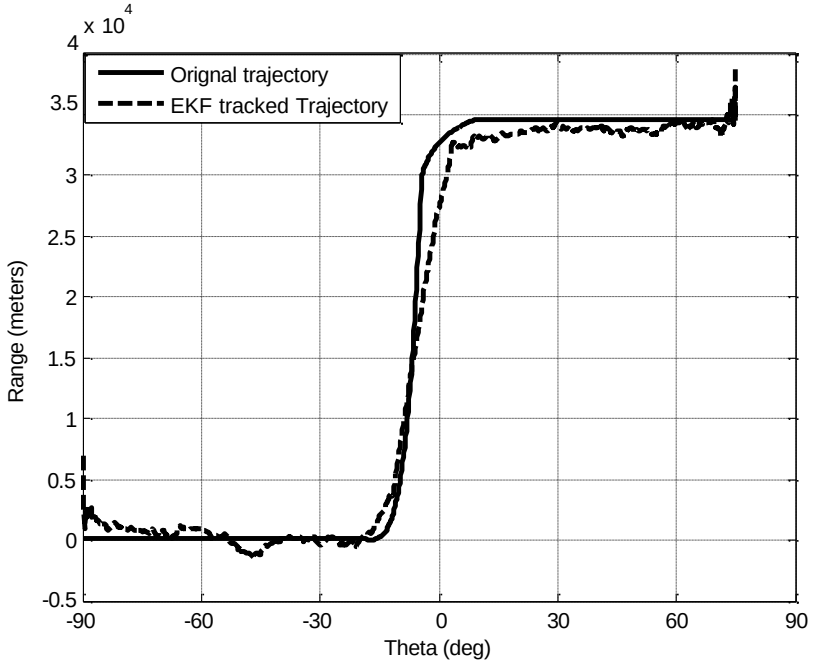

(d) prediction performance of EKF of trajectory 2

Figure- 4. 5: (a) & (c) Observations (b) & (d) target position estimation results using EKF

Figs- 4. 5 (a) & (c) show the trajectory observations, while Figs- 4.5(b) & (d) show the EKF tracking performance. The EKF predicts the target next position with affordable

error. The EKF predicted target position $\left(\hat{\theta}_{0,k+1}, \hat{r}_{0,k+1}\right)$ is tunneled as feedback connecting the receiver to the transmitter.

4.3.5. The transmitter beamforming performance

The receiver sends the predicted position of target $\left(\hat{\theta}_{0,k+1}, \hat{r}_{0,k+1}\right)$ to transmitter i.e., $\left(-30°, 3\times10^5\, m\right)$.The current target position and frequency offset are $\left(-32°, 3.03\times10^5\, m\right)$ and $0.26\, kHz$, respectively. The frequency offset for next cycle is computed and it comes out as $0.25k\, Hz$. Table-4.3 shows the frequency offsets for generating FDA beam pattern with maxima at the predicted target position $\left(\hat{\theta}_{0,k+1}, \hat{r}_{0,k+1}\right)$.

Table-4. 3: Computed frequency offset values corresponding to positions of target

Cycle Instant	(θ, r)	(Δf)
k^{th} (current)	$\left(-32°, 3.03\times10^5\, m\right)$	$0.26k\, Hz$
$(k+1)^{th}$ (predicted)	$\left(-30°, 3\times10^5\, m\right)$	$0.25k\, Hz$

Fig-4.6 (a) shows an FDA beam-pattern with $\Delta f = 0.25k\, Hz$. Figs- 4.6 (b) & (c) show 2-D views of FDA beam pattern, which guarantee maximum power peaks at the target predicted angle $-30°$ and range value $3\times10^5\ m$, respectively.

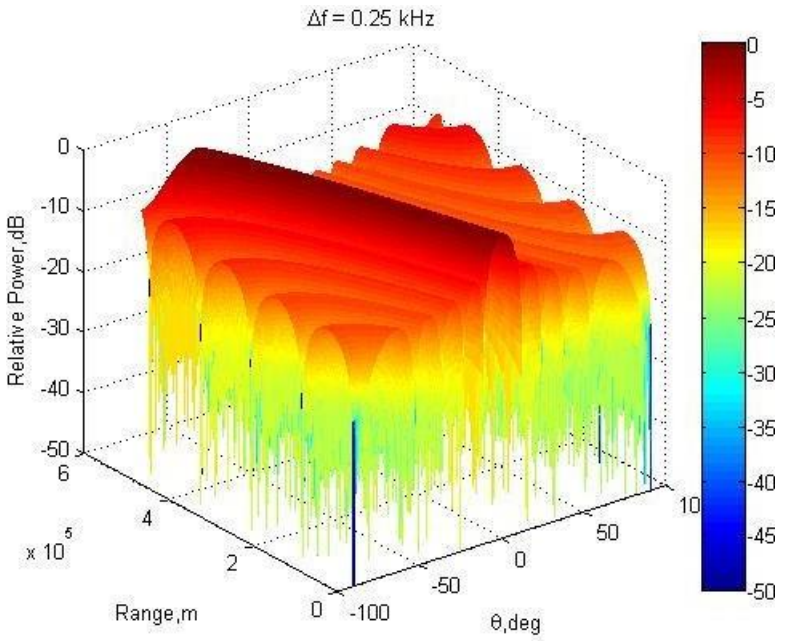

(a)

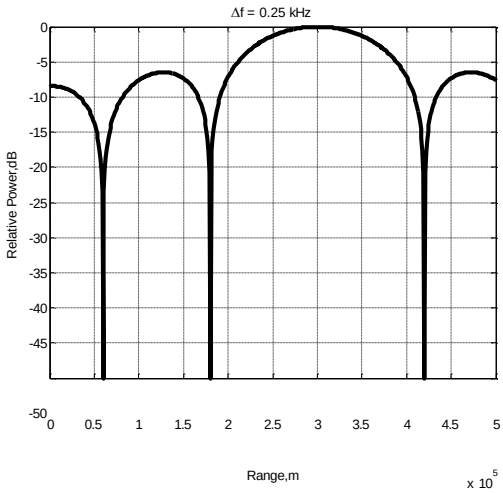

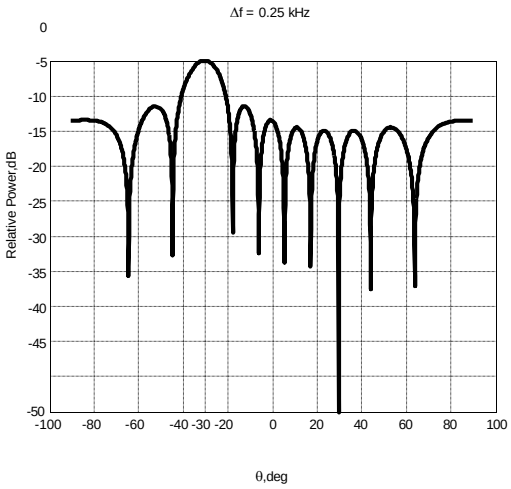

(b) (c)

Figure- 4. 6 : (a)-(c) FDA generated beam pattern with parameters given as $fo=1GHz$, $\Delta f=0.25kHz$, $N=10$, $d=\lambda/2$

Likewise, Fig-4.7 (a) shows an FDA beam pattern with $\Delta f=0.26\,kHz$. Figs. 4.7 (b) & (c) show 2-D view of this FDA beam pattern, which promises peak power towards target

position$\left(-32°, 3.03\times10^{5}\ m\right)$.

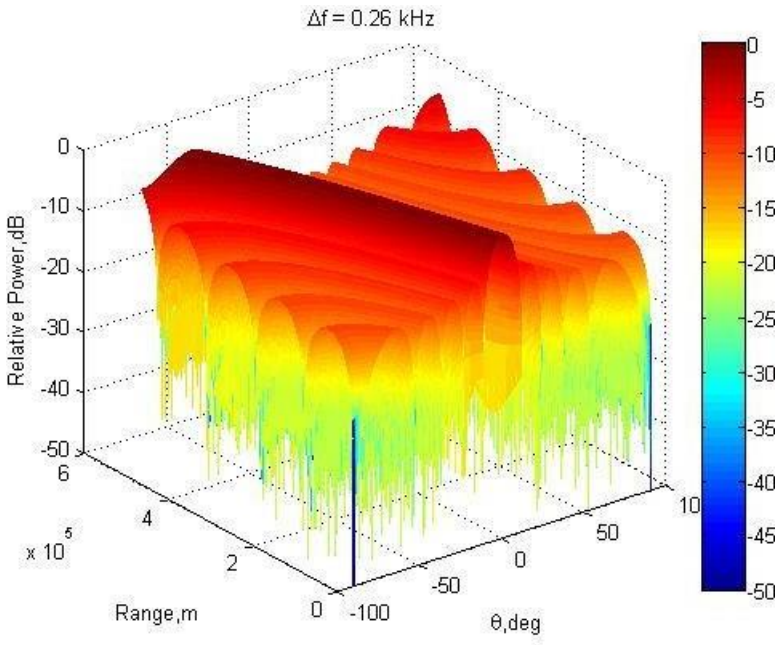

(a)

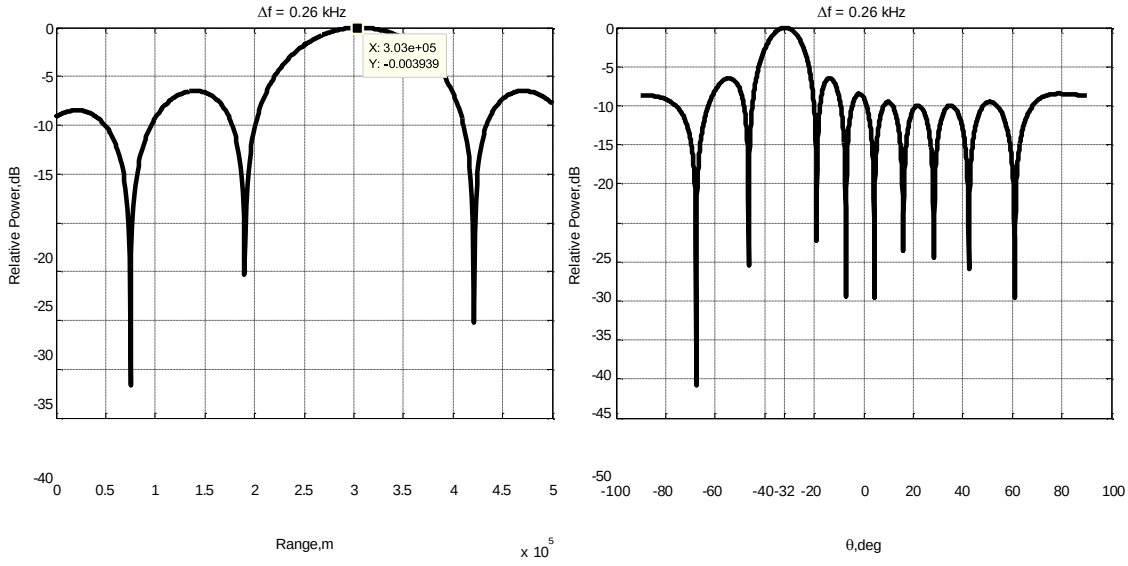

(b) (c)

Figure- 4. 7: (a)-(c) FDA generated beam pattern with parameters given as $fo=1GHz, \Delta f=0.26kHz, N=10, d=\lambda/2$

4.4. Overall SINR and Detection performance of the proposed HCFDA

The SINR and detection performance of the proposed HCFDA is given below. We assume the position of target is at $(0^{\circ}, 300\,km)$, while the position of interferer is at $(10^{\circ}, 350\,km)$. We assume that noise power is fixed to $0\,dB$, while INR is taken as $40\,dB$.

4.4.1. SINR performance of HCFDA

The SINR is computed for a conventional PAR, a cognitive radar with fixed Δf and the proposed technique with adaptive Δf calculated at each cycle. Fig.4.8 confirms a significantly improved SINR using the proposed technique.

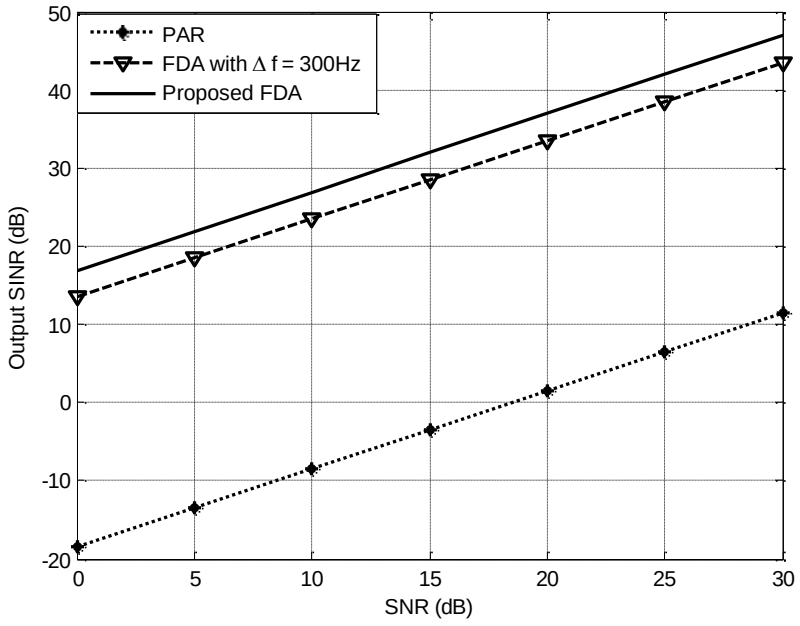

Figure- 4. 8: SNR vs. SINR performance of the cognitive FDA

4.4.2. Detection performance of HCFDA

We have kept a constant false alarm probability p_{fa}, while the SNR= 3dB. Fig. 4.9 shows the detection performance of proposed HCFDA radar as compared to conventional FDA with fixed frequency offset and conventional PAR. The proposed HCFDA radar design achieves improved detection performance due to the fact that a relatively higher SNR is achieved at the receiver.

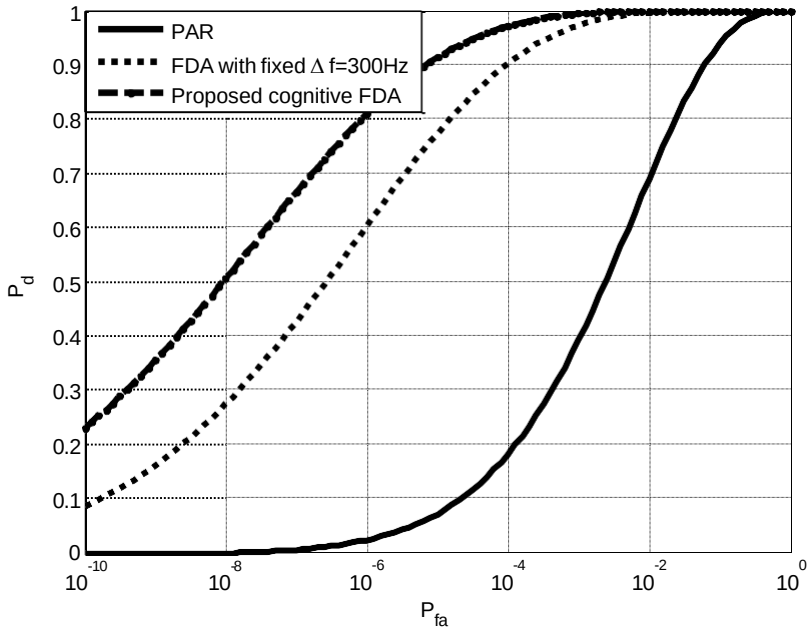

Figure- 4. 9: Comparison of detection performance (probability of false alarm vs. detection probability)

4.5. Conclusion and discussion on HCFDA performance

The proposed design adjusts its attributes, intelligently, based on receiver feedback for improved performance. It ensures power peaks towards the predicted range and direction of the target, which resulted in improved SINR and detection probability.

CHAPTER-5

Hybrid Cognitive Frequency Diverse Array (HCFDA) Radar with Symmetric Non-Uniform Frequency Offset

In this chapter, we have proposed a new design of hybrid cognitive frequency diverse array (HCFDA) radar with non-uniform but symmetric frequency offset applied at the input of array. A brief introduction of FDA and cognitive radar (CR) is presented at the beginning of the chapter followed by the major challenges in a conventional FDA radar. Moreover, four novel methods to compute the non-uniform frequency offsets are presented. The non-uniform frequency offsets enable the transmitter to generate a single maximum range-angle-dependent beam patterns with reduced half power beam width (HPBW).

In the last section of the chapter, the overall performance HCFDA radar design with non-uniform but symmetric frequency offset has been evaluated in terms of SINR, detection performance, range resolution, angle resolution and transmit energy focusing. Cramer Rao lower bounds (CRLB) on range and angle estimations has also been taken into consideration, while evaluating the radar performance.

5.1. Introduction

A frequency diverse array (FDA) radar with uniform inter-element frequency offset generates a range-angle dependent beam pattern, which exhibits maxima at multiple

range and angle values [76]. It also causes broadening of half power beam width (HPBW). Certainly, this multiple maxima property and broadening of the main beam are undesirable due to the facts that they allow the interferers located at any of the maxima to affect the target- returns. Moreover, they also result in decreasing the maximum reachable range and range resolution. Another limitation is its inability to localize the targets and interferences having same direction but different ranges. The ultimate result is weak signal to interference noise ratio (SINR), which degrades the probability of detection and parameter estimation performance.

Non- uniform frequency offsets coefficients, which may be fractional or integer values, achieve a single maximum beam pattern at the target position and sharpen HPBW. This chapter presents the calculations of these non-uniform frequency offset using following four methods:

i) Application of a well-known $mu-law$ [175]–[177] companding schemes for computing non-uniform fractional frequency offset in each step of an iterative cognitive algorithm to generate single maximum range–angle beam pattern.

ii) Application of a well-known genetic algorithm (GA) [153], [162] to compute non-uniform fractional frequency offsets for localizing multiple targets and interferers having same direction but different ranges.

iii) Application of a well-known Hamming window [36], [178], [179] to compute non-uniform tapering fractional frequency offset for improved transmit energy focusing towards the target position.

iv) Application of non-uniform integer coefficients of frequency offsets for achieving sharpened HPBW.

Considering the application of mu-law for HCFDA design, a non-uniform expanded or compressed set of the frequency offset across the array is obtained. This enables the FDA to generate a single maxima beam pattern for interference suppression along with disturbing the main beam pattern in either way i.e., sharpening or broadening. The width of main beam in the proposed scheme is kept inversely proportional to the prediction accuracy for improved performance.

In the second case given above, the GA is used at the transmitter to focus the energy towards the targets positions and suppress interferences having same direction but different ranges. The predicted positions of target and interferences are received through receiver feedback.

In the third case given above, Hamming window has been applied to compute non-uniform frequency offset for focusing the transmit energy with suppressed side lobe levels towards the target predicted position received as feedback from the receiver.

In the fourth case given above, the integer based non-uniform frequency offsets are applied to get sharper HPBW towards the target position received as feedback.

The non-uniform frequency offset values are calculated at each cycle to achieve a better detection probability, an improved SINR, improved range and angle resolution, improved transmit energy focusing and better CRLB on range and angle estimation. The simulations on these parameters are compared to the existing well-known radar designs.

It is also observed that the symmetric pattern [44] of offsets around the central element achieves better null depths as compared to non-symmetric pattern. The effectiveness of proposed scheme has been evaluated in simulations, which indicates an outclass performance as compared to the previous similar works.

In summary, the automatic adjustments of the radar parameters in this case i.e., the selection of suitable inter-element frequency offset values, leads to an improved performance in a moving target situation.

5.2. Proposed HCFDA design with non-uniform frequency offset

This section describes the block diagram of proposed system design. Fig- 5.1 shows the information flow of proposed system. The proposed receiver consists of four sub- blocks i.e., DOA and range estimation, receiver selector, EKF-based predictor and a memory block. The proposed transmitter consist of two sub-blocks i.e., a transmit selector and the FDA antenna block with non-uniform frequency offsets.

The FDA antenna block of transmitter illuminates the radar environment containing potential targets. The DoA and range estimation block of receiver, collect the reflected echoes to estimate the target DoA and range using well known MUSIC algorithm [39], [180], [181] and conventional range estimation formula, respectively. The receiver selector, a sub-block of receiver, calculates the weight vector $\mathbf{w}_R$ using minimum variance distortion less response (MVDR) adaptive beam-former to improve the SINR performance. Consequently, the current target position estimates $\left(\hat{\theta}_{0,k}, \hat{r}_{0k}\right)$ are forwarded to the EKF based predictor for estimating the target predicted position $\left(\tilde{\theta}_{0,k+1}, \tilde{r}_{0,k+1}\right)$.

This estimated position along with the prediction error $\tilde{e}$ is sent as feedback to the transmitter. The transmit selector, a sub-block of transmitter, examines the prediction error e to decide an appropriate method to compute the non-uniform frequency offset values.

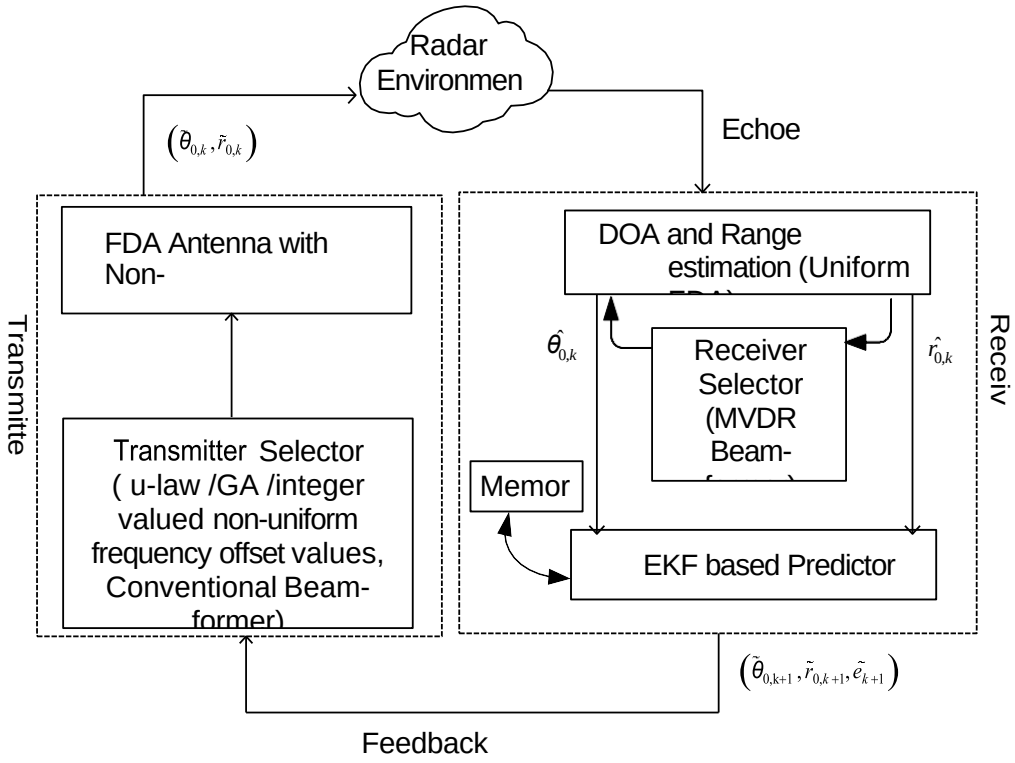

Figure- 5. 1: Block diagram of the proposed radar

The frequency offset values are computed using one of the techniques stated above, i.e., the *mu-law*, the GA, the Hamming window or the non-uniform integer value coefficients. A conventional beam-former calculates the vector $\mathbf{w}_T$ to generate maxima in the target predicted direction $(\tilde{\theta}_{0,k+1}, \tilde{r}_{0,k+1})$. The perception-action cycle keeps on repeating itself for improved performance. The receiver and transmitter of the proposed design are discussed below in detail.

5.2.1. The Receiver

The DOA estimation, range estimation and EKF based prediction algorithm blocks of the receiver have been discussed below.

5.2.1.1. DOA estimation using ROOT MUSIC algorithm

ROOT MUSIC algorithm, one of the well-known DOA or angle of arrival (AOA) estimation algorithms, has been used to estimate the target direction in this chapter. It has the ability to resolve multiple signal directions, simultaneously, with affordable computational time[182].

Consider a conventional symmetric FDA having $M = 2K+1$ elements with inter element distance taken as $d = \lambda/2$. Let θ_0 be the location of the target to be estimated, measured from the middle element i.e., origin of the array in this case. Considering uniform weights at the receiver array, signal received by m^{th} element is given by [82]

$$x_m(t) = s_T\left(t - \frac{r_0}{c}\right)\exp\left\{j2\pi f_m\left(t - \frac{r_m}{c}\right)\right\} + n_m(t);\ \ m = 0, \pm 1, ..., \pm K \tag{5.1}$$

The total signal received at the array input is

$$x_m(t) = s_T\left(t - \frac{r_0}{c}\right)\sum_{m=-K} \exp\left\{j2\pi f_m\left(t - \frac{r_m}{c}\right)\right\} + n_m(t) \tag{5.2}$$

where $f_m = f_0 + m\Delta f;\ m = 0, \pm 1, ..., \pm K$ and $r_m = r_{ref} - md\sin\theta_0$

Defining $\phi_1 = 2\pi f_m\left(t - \frac{r_{ref}}{c}\right)$ and $\phi_m = 2\pi f_m\left(t - \frac{md\sin\theta_0}{c}\right)$

Then, the above equation can be rewritten as

$$x_m(t) = s_T\left(t - \frac{r_0}{c}\right)\exp(j\phi_1)\sum_{m=-K}^{\hat{}} \exp(j\phi_m) + n_m(t) \tag{5.3}$$

Defining $s_T\left(t - \frac{r_0}{c}\right)\exp(j\phi_1) = S(t)$ and representing the above equation in vector form

$$\begin{bmatrix} x_{-K}(t) \\ \vdots \\ x_{K}(t) \end{bmatrix} = S(t) \begin{bmatrix} \exp(j\phi_{-K}) \\ \vdots \\ \exp(j\phi_{K}) \end{bmatrix} + \begin{bmatrix} n_{-K}(t) \\ \vdots \\ n_{K}(t) \end{bmatrix} \tag{5.4}$$

Or equivalently, it can written as

$$\mathbf{x}(t) = \mathrm{S}(t)\left(\mathbf{a}(\phi)\right) + \mathbf{n}(t) \tag{5.5}$$

here $\mathbf{a}(\phi)$ is the steering vector. We assume that F far field target signals are impinging on the array, then the output of array can be written as (ignoring t without the loss of generality)

$$\mathbf{U} = \sum_{l=0}^{F-1} S_l \mathbf{a}(\phi_l) + \mathbf{n} \tag{5.6}$$

The covariance matrix $\mathbf{R}_u$ is given as

$$\mathbf{R}_u = \mathbf{A}\mathbf{R}_s\mathbf{A}^H + \sigma_n^2\mathbf{I} \tag{5.7}$$

If $\lambda_1 \geq \lambda_2 \geq \lambda_3 ..... \geq \lambda_P$ be the Eigen values of this matrix $\mathbf{R}_u$, $v_1 \geq v_2 ..... \geq v_L$ be the Eigen values of $\mathbf{A}\mathbf{R}_s\mathbf{A}^H$ and $\mathbf{q}_1, \mathbf{q}_2, \mathbf{q}_3 ..... \mathbf{q}_P$ be Eigen vectors of $\mathbf{R}_u$, we can state that

$$\lambda_i = \begin{cases} v_i + \sigma_n^2 & i = 1, 2, ..., \mathrm{F} \\ \sigma_n^2 & i = F+1, ..., \mathrm{M} \end{cases} \tag{5.8}$$

Therefore, $\mathbf{A}^H\mathbf{q}_i = 0; i.e.\ a_k^H(\phi) q_i = 0;\ i = F+1, ..., \mathrm{M}$ and $k = 1, 2, ..., \mathrm{F}$

5.2.1.2. Target Range estimation

The time delay to reach the target using FDA beam pattern depends upon the distance of target from transceiver and frequency offset value used [81]. Therefore, time t_d taken by

a transmitted signal to reach a far field target can be given as [81]

$$t_d = \frac{r_0}{c} + \left[g - \frac{d}{\lambda} \sin(\theta_0) \right] \left(\frac{1}{\Delta f} \right) \tag{5.9}$$

where c is speed of light, r_0 is range of far field target, θ_0 is target direction, Δf is frequency offset value used and g is an integer, which stands for grating lobes.

Likewise, the time t_r taken by reflected echo to reach the receiver is given by

$$t_r = \frac{r_0}{c} \tag{5.10}$$

Therefore, the total time delay T_d is expressed as

$$T_d = t_d + t_r = \frac{2r_0}{c} + \left[g - \frac{d}{\lambda} \sin(\theta_0) \right] \left(\frac{1}{\Delta f} \right) \tag{5.11}$$

With the known angle information (θ_0), the target range can be calculated as

$$r_0 = \frac{c}{2} \left| T_d - \left\{ g - \frac{d}{\lambda} \sin(\theta_0) \right\} \left(\frac{1}{\Delta f} \right) \right| \tag{5.12}$$

Hence, the target range can be estimated at every cycle.

5.2.1.3. The EKF algorithm for position prediction estimation

For a radar environment, which is assumed nonlinear but can be made locally linear, extended Kalman filter (EKF) is one of the best choices in hand for implementation of prediction block. The process equation of state space model is described by [48]

$$\mathbf{x}_{k+1} = \tilde{\mathbf{F}} \mathbf{x}_k + \boldsymbol{n}_k \tag{5.13}$$

where $\mathbf{x}_k$ denotes the state of system at discrete time k, $\tilde{\mathbf{F}}$ denotes a nonlinear transition matrix, while $\boldsymbol{n}_k$ denotes process noise and assumed to be zero mean Gaussian noise with

covariance matrix **Q** as

$$\boldsymbol{E}\left[\mathbf{n}_k \mathbf{n}_l^T\right] = \boldsymbol{Q}_k \delta_{lk} \tag{5.14}$$

Likewise, the measurement equation is described as [48]

$$\boldsymbol{z}_k = \tilde{\mathbf{H}}\mathbf{x}_k + \boldsymbol{v}_k \tag{5.15}$$

where $\boldsymbol{z}_k$ denotes an observation vector at discrete time k, $\tilde{\mathbf{H}}$ denotes a nonlinear measurement matrix, while $\boldsymbol{v}_k$ is measurement noise assumed to be zero mean Gaussian with covariance matrix $\mathbf{R}$, given as

$$\boldsymbol{E}\left[\boldsymbol{v}_k \boldsymbol{v}_l^T\right] = \boldsymbol{R}_k \boldsymbol{\delta}_{lk} \tag{5.16}$$

It is also assumed that the process and measurement noises are statistically independent of each other. The Gaussian distribution can be completely characterized by a mean and covariance and so is given as[30], [117]

$$\hat{\mathbf{x}}_{k/k} = E\left[\mathbf{x}_k \mid \mathbf{z}_1^k\right] \tag{5.17}$$

$$\hat{\mathbf{x}}_{k+1/k} = E\left[\mathbf{x}_{k+1} \mid \mathbf{z}_1^k\right] \tag{5.18}$$

Similarly, the filtered and predicted covariance matrices are given as [117]

$$\hat{\mathbf{P}}_{k/k} = E\left[\left(\mathbf{x}_k - \hat{\mathbf{x}}_{k/k}\right)\left(\mathbf{x}_k - \hat{\mathbf{x}}_{k/k}\right)^T \mid \mathbf{z}_1^k\right] \tag{5.19}$$

$$\hat{\mathbf{P}}_{k+1/k} = E\left[\left(\mathbf{x}_{k+1} - \hat{\mathbf{x}}_{k+1/k}\right)\left(\mathbf{x}_{k+1} - \hat{\mathbf{x}}_{k+1/k}\right)^T \mid \mathbf{z}_1^k\right] \tag{5.20}$$

Hence, the state prediction error is defined by

$$\tilde{\mathbf{x}}_{k+1/k} \triangleq \mathbf{x}_{k+1} - \hat{\mathbf{x}}_{k+1/k} \tag{5.21}$$

where $\hat{\mathbf{x}}_{k+1/k} = \tilde{\mathbf{F}}\hat{\mathbf{x}}_{k/k}$.

Similarly, the prediction measurement error $\tilde{\mathbf{e}}$ is defined as

$$\tilde{\mathbf{e}}_{k+1/k} \triangleq \mathbf{z}_{k+1} - \hat{\mathbf{z}}_{k+1/k} \tag{5.22}$$

where $\hat{\mathbf{z}}_{k+1/k} = \tilde{\mathbf{H}}_{k+1}\hat{\mathbf{x}}_{k+1/k}$

The prediction error and prediction measurement error are meant to be minimized and are strongly dependent on the returned echoes. But in the case of more non-stationary radar environment, the target position prediction and filtering may become a challenging task. As all estimators have inherent errors and their magnitude is a function of target maneuver. If beam positional resolution does not match actual spatial dislocation of target, beam will frequently lose track and enter search mode. Consequently, the detection performance may deteriorate.

To cope up with this problem, the transmitter of proposed radar system is linked with the receiver to intelligently change its parameters keeping in touch with the environmental changes, as done by a cognitive radar. Therefore, the predicted target position computed at the receiver along with the estimation errors are tunneled as feedback to the transmitter to adjust its parameters adaptively.

5.2.2. The Transmitter:

The non-uniform FDA design, calculation of non-uniform frequency offsets and non-uniform FDA transmit beamforming have been discussed below.

5.2.2.1. Non-uniform FDA antenna

Fig. 5.2 shows the proposed uniformly-spaced FDA antenna with non-uniform frequency offsets, having symmetrical elements around the origin. This symmetry is with respect to frequency offsets. The inter-element distance is d and total number of elements is $N = 2P + 1$, here P is the maximum number of elements on each side of array from origin, while w_n are the transmitter weights.

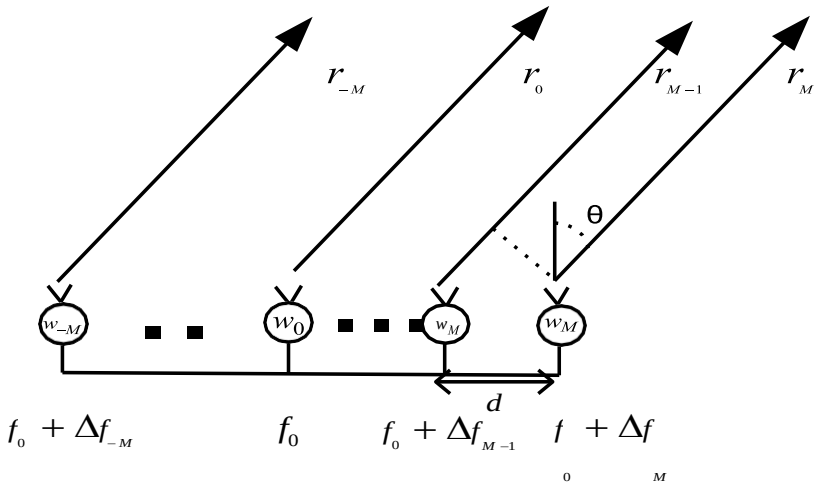

Figure- 5. 2: The proposed frequency diverse array structure

The frequency input at n^{th} element is given as

$$f_n = f_0 + \Delta f_n \; ; \qquad n = 0, \pm 1, ..., \pm P \tag{5.23}$$

here, f_0 is the fundamental frequency, Δf_n is the frequency offset of n^{th} element with reference to f_0 , and is given by

$$\Delta f_n = \alpha_n \Delta f \tag{5.24}$$

α_n are a set of non-uniform frequency offset coefficients. These coefficients are either integers or fractional values but non-uniform. In the fractional coefficient computation case, these are further divided into three categories i.e., the computation using the *mu- law*, the GA or the Hamming window according to the requirement.

5.2.2.2. Non-uniform FDA beam pattern and Transmit Beamforming

Consider a far field target, the phase of signals transmitted by the middle (reference) and adjacent elements are given by [83]

$$\Psi_0 = \frac{2\pi f_0}{c} r_0 \qquad and \qquad \Psi_1 = \frac{2\pi f_1}{c} r_1 \tag{5.25}$$

here, c is speed of light, while r_0 and r_1 are the target distances from reference and adjacent elements, respectively. The frequency f_1 is given as $f_1 = f_0 + \Delta f_1$, while $\Delta f_1 = \alpha_1 \Delta f$ and $r_1 = r_0 - d\sin\theta$, where θ is the target direction. The phase difference of these signals is given as

$$\Psi_1 - \Psi_0 = -\frac{2\pi d \sin\theta}{c}\left[f_0 + \alpha_1 \Delta f - \frac{\alpha_1 \Delta f r_0}{d\sin\theta} \right] \tag{5.26}$$

Similarly, the phase difference between reference and P^{th} element can be written as

$$\Psi_M - \Psi_0 = -\frac{2\pi d \sin\theta}{c}\left[f_0 P + \alpha_P P\Delta f - \frac{\alpha_P \Delta f r_0}{d\sin\theta} \right] \tag{5.27}$$

since $f_0 \gg \alpha_P \Delta f$ and $r_0 \gg \alpha_P d\sin(\theta)$, hence the term containing their product, i.e., $\frac{2\pi \alpha_p P \Delta f d \sin\theta}{c}$ may be neglected. In case of far filed targets i.e., $r_n \approx r$, the steering vector $\mathbf{a}(\theta, r, \alpha)$ can be taken as

$$\mathbf{a}(\theta,r,\alpha) = \begin{bmatrix} e^{j\left(\frac{2\pi f_0 P d \sin\theta}{} - \frac{2\pi . \alpha_{EP} \Delta f . r}{}\right)}, \ldots, e^{j\left(\frac{2\pi f_0 d \sin\theta}{} - \frac{2\pi . \alpha_{E1} \Delta f . r}{}\right)}, \\ 1, e^{-j\left(\frac{2\pi f_0 d \sin\theta}{} - \frac{2\pi . \alpha_{\theta} . \Delta f . r}{}\right)}, \ldots, e^{-j\left(\frac{2\pi f_0 P d \sin\theta}{} - \frac{2\pi . \alpha_P \Delta f . r}{}\right)} \end{bmatrix} \tag{5.28}$$

It can be represented in vector form, given as

$$\mathbf{a}(\theta, r) = \mathbf{a}(\theta) \odot \mathbf{a}(r, \alpha) \tag{5.29}$$

where

$$\mathbf{a}(\theta) = \left[e^{j\left(\frac{2\pi f_0 P d \sin\theta}{}\right)}, \ldots, e^{j\left(\frac{2\pi f_0 d \sin\theta}{}\right)}, 1, e^{-j\left(\frac{2\pi f_0 d \sin\theta}{}\right)}, \ldots, e^{-j\left(\frac{2\pi f_0 P d \sin\theta}{}\right)} \right] \tag{5.30}$$

and

$$\mathbf{a}(r,\alpha)=\left[e^{-j\left(\frac{2\pi.\alpha_{eP}\Delta f.r}{c}\right)},...,e^{-j\left(\frac{2\pi.\alpha_{e1}\Delta f.r}{c}\right)},1,e^{j\left(\frac{2\pi.\alpha_{1}\Delta f.r}{c}\right)},...,e^{j\left(\frac{2\pi.\alpha_{P}\Delta f.r}{c}\right)}\right] \tag{5.31}$$

It can be noted that these non-uniform frequency offsets only affect the range steering vector i.e., $\mathbf{a}(r,\alpha)$. The FDA beam pattern is a function of angle (θ) and range (r), therefore, following observations are in line [80]:

(i): If we take $\Delta f=0$, then it reduces to a conventional phased array radar (PAR) pattern.

(ii): If the values of α_n are taken uniform, a conventional FDA beam pattern is generated.

(iii): The non-uniform frequency offset does not affect the angle dimension of beam pattern as there is no α_n in $\mathbf{a}(\theta)$ vector.

If a desired target position is at $(\hat{\theta_0},\hat{r_0})$, then the weights for steered beam pattern to achieve a maximum gain, can be given as

$$w_{T,n}=\exp\left\{-j2\pi f_n\left(\frac{\alpha_n\Delta f\hat{r_0}}{c}+\frac{ndsin(\hat{\theta}_0)}{c}\right)\right\},\quad n=0,\pm1,...,\pm P \tag{5.32}$$

where $w_{T,n}$ is a weight of n^{th} transmitter element. The array factor of a FDA system is given by

$$AF=\sum_{n=-P}^{P}w_n\exp\left\{-j\left(\frac{2\pi f_0 nd\sin\theta}{c}-\frac{2\pi.\alpha_n\Delta f.r}{c}\right)\right\} \tag{5.33}$$

The beam pattern towards the desired target can be approximated as the magnitude squared of the array factor [115] and is given by

$$P_{FDA}\left(r_0,\theta_0,\alpha\right)\approx\left|\sum_{n=-P}^{P}\exp\left\{-j2\pi\left[\frac{fnd_0\left(\sin\theta-\sin\theta_0\right)}{c}-\frac{\alpha_n\Delta f\left(r-\hat{r_0}\right)}{c}\right]\right\}\right|^2 \tag{5.34}$$

This expression cannot be further simplified to get a closed form solution [98], [115], therefore, simulations have been carried out to show the beam pattern results for given target position $\left(\hat{\theta},\hat{r_0}\right)$.

5.2.3. Calculation of non-uniform frequency offset values

Now, we will discuss each method either fractional or integer based computation of non-uniform frequency offset values with their effects on transmit beamforming in detail.

5.2.3.1. Calculation of non-uniform frequency offset values using mu-law companding schemes

In the first case of fractional coefficient calculation, α_n is not an integer, instead it represents a non-uniform fractional coefficient of frequency offset value Δf. The value of middle coefficient is kept zero i.e.,$\alpha_0=0,$ so that it can transmit waveform with fundamental frequency f_0. In the proposed design, Δf_n values are calculated using well known *mu-law* formula due to its non-uniformity property. Previously in literature, mu-law has been used in literature for non-linear quantization of pulse coded modulation (PCM) and reducing peak-to-average-power-ratio (PAPR) of orthogonal signals of OFDM systems etc., [176], [177], but here we will use it to compute the non-uniform frequency offsets to generate a single maximum beam pattern.

In the given scenario, where the predicted target positions are tunneled as feedback

to the transmitter, the accuracy of the estimator at the receiver plays a vital role. If the position of the target is accurately predicted, the transmitter directs its sharp beam

pattern peak, regardless of generated high side lobes, to detect the target. On the contrary, if the target range and angle values are not in the given range or the estimated prediction error is not affordable, the transmitter is set to increase the beam width of the main lobe towards the target previous position to detect the target in the next cycle.

Based on the accuracy of the predictor block, there can be two cases, i) the estimate is accurate or with affordable error, ii) the estimate is not accurate or the predicted target position is out of range (i.e., the target is lost).

For both the cases, the transmitter selector, a sub-block of transmitter computes the non-uniform frequency offset values by selecting an appropriate companding factor (i.e., suitable values of *mu*) according to the requirement.

Therefore, a linearly increasing frequency offset vector i.e., $\left[-P\Delta f,...,-2\Delta f,-\Delta f,0,\Delta f,2\Delta f,...,P\Delta f\right]$ is transformed into a non-uniform frequency offset vector i.e. $\left[-\alpha_P\Delta f,...,-\alpha_2\Delta f,-\alpha_1\Delta f,0,\alpha_1\Delta f,\alpha_2\Delta f,...,\alpha_P\Delta f\right]$.

The *mu-law* compression expression used in this paper, is given as

$$\Delta f_n = \operatorname{sgn}(n\Delta f)\frac{\ln\left(1+\mu\left(n\Delta f\right)\right)}{\ln(1+\mu)};\ \ n=0,\pm1,...,\pm P \tag{5.35}$$

where $n\Delta f$ is the input frequency offset, while Δf_n is the calculated frequency offset and μ is a compression factor. Similarly, the *mu-law* expansion expression used in this paper, is given as

$$\Delta f_n = \frac{1}{\mu}\left(\exp\left(\ln\left(1+\mu\right)n\Delta f\right)-1\right)\operatorname{sgn}\left(n\Delta f\right);\ n=0,\pm1,...,\pm P \tag{5.36}$$

Since, we are assuming a symmetric FDA with $N = 2P+1$ elements, Fig- 5.3 shows the employed frequency offsets of one side i.e. P elements. We can see that $\mu = 0$ assures no change, solid lines show the compression, while black dotted lines show the expansion expression results for different values of μ .

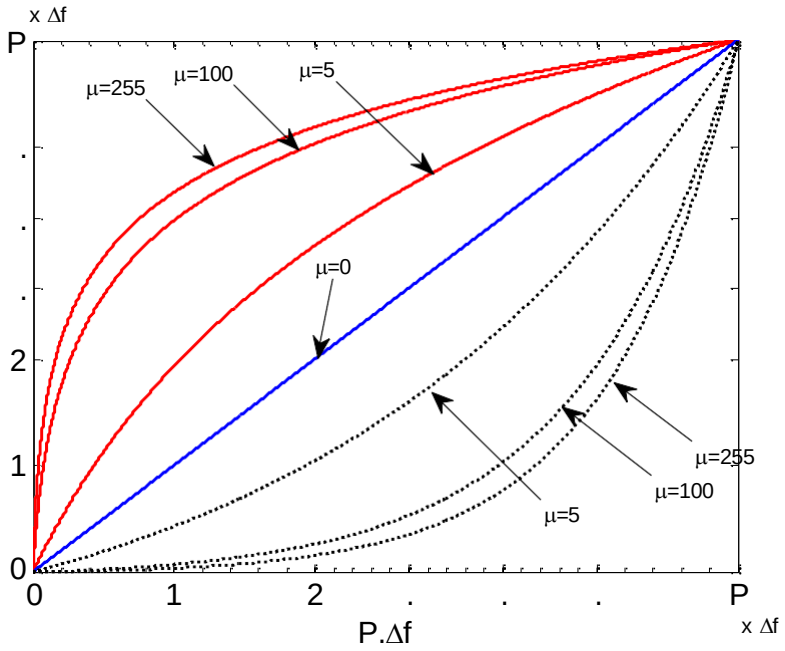

Figure- 5. 3: Non-uniform frequency offset calculation using *mu-law* companding schemes

To study the effect of *mu-law* compressing and expanding schemes on calculated frequency offsets, Fig-5.4 shows a comparison of compression and expansion curves with $\mu = 5$.

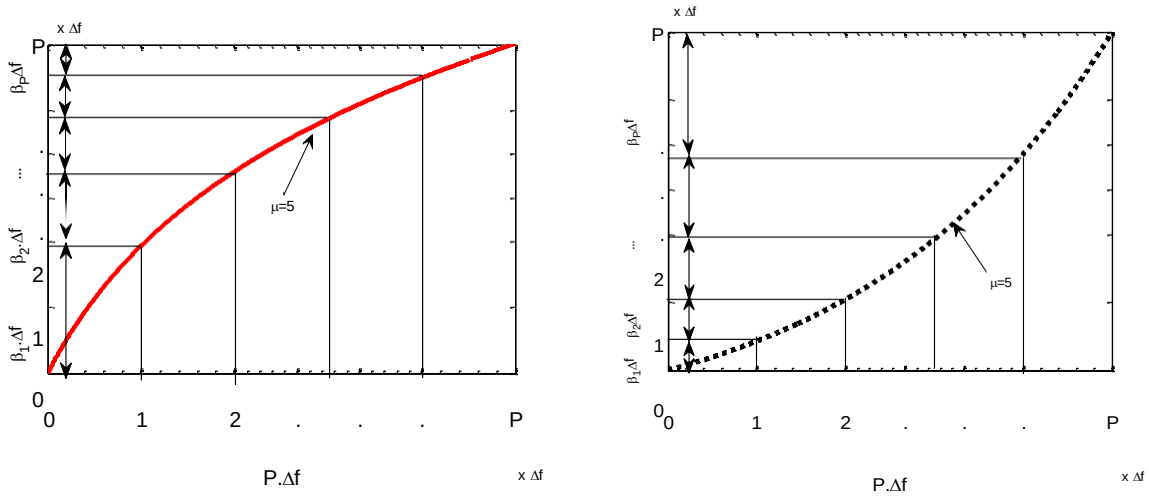

(a) Compression (b) Expansion

Figure- 5. 4: Effect of *mu-law* companding schemes on uniform frequency offsets

The frequency offset for reference element is zero, i.e., $\Delta f_0 = 0$ and therefore, the frequency offset difference between first and reference element is

$$\Delta f_1 - \Delta f_0 = \beta_1 \Delta f = \alpha_1 \Delta f \tag{5.37}$$

Similarly, the difference for subsequent pairs of adjacent elements, as shown in Fig 5.4, is

$$\Delta f_2 - \Delta f_1 = \beta_2 \Delta f \tag{5.38}$$

$$\Delta f_3 - \Delta f_2 = \beta_3 \Delta f \tag{5.39}$$

By generalizing it for M elements on each side of symmetric array, we have

$$\Delta f_P - \Delta f_{P-1} = \beta_P \Delta f \tag{5.40}$$

In the case of *mu-law* compression scheme, we note that this frequency offset difference is maximum at the first element and decreases as we go away from reference to the last elements. On the contrary, in the expanding scheme this difference is minimum at the first element, while it keeps on increasing. Applying these results on the symmetric array, we

get two different cases as shown in Fig-5.5.

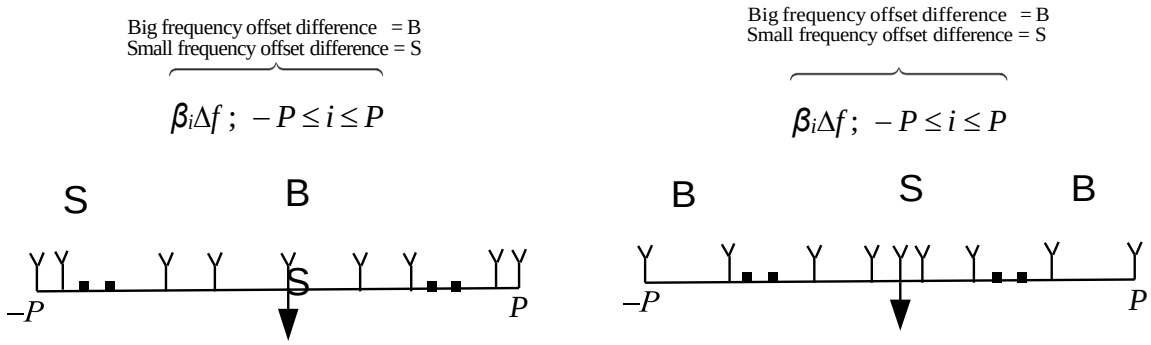

(a) SBS array (based on compression scheme) (b) BSB array (based on expansion scheme)

Figure- 5. 5: Two array structures with respect to the frequency offset difference

The SBS (small-big-small) and BSB (big-small-big) offset structures effect the side lobes level (SLL)[18], [23], [43], [54] of generated single maximum FDA beam pattern. Thus, with a constant energy constraint of the array, these SLL are proportional to the beam width of FDA pattern [18]. Therefore, BSB offset array structure generates a single maximum FDA broad beam pattern with low SLL, while SBS generates a sharp beam with high SLL.

The transmitter array structure along with the companding factor value μ, are selected according to the environmental changes received as feedback (a cognitive radar property).

The non-uniform coefficient of frequency offset for 1^{st} element is given as

$$\alpha_1 = \beta_1 \tag{5.41}$$

and

$$\alpha_2 = \beta_1 + \beta_2 \tag{5.42}$$

Similarly, generalizing it for M^{th} value

$$\alpha_3 = \beta_1 + \beta_2 + \beta_3 \tag{5.43}$$

$$\vdots$$

$$\alpha_P = \beta_1 + \beta_2,...,+\beta_P \tag{5.44}$$

Consequently, we can write

$$\alpha_P = \alpha_{P-1} + \beta_P \tag{5.45}$$

Therefore, a recursive formula for calculating frequency offset for a symmetric array is given as

$$\Delta f_n = \left(\alpha_{n-1} + \beta_n\right)\Delta f; \quad n = \pm 1, \pm 2,..., \pm P \tag{5.46}$$

The use of non-uniform symmetric frequency offset affects the null depth of FDA pattern. Therefore, Fig-5.6 shows comparison of the FDA beam pattern for non-uniform inter-element frequency offset and symmetric non-uniform inter-element frequency offset coefficients.

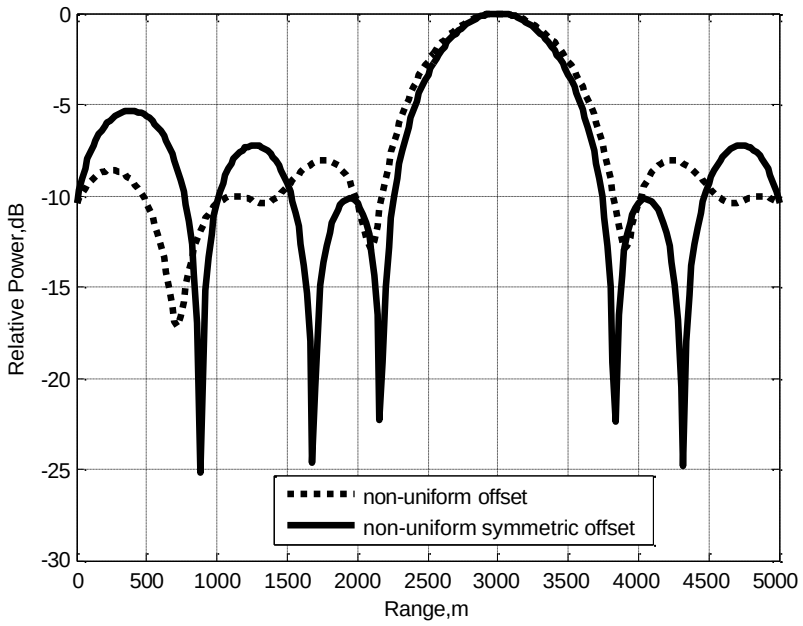

Figure- 5. 6: Comparison of null depths of FDA using non-uniform non-symmetric and symmetric offsets in range dimension $N = 11, \hat{r_0} = 3km, f_0 = 10GHz, \Delta f = 30kHz$

It can be seen that by using the symmetric offsets, the disadvantage of losing null depths can be reduced. Therefore, the frequency offset symmetry around the middle element has been maintained for the subsequent sections.

Manipulating with non-uniform symmetric frequency offsets, it can be noted that for higher values of μ for *mu-law* compression scheme, the frequency offset value adjacent to the middle element increases as compared to other frequency offset values. It results in more directional beam i.e., half power beam width (HPBW) decreases but at the same time, side lobe levels increase. Fig- 5.7 shows a beam pattern comparison with different values of μ on range axis.

It is noteworthy that the HPBW for considered three cases decreases gradually, i.e., approximately $1800\,m$, $1500\,m$ and $1000\,m$, respectively, while side lobes levels increase.

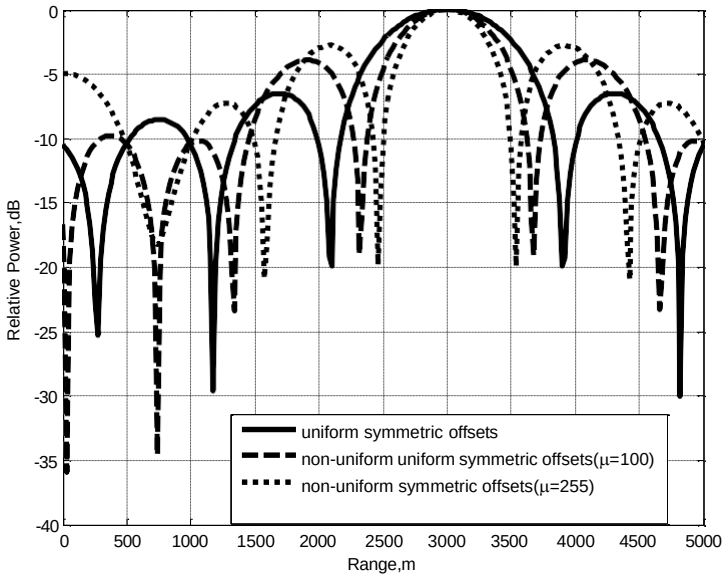

Figure- 5. 7: Comparison of range resolution (i.e. HPBW) among non-uniform symmetric frequency offsets vectors. $N=11, \hat{r_0}=3km, f_0=10GHz, \Delta f=30kHz$

On the contrary, it is also evident that using expanding scheme of *mu-law*, the frequency offsets near the middle element increase slowly, while increase fast as we go towards end of the array. Therefore, it results in increased HPBW and low side lobe levels (SLL). Lower SLL can be achieved by using higher values of μ in expansion scheme.The transmitter selector, a sub-block of transmitter, decides a suitable value of μ along with *mu-law* compression or expansion scheme, based on the feedback i.e. $\left(\theta_{0,k+1}, r_{0,k+1}, \epsilon\right)$.

Fig- 5.8 shows the FDA generated beam patterns using these non-uniform frequency offset values. We assume that the target is located at $\left(30^{\circ}, 3km\right)$. Fig-5.8(a) & (b) show the normalized 3-D and 2-D FDA beam pattern using uniform frequency offset along the array, which shows number of range-angle pairs in the surveillance region have been illuminated. This multiple maxima property may deteriorate the SINR as it can allow many interferes to affect the target-returns. In contrast, we can note from Figs-5.8 (c)-(f) that the non-uniform frequency offset calculated using mu-law facilitate to generate a single maximum beam pattern. Different values of mu are selected on the base of receiver feedback about the estimation error, which are given in fig-5.8(g).

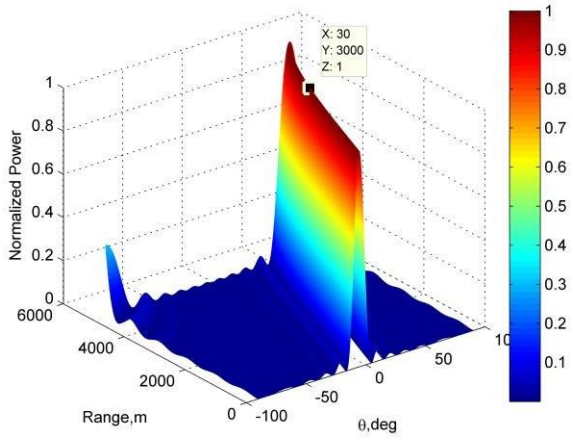

(a) 3-D view using uniform frequency offset values

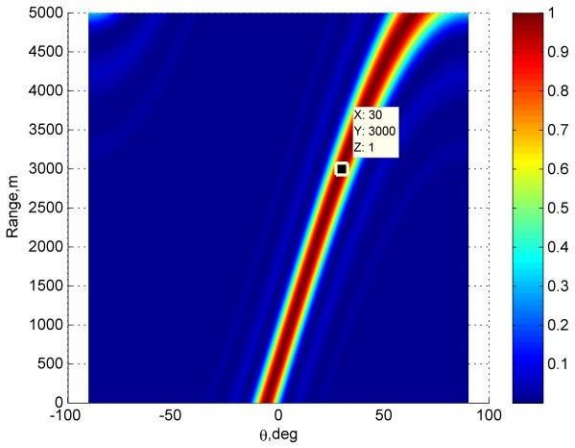

(c) 2-D view using uniform frequency offset values

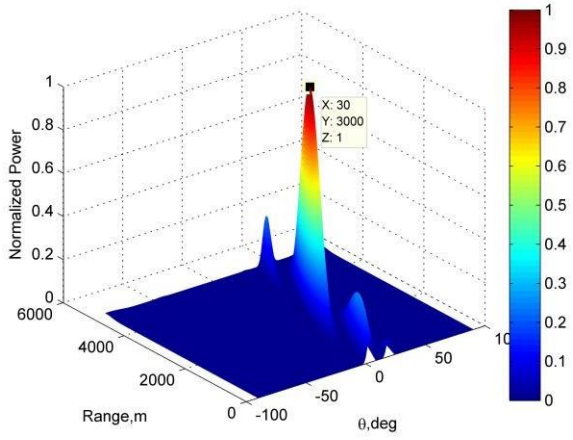

(b) 3-D view using frequency offset values with compression ($\mu = 5$)

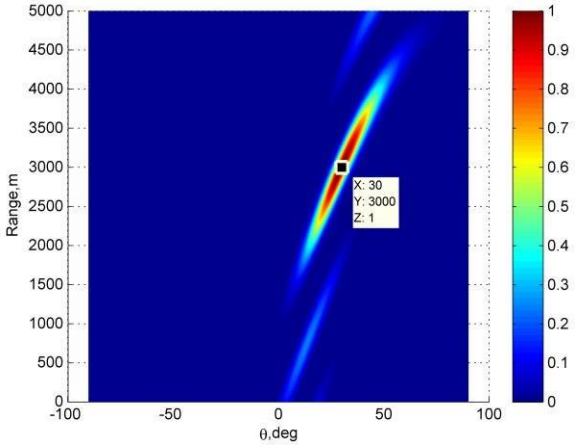

(d) 2-D view frequency offset values with compression ($\mu = 5$)

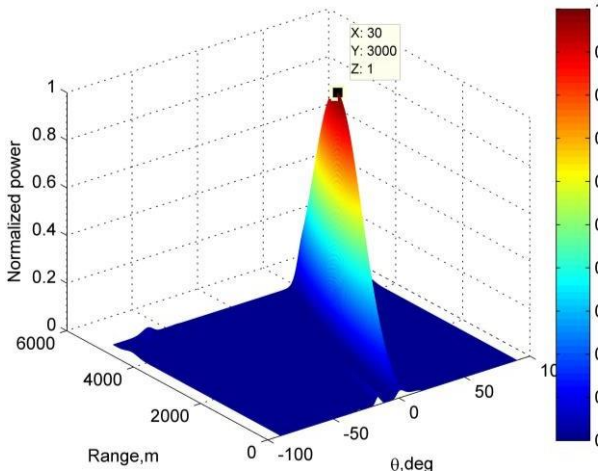

(e) 3-D view using frequency offset values with expansion ($\mu = 15$)

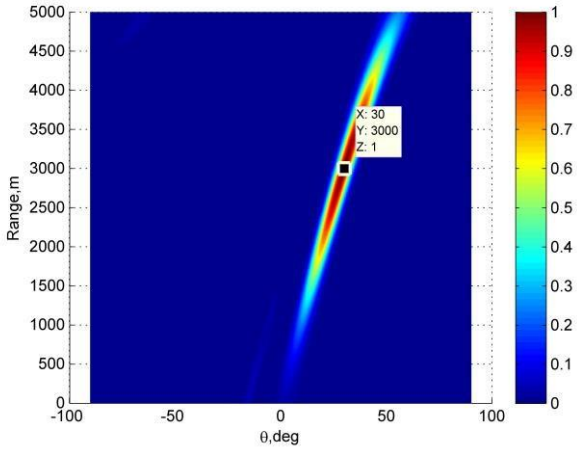

(f) 2-D view using frequency offset values with expansion ($\mu = 15$)

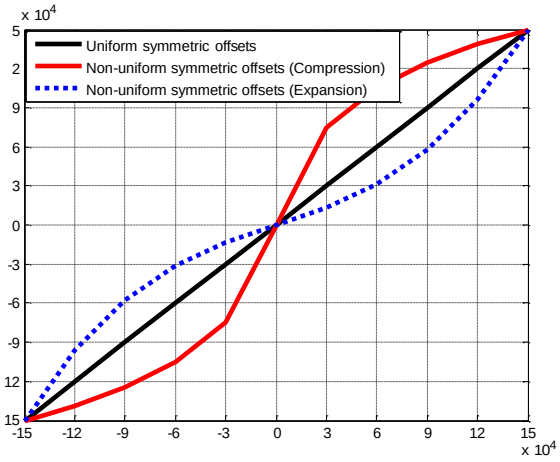

(g) Non-uniform frequency offset values used for proposed system

Figure- 5. 8: FDA generated beam patterns with $N = 11, r_0 = 3km, f_0 = 10GHz, \Delta f = 30kHz$ (a) & (b) 3-D and 2-D views using uniform symmetric frequency offsets (c) & (d) 3-D and 2-D views using non-uniform symmetric frequency offsets (compressed) (e) & (f) 3-D and 2-D views using non-uniform symmetric frequency offsets (expanded) (g) calculated non-uniform frequency offset using mu-law for the proposed HCFDA system.

5.2.3.2. Calculation of non-uniform frequency offset values using the GA

In this section, the GA has been used to compute the non-uniform frequency offset values for localizing the targets and interference with same direction but different ranges. First of all, the problem is formulated then the GA has been applied to compute such non-uniform frequency offset values which enable the FDA transmitter to illuminate the target positions only and suppress the interferences, simultaneously.

5.2.3.2.1. Problem formulation

As soon as the radar is switched on, it connects with its surrounding environments through electromagnetic link to sense it. The radar strongly depends upon the reflected echoes form one scan to the next to identify targets of interest on unknown locations in the surrounding environment. Assume that there are u targets and v interferes at unknown locations having same direction and different ranges. These targets reflect $u+v$ number of plane waves that impinge on the linear array. Due to the same direction of targets, it is not possible for a linear array antenna to localize them in the range dimension as PAR will consider them as a single target. Figure 5.9 shows the target constellation, where $u+v$ number of reflectors, with same direction but different ranges contribute the target returns.

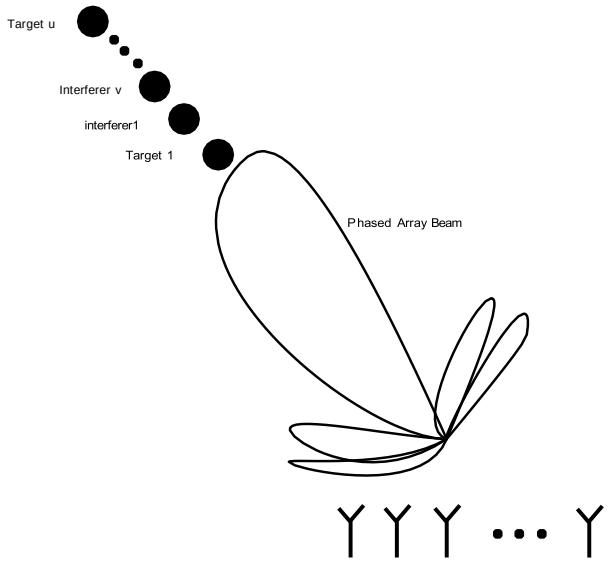

Figure- 5. 9: u targets and v interferers constellation in space

5.2.3.2.2. Proposed solution

In this context, an intelligent and adaptive transmitter that can direct the power peaks in the targets direction and their ranges to get high signal to noise ratios (SNR) at the receiver for their localization. Once these targets and interferers are declared in environment by the radar receiver, a state space model of surrounding environment is needed to estimate the certain parameters and recursively updating the state vectors. The design illustrates that the transmitter illuminates the radar environment containing multiple targets and interferes of considered constellation at time instant $k-1$ as shown in proposed HCFDA design in Fig-5.10.

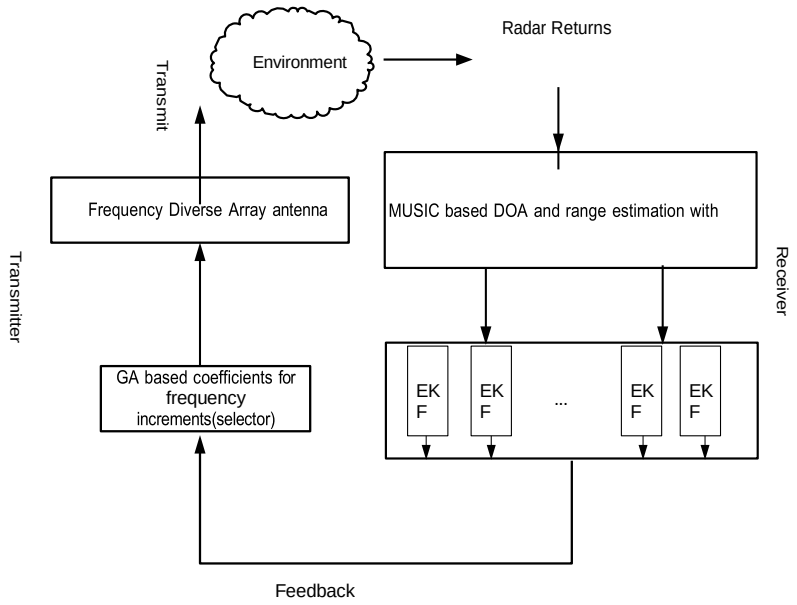

Figure- 5. 10: Block diagram of the proposed radar

The radar returns denoted as z_k are received by the receiver MUSIC based DOA and range estimation block. At first cycle, we suppose there are u targets and v interferers in space with same direction and different ranges. The filtered target position estimate $\left(\hat{\theta}_{0,k}, \hat{\boldsymbol{r}}_{1:u+v,\,k}\right)$ at k^{th} instant are calculated, where $\hat{\epsilon}_{0,k}$ denotes the direction of targets and $\hat{\boldsymbol{r}}_{1:u+v,\,k}$ denotes the range vector containing the range values of u targets and v interferers at any time k. This extracted information is given to the EKF block to predict the targets next positions $\left(\hat{\theta}_{0,k+1}, \hat{\boldsymbol{r}}_{1:u+v,k+1}\right)$. The predicted positions of targets are sent as feedback to the transmitter.

There are two cases regarding inter-targets distances, which are at the same angle. First case is that if the targets are at periodic ranges (inter-targets distance is equal) then due to the range periodicity property of FDA beam pattern, an appropriate frequency

offset value is computed to put the peak power at these ranges. On the contrary, if the targets with same direction are not at the periodic ranges (inter- targets distances are not equal), then non-uniform fractional coefficients of the frequency offsets have been calculated using the GA algorithm. The fitness function is taken as the mean square error (MSE) between the desired and the estimated FDA beam patterns and given as

$$MSE = \left| P_{FDA\_d}(\theta, r) - \hat{P}_{FDA\_e}(\theta, r) \right|^2 \tag{5.47}$$

Where $P_{FDA\_d}(\theta, r)$ is the desired beam pattern, while $\hat{I}_{FDA\_e}(\theta, r)$ is the estimated symmetric FDA beam pattern and given as

$$\hat{P}_{FDA\_e}(\theta, r) = \sum_{n=-P}^{P} \exp\left\{ -j2\pi n \left(\hat{\alpha}_n \Delta f \frac{\hat{r}_0}{c} - \frac{d \sin(\hat{\theta})}{\lambda_0} \right) \right\} \tag{5.48}$$

where $\hat{\alpha}_n$ are the coefficients to be estimated by the GA for non-periodic target ranges. For the periodic range case these $\hat{\alpha}_n$ are taken unity and suitable frequency offset value Δf is computed using the range periodicity formula i.e., $\Delta f = \frac{c}{r_0}$ where c is speed of light and r_0 is the range of first target at each cycle.

5.2.3.2.3. Beam pattern synthesis with calculated non-uniform frequency offsets using the GA

In case of non-periodic ranges of targets, by tuning the frequency offset (Δf) with suitable coefficients $\hat{\alpha}_n$, the range-angle dependent beam pattern can be

controlled for putting power peaks at required ranges and angles, simultaneously.

Case 1: The inter-targets distances are at equal (at periodic ranges)

The target predicted positions are sent as a feedback from the receiver for five targets given as $\left(\hat{\theta}_{0,k+1}, \hat{\boldsymbol{r}}_{0:4,k+1}\right) = \left(40°, 0.5\times10^5\, m, 1.5\times10^5\, m, 2.5\times10^5\, m, 3.5\times10^5\, m, 4.5\times10^5\, m\right)$.

We can see that inter-targets distance is equal. The selectors, selects the frequency offset $\Delta f = 3000\, Hz$ that enables the beam pattern to generate power peaks at required target angle and ranges. Figs-5.11 (a),(b),(c) shows the FDA generated range-angle dependent pattern and its angle response and range response respectively.

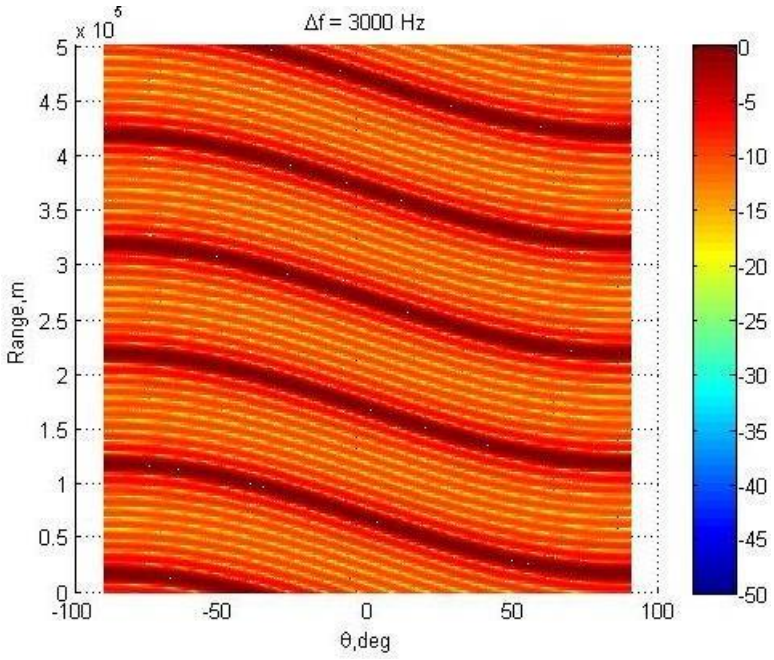

(a)

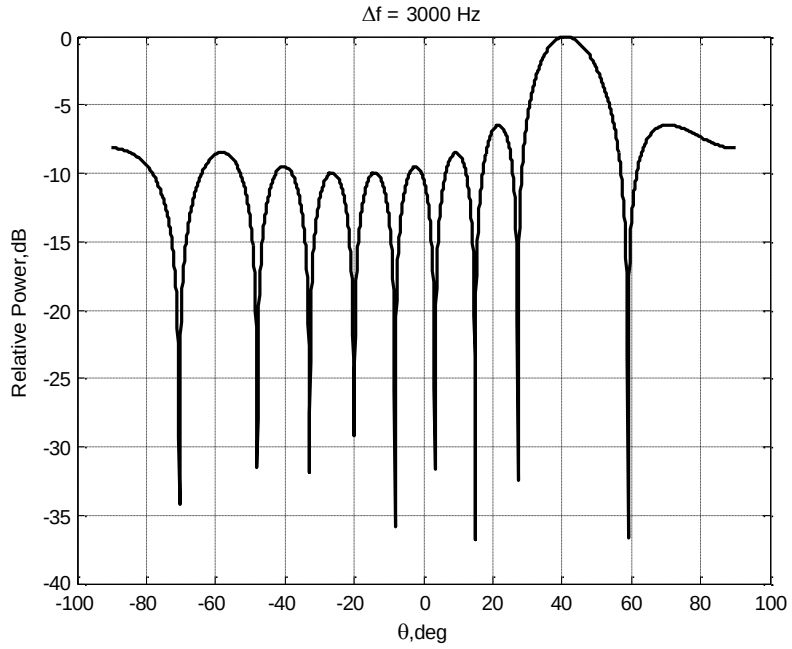

(b)

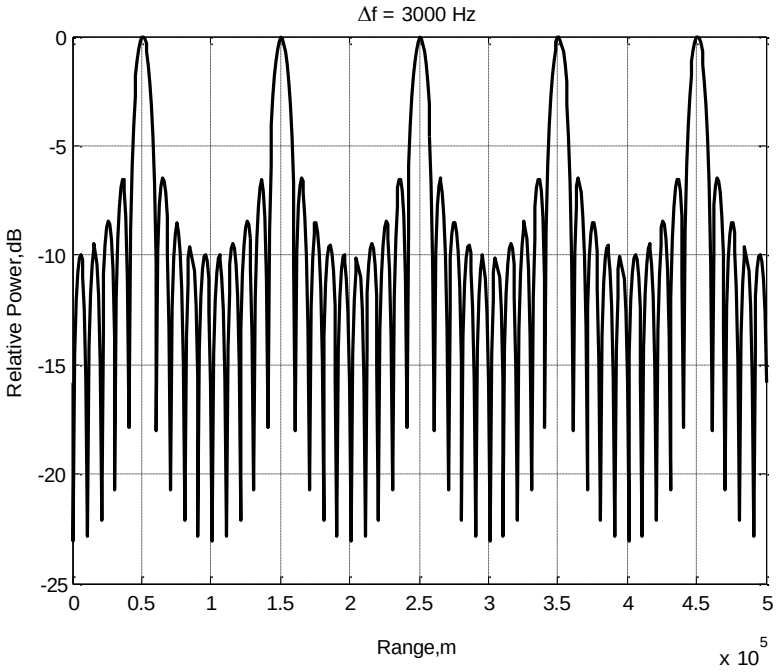

(c)

Figure- 5. 11 (a)-(c) FDA beam pattern (linear frequency offsets) with parameters $f_0 = 10GHz, \Delta f = 3kHz$, $N = 11, d = \lambda / 2$

Case 2: The inter-target distances are not equal (at non-periodic ranges)

The predicted target positions of targets sent as feedback for five targets are taken as $\left(\hat{\theta}_{0,k+1}, \hat{\boldsymbol{r}}_{1:5+1,k+1}\right) = \left(0°, 0.5\times10^5\, m, 2\times10^5\, m, 2.5\times10^5\, m, 3.5\times10^5\, m, 4.4\times10^5\, m, 4.7\times10^5\, m\right)$ in the second case. Since these target are at same angle but the inter-targets distances is not equal. Likewise the interference is at $\left(0°, 4.7\times10^5\, m\right)$. In this case, the selector adaptively use the nonlinear frequency offset vector calculated by GA to allow to the range-angle beam pattern with peaks at the desired positions and nulls in the desired interferer range value. Figure 5.12 (a),(b),(c) shows the FDA generated range-angle dependent pattern and its angle response and range response, respectively.

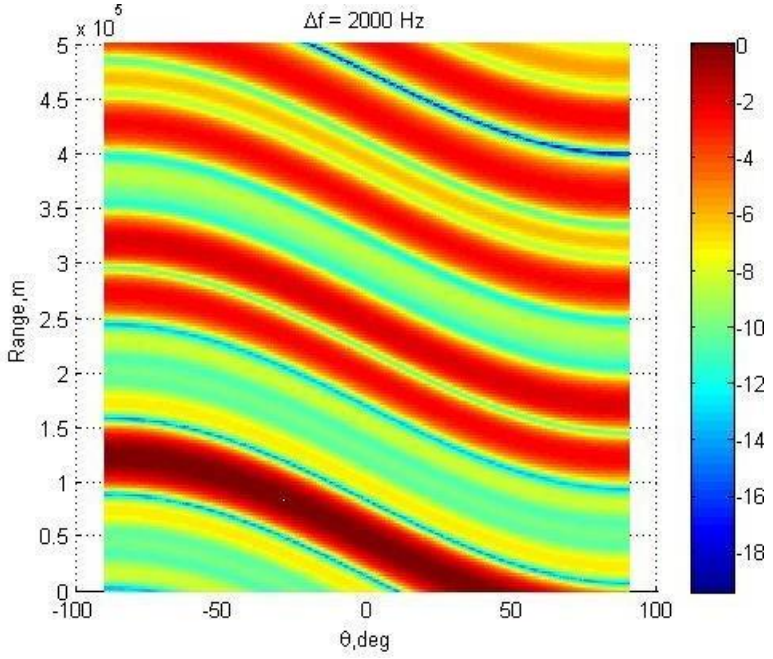

(a)

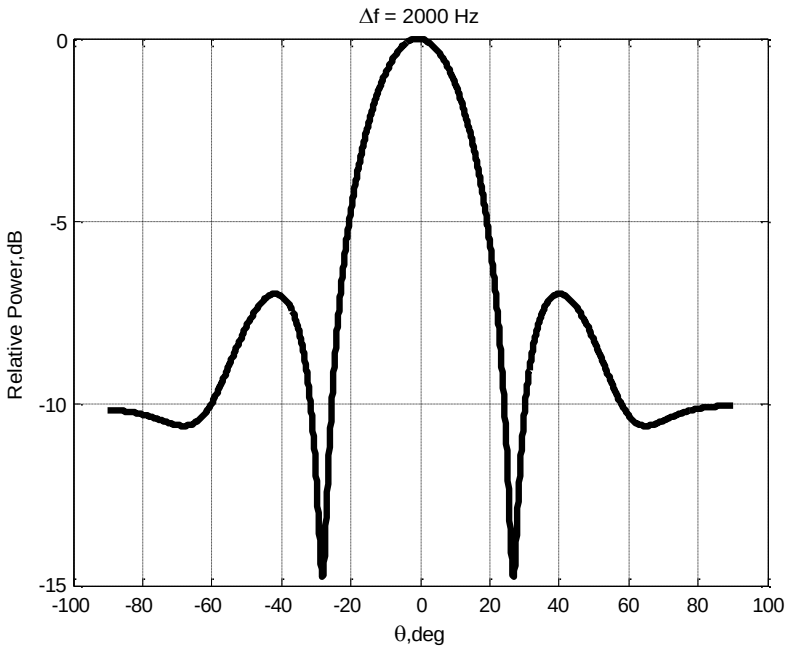

(b)

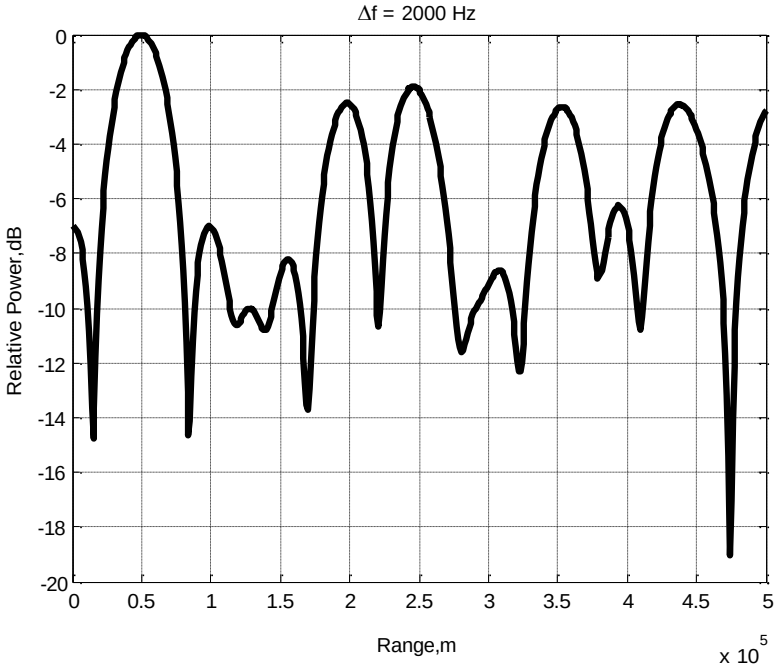

(c)

Figure- 5. 12 (a)-(c) FDA beam pattern generated using GA based non-linear fractional frequency offset $f_0 = 10GHz, \Delta f = 2kHz$, $N = 11, d = \lambda / 2$

The GA parameter settings of *optimtool* toolbox of MATLAB for this problem are given

in Table-5.1.

Table-5. 1: The GA parameter settings for computing non-uniform frequency offset

GA parameters settings								
parameters	Chromosome Size	Creation function	Crossover function	Function tolerance	Migration direction	No. of generations	Population Size	Selection function
Settings	10	Uniform	Heuristic	1e-4	Both	400	40	Uniform

It is clear from Figs-5.11 and 5.12, that the proposed design generate the beam pattern with maxima at the target directions and ranges, simultaneously. The non-uniform frequency offsets are computed through the GA. The convergence performance of GA for computing non-uniform frequency increment for the given problem is shown in Fig-5.13. We can find that in about 60 iterations, the cost function mean square error is affordable, which justify its practical implementation.

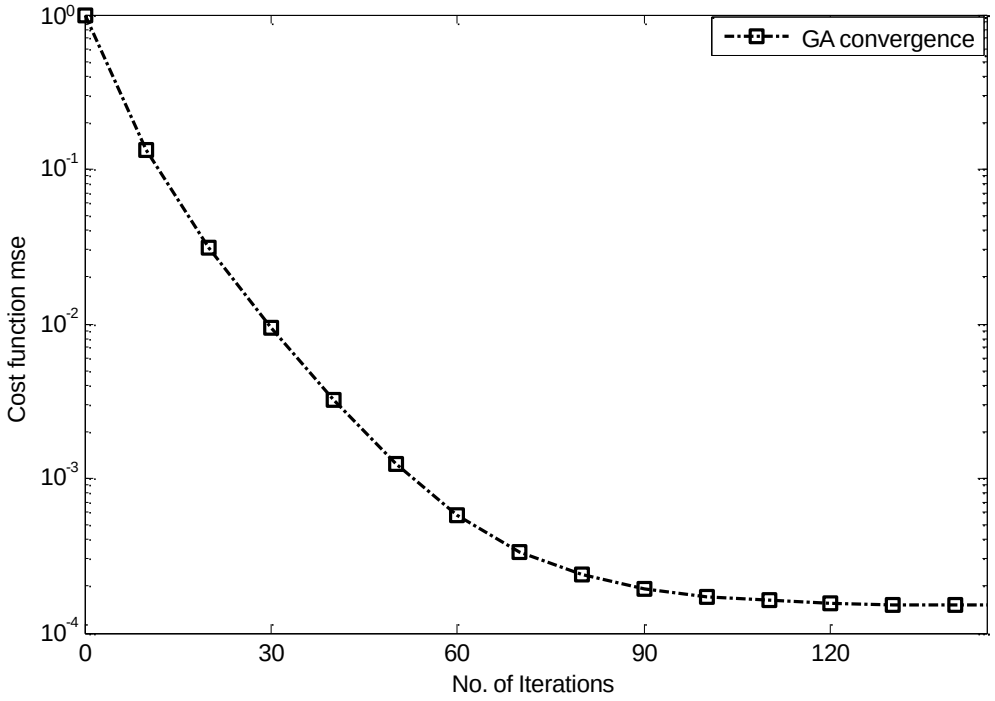

Figure- 5. 13: Convergence of GA i.e., no. of iterations vs. cost function MSE

5.2.3.3. Calculation of non-uniform frequency offset using Hamming window

In this section, the well- known Hamming window has been used to compute the non-uniform frequency offset, which outperforms all the existing techniques in terms of transmit energy focusing and side lobe suppression towards the target of interest.

5.2.3.3.1. Problem formulation

The FDA range-angle dependent pattern offers the flexibility of transmit energy focusing in a desired range-angle space, while rejecting the range-dependent interferences to improve received SINR [76]. On the other hand, it generates a range- angle dependent S-shaped beam pattern that exhibits maxima at multiple range and angle values. This property allows a number of reflectors positioned at any of the maxima to interfere the target-returns, thus weakening the received signal to interference and noise ratio (SINR).

In the HCFDA design scenario, once the receiver sends the feedback about the target predicted position to the transmitter, it is very important for a transmitter to focus as much energy as it can, towards the target position, while suppressing the side lobes outside the area of interest.

A uniformly spaced linear FDA with logarithmically increasing frequency offset i.e. log-FDA has been proposed in [115], which achieves a single maximum non-periodic beam pattern to reject range-dependent interferences for improved SINR. Although, this technique produces a single maximum beam pattern, but it achieves a poor resolution in range and angle dimensions, which may degrade the radar performance in terms of range and angle estimations.

5.2.3.3.2. Proposed solution

In this section, we have proposed a uniformly spaced linear FDA radar with a hamming window based tapering non-uniform frequency offsets applied along the symmetric array. The proposed strategy generates an improved transmit single maximum beam pattern that achieves better resolution in range and angle dimensions than that of all existing techniques. Moreover, it outperforms the existing Log-FDA technique in side-lobe suppression and transmit energy focusing.

In literature, different types of filtering windows such as Hamming, Hanning, Binomial windows etc., have been applied to different types of arrays for spatial filtering and side lobe reduction. due to moderate behavior of hamming window between narrowband and wideband applications it has been used to find the frequency offset applied at each element. The frequency offsets Δf_n can be expressed as

$$\Delta f_{P-n} = \Delta f \left(0.54 - 0.46 \cos\left(\frac{2\pi n}{2P} \right) \right); \quad n = 0,1,...,2P \tag{5.48}$$

where $(.)$ is the general hamming window equation used in literature.

5.2.3.3.3. Beam pattern synthesis with calculated non-uniform frequency offsets using Hamming window

Due to the tapering offsets calculated using a hamming window function, it is noteworthy that transmitted frequency decreases on both sides from the central element till the last elements of the symmetric array, while central element transmits the waveform with maximum frequency as shown in Fig- 5.14.

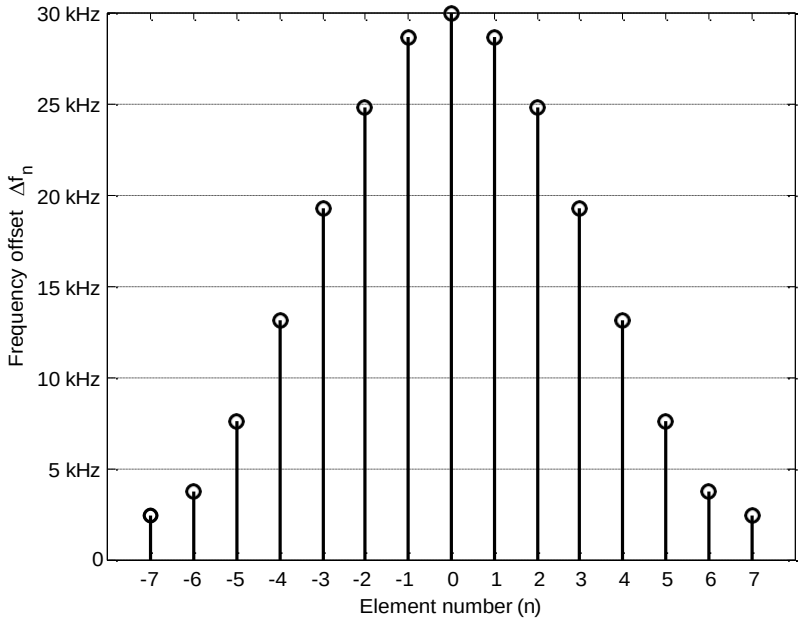

Figure- 5. 14: Frequency offset values used for the proposed symmetric FDA with 15 elements

Fig-5.15 shows the synthesized normalized transmit beam pattern using our proposed method. The synthesized beam pattern generates a focused maxima at the target position. To make the comparison, log-FDA based normalized beam pattern has been plotted in Fig-5.16. Both schemes generate maxima at the target position, but the proposed scheme outperforms the log-FDA as it generates a more focused maxima at the target position, which will result in increased SINR. The proposed pattern also outperforms the log-FDA in terms of side lobe levels, as it has lower side lobe levels in the undesired directions.

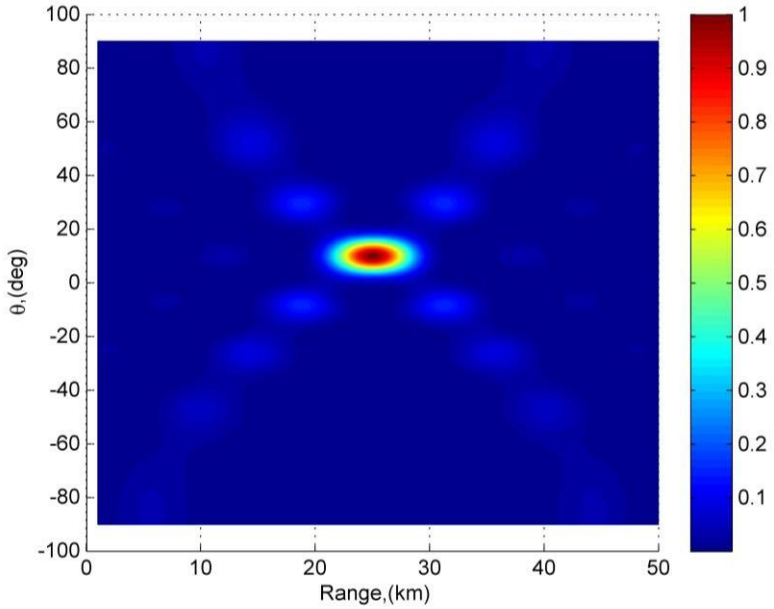

Figure- 5. 15: Normalized pattern with our scheme having parameters $N = 15, \hat{\theta} = 10^{\circ}, \hat{r} = 25\,km, f = 10\,GHz, \Delta f = 30\,kHz$

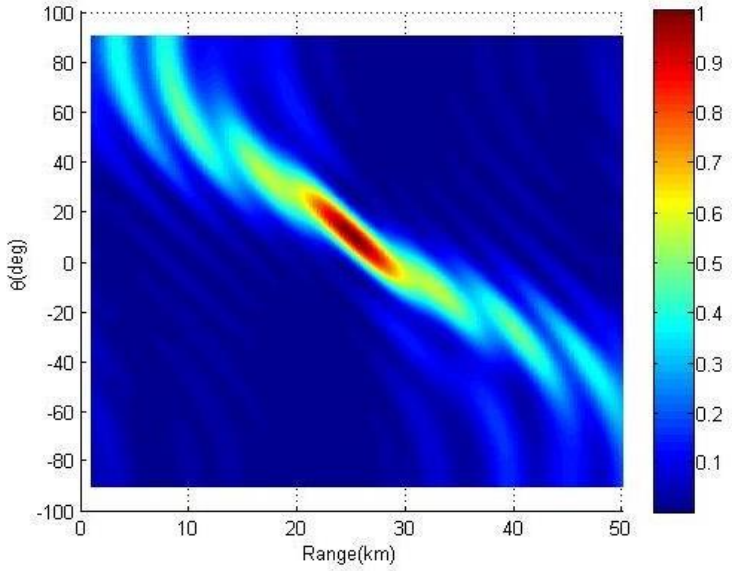

Figure- 5. 16: Normalized pattern of log-FDA scheme with parameters $N = 15, \hat{\theta} = 10^{\circ}, \hat{r} = 25\,km, f = 10\,GHz, \Delta f = 30\,kHz$

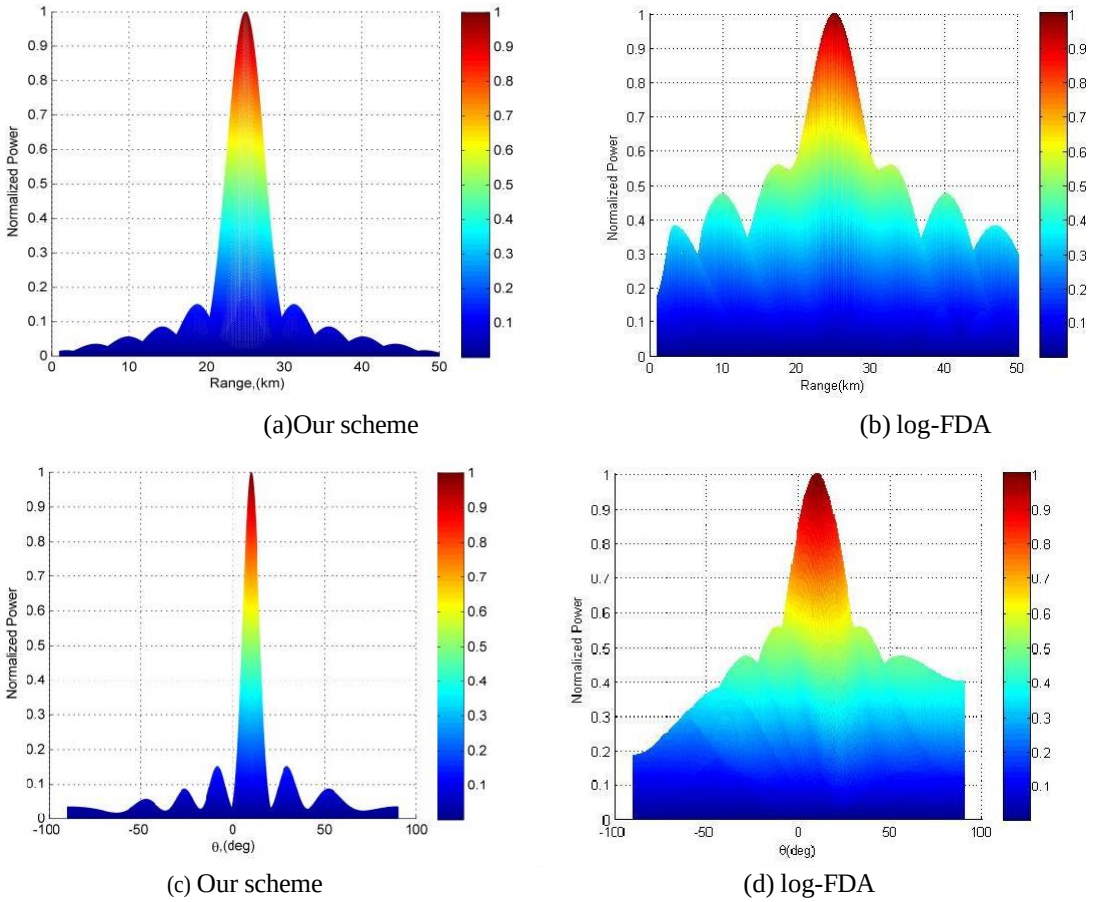

(a)Our scheme (b) log-FDA

(c) Our scheme (d) log-FDA

Figure- 5. 17: (a) & (b) Comparison of normalized beam pattern in range dimensions (c) & (d) comparison of normalized beam pattern in angular dimension

To analyze the range and angular resolution of the proposed scheme, Fig-5.17 shows the comparison of range and angle dimensions normalized beam patterns of our proposed scheme and log-FDA scheme. It also verifies the better resolution of our scheme as range span and angle span of the proposed scheme is much better than that of a log-FDA. In this specific case, the range span of generated beam pattern through our scheme is less than 8km, while log-FDA scheme has a much wider span. Likewise, the angle span of beam pattern generated using our scheme is less than 25 degrees, while the

log-FDA angle span is much wider than this. By utilizing these advantages a beam can be steered more precisely towards the desired target. This scheme also eliminates the periodic behavior of pattern, which is used for suppression of interferences located outside the target area. This property makes it more useful than that of conventional FDA schemes.

This proposed scheme generates a more focused beam pattern with suppressed side-lobes towards the desired target position. As a result a better range and angle resolution compared to log-FDA has been achieved. This scheme also facilitates the generation of a non-periodic beam pattern, which significantly suppresses interferences located outside the target area.

5.2.3.4. Using non-uniform symmetric but integer frequency offset values

In the case of non-uniform symmetric but integer frequency offset values, the α_n is taken as integer coefficient of the frequency offset applied at the n^{th} element. This design is same as the conventional FDA, except for the coefficients $\alpha = [\alpha_{-P},...,\alpha_{-1},\alpha_0,\alpha_1 \ldots,\alpha_P]$ that are non-uniform but integers. The value of the middle coefficient is kept zero i.e., $\alpha_0 = 0$, so that the middle element transmits signal with fundamental frequency f_0.

5.2.3.4.1. Problem formulation

All of the FDA based schemes with uniform frequency offsets cause broadening of half power beam width (HPBW). Certainly, this broadening of the main beam is undesirable due to the fact that it decreases the maximum reachable range and at the same

time it allows interferes to affect the target- returns. The net effect is weak signal to interference noise ratio (SINR), which deteriorates the performance.

A new FDA with non-uniform integer frequency offsets applied along the array is proposed. The proposed design avoids the broadening of main beam and hence may provide a better range resolution as compared to the previous designs.

5.2.3.4.2. Beam pattern synthesis with non-uniform but integer frequency offsets

The FDA with non-uniform frequency offset beam pattern expression has been simulated with different combinations of non-uniform frequency offset integer co-efficients $\alpha = [\alpha_{-P},...,\alpha_{-1},\alpha_0,\alpha_1 \ldots,\alpha_P]$. The coefficient of middle element has been assigned zero, i.e., $\alpha_0 = 0$, this is to take it as reference having signal with the fundamental frequency f_0. The results are compared with conventional FDA for a given target position $(\hat{\theta_0}, \hat{r_0}) = (30°, 3km)$. The fundamental frequency is taken as $10GHz$ and frequency offset value is taken as $\Delta f = 30kHz$, while the array elements are $N = 11$ and the inter-element distance is taken as $\lambda / 2$ to avoid the grating lobes in angle dimensions. Since, the angle dimension does not change due to non-uniform frequency offsets, therefore only the range dimension results have been plotted and compared.

Manipulating with non-uniform symmetric frequency offsets, some other interesting results have been obtained. For example, keeping all other parameters alike, the following symmetric coefficients have been taken:

$$\alpha_{uniform} = [-5,-4,-3,-2,-1,0,1,2,3,4,5]$$
$$\alpha_{non-uniform\_symm1} = [-6,-5,-4,-3,-2,0,2,3,4,5,6]$$
$$\alpha_{non-uniform\_symm2} = [-7,-6-5,-4,-3,0,3,4,5,6,7]$$

In the non-uniform symmetric cases, the offsets coefficients adjacent to the middle element differs with an additional Δf in each case i.e., $2\Delta f$ and $3\Delta f$, respectively, but all the other coefficients remain uniformly increasing.

Fig-5.18 shows, if the difference of frequency offset between the middle element and the adjacent elements is increased, a better half power beam width (HPBW) is obtained. i.e., the HPBW for the considered three cases is approximately 1800 *m,*1500 *m*and 1000 *m* , respectively. On the other hand, it is also evident that by increasing offset difference the side lobes levels also increase, which is not desirable. Therefore, to deal with this problem, the progressive increase of frequency offset can be utilized, shown in Fig-5.19, i.e., the coefficient vector is taken as:

$$\boldsymbol{\alpha}_{nou-uniform-progressive} = [\ -9 \quad -8 \quad -5 \quad -3 \quad -2 \quad 0 \quad 2 \quad 3 \quad 5 \quad 8 \quad 9]$$

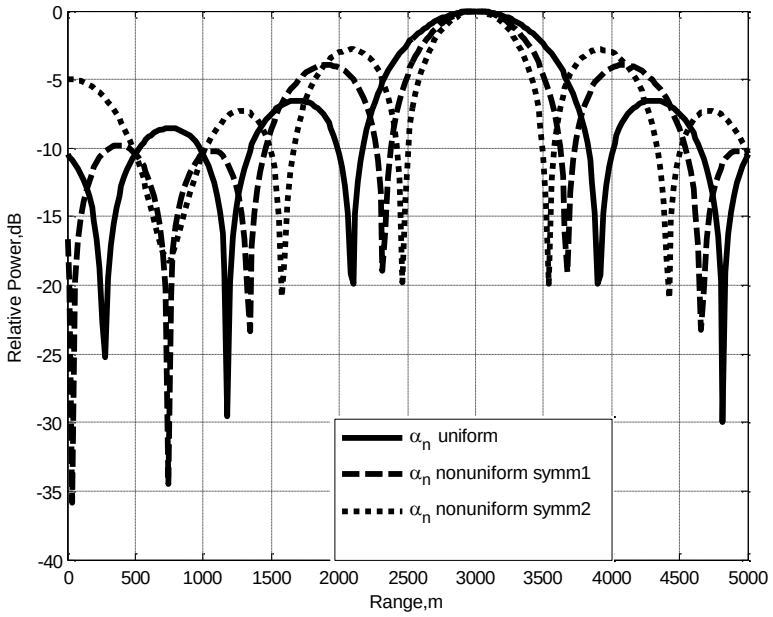

Figure- 5. 18: Comparison of range resolution (i.e. HPBW) among non-uniform symmetric frequency offsets vectors. $N = 11, \hat{r_0} = 3km, f_0 = 1GHz, \Delta f = 30kHz$

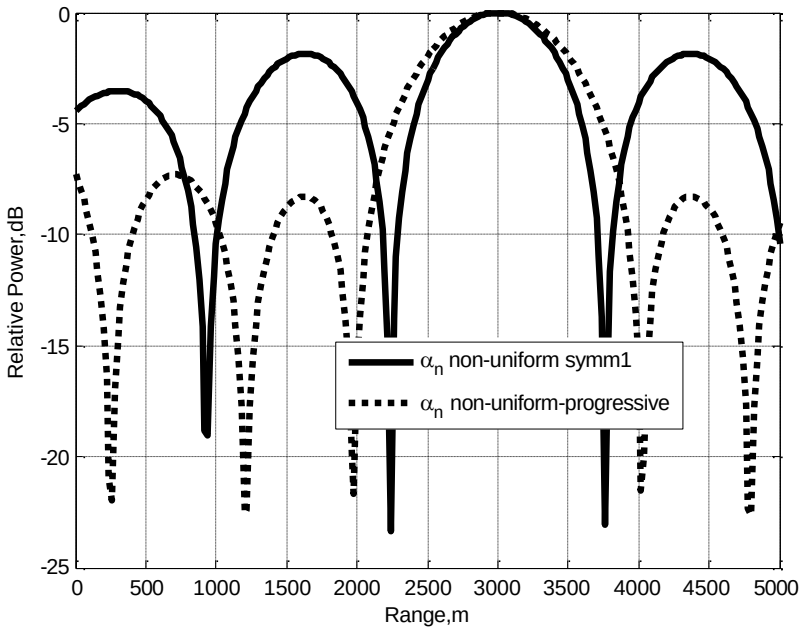

Figure- 5. 19: Comparison of side lobes between the range profiles generated by non-uniform symmetric and non-uniform symmetric progressive frequency offset

$N = 11, r_0^{\wedge} = 3km, f_0 = 1GHz, \Delta f = 30kHz$

Fig-5.19 also shows the comparison between the generated range profiles using $\boldsymbol{\alpha}_{non-niform\_symm1}$ and $\boldsymbol{\alpha}_{non-uniform-progssive}$. Clearly, the use of more nonlinear frequency offset coefficient vector decreases the side lobe level, approximately 8dB, than that of non-uniform symmetric frequency offset coefficients on the cost of a little bit increase in HPBW. The conventional FDA exhibit a periodic behavior in its beam pattern due to the usage of a uniform frequency offset. Therefore, it is worth knowing that does the proposed nonlinear frequency offset scheme affect the range periodicity?

The simulations are repeated for a ten times bigger range axis and results are shown in Fig-5.20 with uniform offset coefficients $\boldsymbol{\alpha}_{uniform}$, non-uniform symmetric offset coefficients $\boldsymbol{\alpha}_{non-niform\_symm3}$ and non-uniform progressive coefficients $\boldsymbol{\alpha}_{non-uniform-progssive3}$

given as:

$$\alpha_{uniform} = [-5, -4, -3, -2, -1, 0, 1, 2, 3, 4, 5]$$

$$\alpha_{non-uniform\_symm3} = [-8, -7, -6, -5, -4, 0, 4, 5, 6, 7, 8]$$

$$\alpha_{nou-uniform-progssive3} = [-11, -10, -7, -5, -4, 0, 4, 5, 7, 10, 11]$$

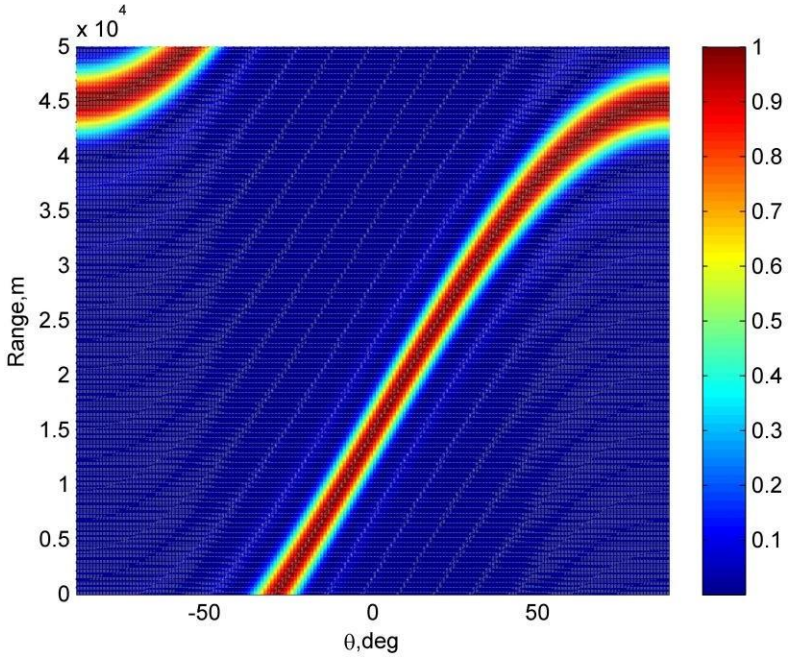

(a)

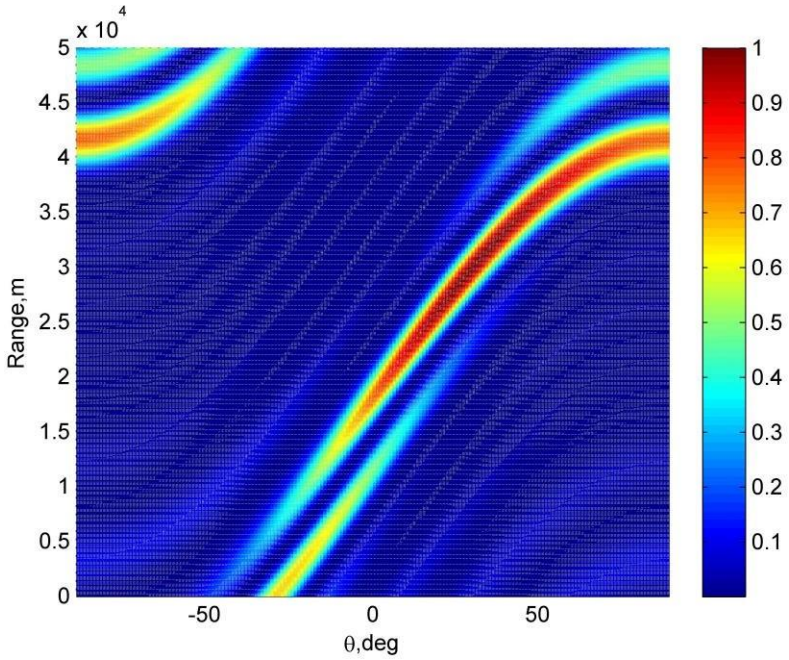

(b)

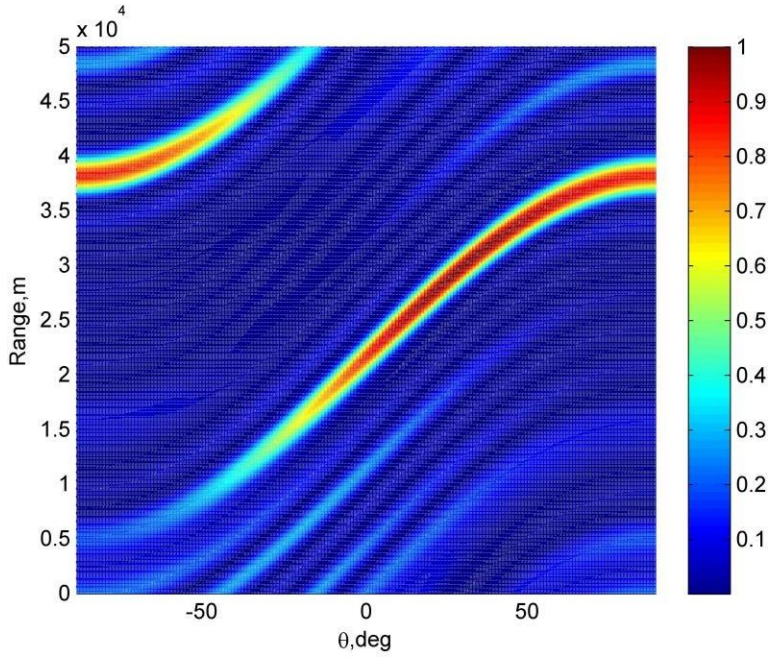

(c)

Figure- 5. 20: (a) -(c): Comparison of range periodicity between the range profiles generated by non-uniform symmetric and non-uniform symmetric progressive frequency offset $N = 11, \hat{r} = 30\,km, \hat{\theta} = 30^{\circ}, f = 1GHz, \Delta f = 50\,kHz$

Fig-5.20 suggests that the nonlinear frequency offsets does not affect the periodicity of the FDA beam pattern as there are the same number of maxima in each case (i.e., Fig-5.20 (a)-(c)) and repetition period $\frac{c}{\Delta f}$ as given in [81].

5.2.4. Overall performance of the HCFDA design

This section discusses the overall performance of the proposed HCFDA with non-uniform frequency offsets. The performance is evaluated based on the transmit/receive beamforming, SINR performance, detection performance and CRLB on target range and

estimation performance.

5.2.4.1. Transmit/receive beamforming:

The proposed FDA antenna has the ability to direct beam pattern maximum towards the target look angle and range. Let the signal received at target be given as [31]

$$\mathbf{w}_T^H \mathbf{a}(\theta, r, \alpha) s(l) \tag{5.49}$$

where $\mathbf{a}(\theta, r, \alpha)$ is the transmit steering vector of an FDA, $s(l)$ is a transmit baseband signal samples of transmitted waveform at any discrete time interval l and $\mathbf{w}_T^H$ is the transmit beamforming weight vector.

Consider that the target is located at a position (θ_0, r_0) and the interference sources are located at positions (θ_i, r_i). Therefore, the signal at uniform FDA receiver is given by [30], [117]

$$y(l) = \beta_0 \mathbf{b}(\theta_0, r_0, \Delta f) s(l) + \sum_i \beta_i \mathbf{b}(\theta_i, r_i, \Delta f) s(l) + n(l) \tag{5.50}$$

where $\beta_0 = \mathbf{w}_T^H \mathbf{a}(\theta_0, r_0, \alpha)$, is directional gains towards the target direction and range, while $\beta_i = \mathbf{w}_T^H \mathbf{a}(\theta_i, r_i, \alpha)$ is the directional gain in the interference directions θ_i and ranges r_i, respectively. $\mathbf{b}(\theta_0, r_0, \Delta f)$ is receive steering vector, while $n(l)$ is zero mean additive white Gaussian noise with σ_n^2 variance.

Defining $\mathbf{u}_i(\theta_i, r_i, \Delta f) \triangleq \beta_i \mathbf{b}(\theta_i, r_i, \Delta f)$ and $\mathbf{u}_0(\theta_0, r_0, \Delta f) \triangleq \beta_0 \mathbf{b}(\theta_0, r_0, \Delta f)$, the array output $\mathbf{y}$, in vector form, after match filtering is given by [31]

$$\mathbf{y} = \mathbf{u}_0(\theta_0, r_0, \Delta f) + \sum_i \mathbf{u}_i(\theta_i, r_i, \Delta f) + \mathbf{n} \tag{5.51}$$

The minimum variance distortion less response (MVDR) beam former calculates the receiver weight vector $\mathbf{w}_R$ to suppress the interferences, while giving distortion less response in the target direction and range, is given by [32]

$$\mathbf{w}_R = \frac{\hat{\mathbf{R}}_{i+n}^{-1}\mathbf{u}_0(\theta_0, r_0, \Delta f_0)}{\mathbf{u}_0^H(\theta_0, r_0, \Delta f_0)\hat{\mathbf{R}}_{i+n}^{-1}\mathbf{u}_0(\theta_0, r_0, \Delta f_0)} \tag{5.52}$$

$\hat{\mathbf{R}}_{i+n}$ is interference plus noise covariance matrix and is given as [32]

$$\hat{\mathbf{R}}_{i+n} = \sum_i \sigma_i^2 \mathbf{u}_i(\theta_i, r_i, \Delta f_i)\mathbf{u}_i^H(\theta_i, r_i, \Delta f_i) + \sigma_n^2 \mathbf{I} \tag{5.53}$$

5.2.4.2. SINR analysis

Here, it is assumed that the target/ interferences complex amplitudes are mutually uncorrelated with zero mean and variance σ_i^2. The signal to interference noise ratio (SINR) is evaluated as [30], [32]

$$SINR = \frac{\sigma_s^2 \left|\mathbf{w}_R^H \mathbf{u}_0(\theta_0, r_0, \Delta f_0)\right|^2}{\mathbf{w}_R^H \hat{\mathbf{R}}_{i+n}^{-1} \mathbf{w}_R} \tag{5.54}$$

$$= \frac{\sigma_s^2 N^2 P^2}{\sum_i \sigma_i^2 \left|\mathbf{a}^H(\theta_0, r_0, \alpha_0)\mathbf{a}(\theta_i, r_i, \alpha_i)\right|^2 \left|\mathbf{b}^H(\theta_0, r_0, \Delta f_0)\mathbf{b}(\theta_i, r_i, \Delta f_i)\right|^2 + \sigma_n^2 P} \tag{5.55}$$

Here, σ_s^2 is variance of the desired target. If a desired target is in the background of weak interferences that are well separated from target, then SINR term reduces to [32]

$$SINR \simeq \frac{\sigma_s^2 N^2 P}{\sigma_n^2} \tag{5.56}$$

But if a desired target is in the background of a strong interference, then we can ignore the noise power as compared to interference power and SINR term can be expressed as [30], [32]

$$SINR \simeq \frac{\sigma_s^2 N^2 P^2}{\sum_i \sigma_i^2 \left|\mathbf{a}^H(\theta_0, r_0, \alpha)\mathbf{a}(\theta_i, r_i, \alpha)\right|^2 \left|\mathbf{b}^H(\theta_0, r_0, \Delta f)\mathbf{b}(\theta_i, r_i, \Delta f)\right|^2} \tag{5.57}$$

These equations provide a proof that a strong echo from the target, which is the result of proposed transmitter FDA design can indeed increase the SINR.

5.2.4.3. Detection probability analysis

The signal at receiver array after interference suppression, can be given as

$$\mathbf{y} = \mathbf{w}_T^H \mathbf{a}(\theta_0, r_0, \alpha)\mathbf{b}(\theta_0, r_0, \Delta f) + \mathbf{n} \tag{5.58}$$

Where $\mathbf{b}(\theta_0, r_0, \Delta f)$ is the receive steering vector, while $\mathbf{w}_T^H \mathbf{a}(\theta_0, r_0, \alpha)$ is complex amplitude of the steered target and is a scalar value. $\mathbf{n}$ is the zero mean Gaussian noise with variance σ_n^2.

The hypothesis testing problem of a radar detection can be modeled as [30], [104]

$$\begin{cases} H_0 : \mathbf{y} = \mathbf{n} \\ H_1 : \mathbf{y} = \mathbf{w}_T^H \mathbf{a}(\theta_0, r_0, \alpha)\mathbf{b}(\theta_0, r_0, \Delta f) + \mathbf{n} \end{cases} \tag{5.59}$$

Here we assume that noise process is independent and identically distributed (i.i.d) Gaussian random noise with zero mean and variance σ_n^2.

The probability density function (PDF) i.e. the likelihood for a random variable $\mathbf{y}$ to take on a given value of H_0, is given by [104]

$$p(\mathbf{y}; H_0) = \exp\left(-\frac{\|\mathbf{y}\|^2}{\sigma_n^2}\right) \tag{5.60}$$

The PDF of H_1 is given by [104]

$$p(\mathbf{y};H_1)=\exp\left(-\frac{\|\mathbf{y}\|^2}{\sigma_n^2}\right)\times\exp\left(-\frac{\left|\left\|\mathbf{w}_T^H\mathbf{a}(\theta_0,r_0,\alpha)\right\|^2\left\|\mathbf{b}(\theta_0,r_0,\Delta f)\right\|^2+n\right|^2}{2\sigma_n^2}\right) \tag{5.61}$$

The likelihood ratio test is given as [104]

$$\wedge=\log\frac{p(\mathbf{y};H_1)}{p(\mathbf{y};H_0)}=\left|\left\|\mathbf{w}_T^H\mathbf{a}(\theta_0,r_0,\alpha)\right\|^2\left\|\mathbf{b}(\theta_0,r_0,\Delta f)\right\|^2+n\right|^2\underset{H_0}{\overset{H_1}{\gtrless}}\delta \tag{5.62}$$

where δ is threshold for detection. We suppose that the target signal is a Gaussian process with zero mean and variance σ_s^2. The Neyman-Pearson criterion based probability of detection and false alarm can be given as [30], [104]

$$p_{fa}=p(\wedge>\delta\mid H_0)=1-F_{\chi^2_{(2)}}\left(\frac{2\delta}{\sigma_n^2}\right) \tag{5.63}$$

$$p_d=p(\wedge>\delta\mid H_1)=1-F_{\chi^2_{(2)}}\left(\frac{\sigma_n^2F^{-1}_{\chi^2_{(2)}}(1-p_{fa})}{\sigma_s^2N^2M^2+\sigma_n^2}\right) \tag{5.64}$$

where M and N are the receiving and transmitting array elements respectively, $\chi^2_{(2)}$ is the chi-square distribution with 2 degrees-of-freedom, while $F(.)$ is cumulative distribution function. In this case, the strong received echoes increase the probability of detection (p_d) .

5.2.4.4. CRLB analysis

In this section, the performance of proposed scheme has been analyzed in terms of Cramer-Rao Lower Bound (CRLB) criteria for range and angle estimation. For CRLB, the data vector can be taken as [183]

$$\mathbf{y} = \left(\mathbf{w}_T^H \mathbf{a}\left(\theta_0, r_0, \alpha\right) \right) \mathbf{b}\left(\theta_0, r_0, \Delta f\right) + \mathbf{n} \tag{5.65}$$

where $\mathbf{b}(\theta_0, r_0, \Delta f)$ is receive steering vector, while $\mathbf{w}^H \mathbf{a}(\theta_0, r_0, \alpha)$ is complex amplitude of the steered target that provides improved SNR in this case. The improved SNR is due to the use of non-uniform frequency offsets along the transmitter FDA elements. $\mathbf{n}$ is the zero mean Gaussian noise with unit variance. Therefore, we can write array output in SNR terms given as

$$\mathbf{y} = \sqrt{SNR}\,\mathbf{b}(\theta_0, r_0, \Delta f) + \mathbf{n} \tag{5.66}$$

We assume that angle and range parameter vector i.e., $\gamma = [\theta_0, r_0]^T$ is unknown. The mean ε and covariance $\mathbf{\Gamma}$ of the array output $\mathbf{y}$ are given as

$$\varepsilon = \sqrt{SNR}\,\mathbf{b}(\theta_0, r_0, \Delta f) \tag{5.67}$$

$$\mathbf{\Gamma} = \mathbf{I} \tag{5.68}$$

The Fisher information matrix (FIM) is derived as [30], [183]

$$\mathbf{J} = 2\,\mathrm{Re}\left[\frac{d\varepsilon^*}{d\gamma}\,\mathbf{\Gamma}^{-1}\,\frac{d\varepsilon^T}{d\gamma}\right] = 2SNR\begin{bmatrix} J_{\theta_o\theta_o} & J_{\theta_o r_0} \\ J_{r_0\theta_0} & J_{r_0 r_0} \end{bmatrix} \tag{5.69}$$

Where the related values of $J_{\theta_o\theta_o}$ and $J_{r_0 r_0}$ are derived as [31], [183]

$$J_{\theta_o\theta_o} = \frac{4\pi^2 f_0^2 d^2 \cos^2(\theta_0)}{c^2} \sum_{n=-K}^{K} n^2 \tag{5.70}$$

$$J_{r_0 r_0} = \frac{4\pi^2 \Delta f^2}{c^2} \sum_{n=-K}^{K} n^2 \tag{5.71}$$

while, $J_{\theta_0 r_0}$ and $J_{r_0\theta_0}$ are derived as [31], [183]

$$J_{\theta_0 r_0} = J_{r_0\theta_0} = \frac{4\pi^2 f_0 \Delta f d \cos(\theta_0)}{c^2} \sum_{n=-K}^{K} n^2 \tag{5.72}$$

The CRLB for the target angle and range estimates can be given as the diagonal elements of the inverse J matrix i.e.

$$CRLB_{\theta_0\theta_0} = \left\lceil \left\lfloor \mathbf{J}^{-1} \right\rfloor \right\rceil_{1,1} \tag{5.73}$$

$$CRLB_{r_0 r_0} = \left\lceil \left\lfloor \mathbf{J}^{-1} \right\rfloor \right\rceil_{2,2} \tag{5.74}$$

The improved CRLB results are shown in simulations. The performance improvement is due to proposed scheme which directs the maximum energy towards the target.

5.2.5. Performance analysis of HCFDA with the proposed non-uniform FDA transmitter designs

This section describes the simulations and results. We assume a symmetric FDA of $N = 11$ transmitting array elements and M receiving array elements with half wave length inter-element distance. The AWGN is modeled as having a zero mean and equal variance at both ends. Likewise, we assume the carrier frequency $f_0 = 10GHz$ and frequency offsets $\Delta f = 30kHz$.

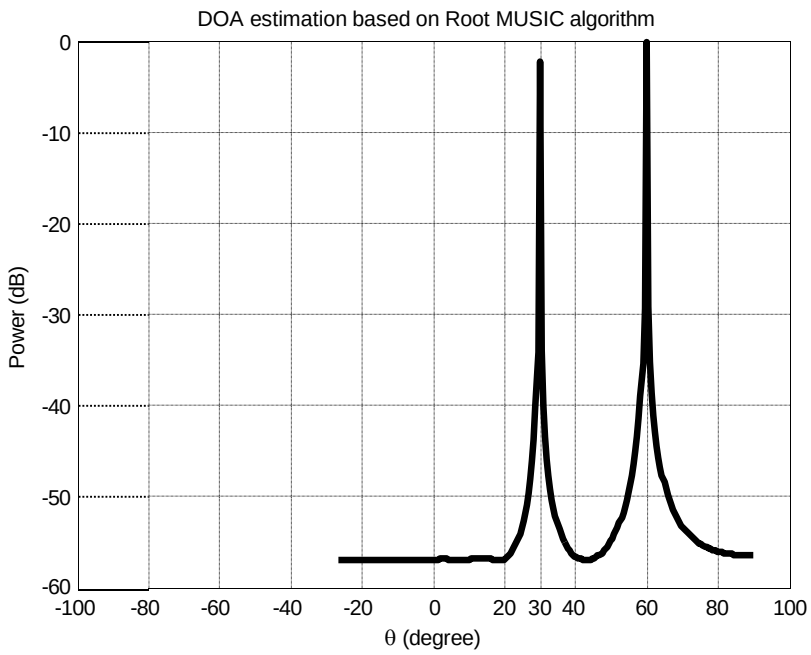

Figure- 5. 21: DOA estimation performance using Root Music algorithm

For DOA estimation, the Root MUSIC algorithm has been used. The SNR of received signal is assumed to be $20\,dB$. We assume that two signals imping on the receiving array from 30° and 60°. The employed algorithm estimates the target DOA quite accurately. Fig- 5.21 shows the DOA estimation results of Root MUSIC algorithm.

We assume that 30° is the target direction, while 60° is the direction of interference to be suppressed. Likewise, the range of these targets can easily be estimated using the conventional range estimation formula.

The current estimated range and direction of the target i.e., $\left(\hat{\theta}_{0,k}, \hat{r}_{0,k}\right)$, along with the previously estimated positions kept in the memory i.e., $\left(\hat{\theta}_{0,k-1}, \hat{r}_{0,k-1}\right), \left(\hat{\theta}_{0,k-2}, \hat{r}_{0,k-2}\right), \left(\hat{\theta}_{0,k-3}, \hat{r}_{0,k-3}\right), \ldots$, are forwarded to the EKF based prediction block of receiver to estimate target future direction i.e., $\left(\tilde{\theta}_{0,k+1}, \tilde{r}_{0,k+1}\right)$. Instead of taking

the target trajectory in Cartesian plane, we convert it to range (r) and theta (θ) axis for making is more relevant to range-angle dependent beamforming of FDA. The target motion is modelled using well-known coordinated turn model. We assume a nonlinear state vector denoted as $\mathbf{x} = [\theta \dot{\theta} r \dot{r} \xi]^T$, here θ and $\dot{\theta}$ are the target position and its velocity component along angle axis, while r and $\dot{r}$ are the range and its velocity component along range axis and ξ denotes the turn rate. The nonlinear transitional and measurement matrices are taken as

$$F = \begin{bmatrix} 1 & 0 & 0 & 0 & 0 \\ 0 & \xi & 0 & 0 & 0 \\ 0 & 0 & 1 & 0 & 0 \\ 0 & 0 & 0 & \xi & 0 \\ 0 & 0 & 0 & 0 & 0 \end{bmatrix} \text{ and } \tilde{H} = \begin{bmatrix} 1 & 0 & 0 & 0 & 0 \\ 0 & 0 & 1 & 0 & 0 \end{bmatrix}$$

Likewise, the process and measurement noises are taken as zero mean Gaussian with covariance matrices $\mathbf{Q}$ and $\mathbf{R}$, respectively, where $\mathbf{Q} = diag[0, \sigma_1^2, 0, \sigma_2^2, \sigma_2^2]$ with $\sigma_1^2 = \sigma_2^2 = 0.25$ and

$\mathbf{R} = diag([\sigma_\theta^2, \sigma_r^2])$ with $\sigma_\theta^2 = 0.01$ and $\sigma_r^2 = 0.2$. The SNR is taken as 10dB.

Fig-5.22 shows the prediction performance of this EKF based prediction block. Fig-5.22 (a) shows the observations of the target trajectory and Fig- 5.22 (b) shows the EKF based target position prediction performance. Fig-5.22 (c) & (d) show the comparison of Kalman filter (EKF) and EKF based prediction with the help of feedback performances in terms of measured mean square error with respect to angle and range.

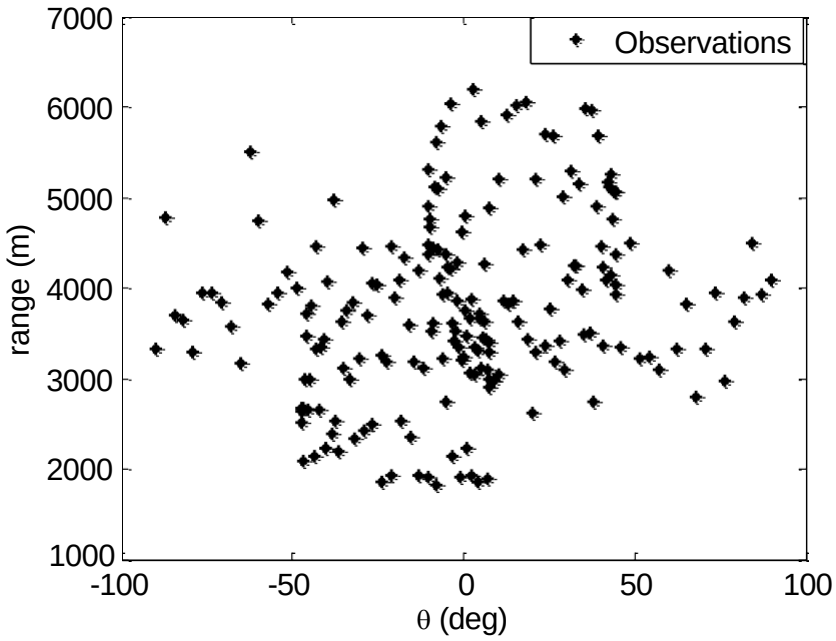

(a) Observations

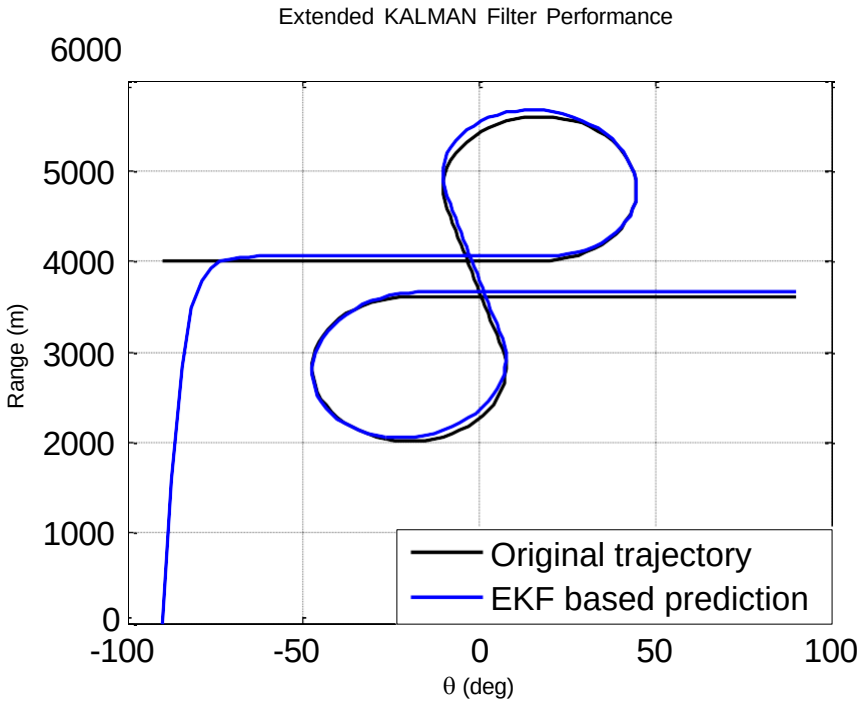

(b) EKF based prediction

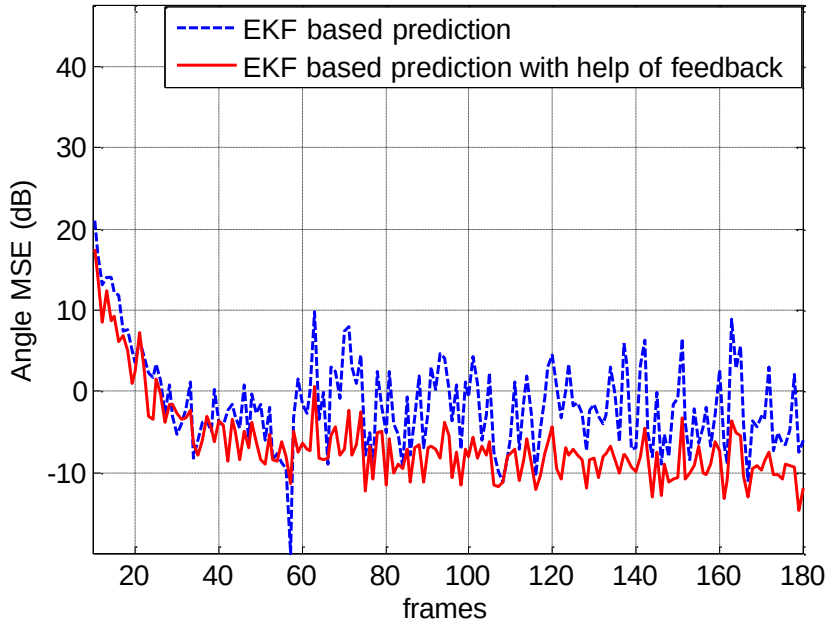

(c) Angle MSE

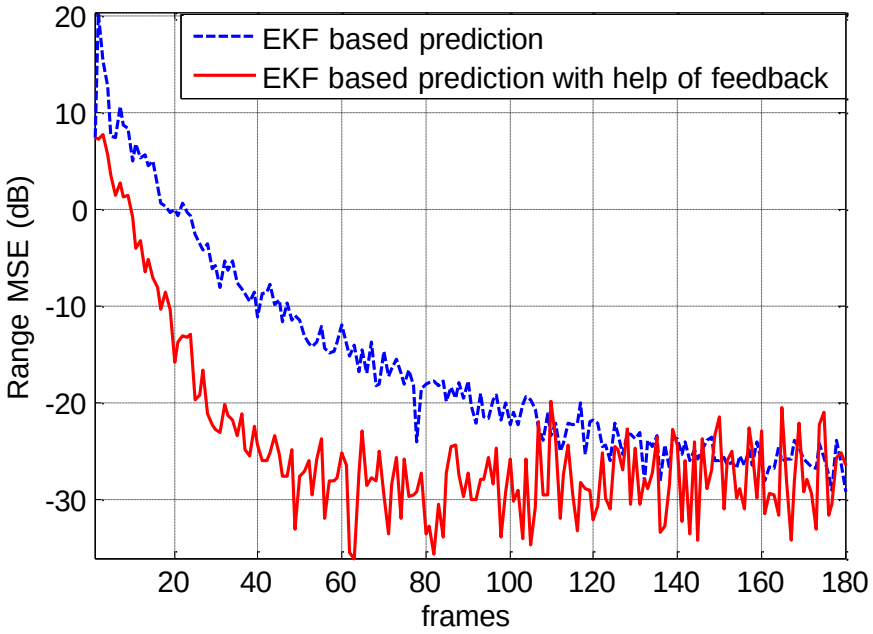

(d) Range MSE

Figure- 5. 22 : Performance Analysis of EKF based target position estimation

It can be noted that EKF with the help of feedback loop predicts the target position quite accurately. But if the environment becomes more non-stationary, the feedback property of cognitive radar helps the proposed system to maintain its performance. Therefore, this predicted estimate and estimation error of the target position is sent to the proposed transmitter for calculating the non-uniform frequency offsets using a suitable companding factor μ .

For SINR analysis, we assume that an interference is located at $\left(60^{\circ}, 4\,km\right)$, we fix the interference plus noise ratio (INR) equal to 30 dB. Fig-5.23 shows the output SINR vs SNR graph for the conventional and proposed FDA design. It can be noticed that the proposed radar has a better SINR performance than that of a conventional FDA radar.

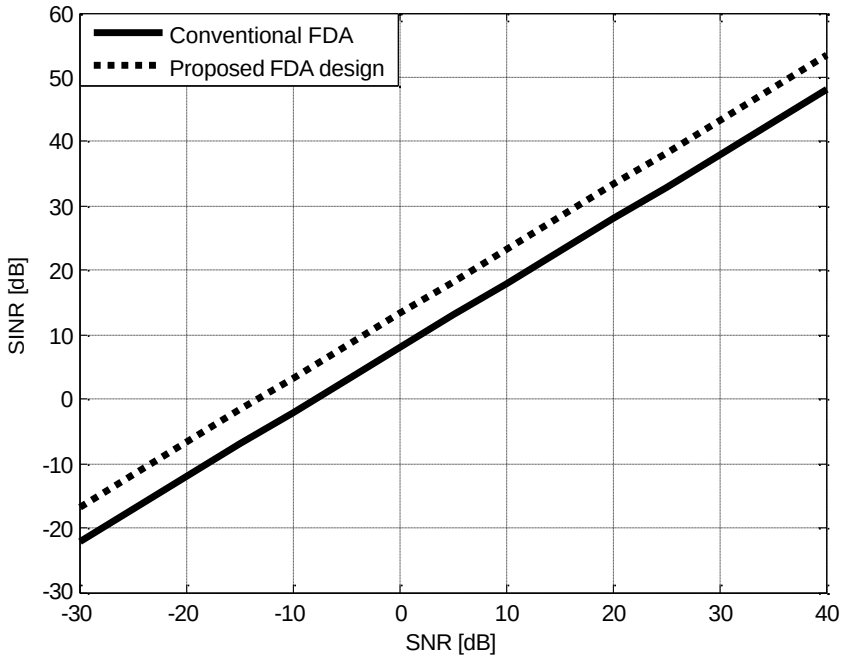

Figure- 5. 23: The comparison of output SINR vs SNR of proposed and conventional FDA at fixed INR=30 dB $N = P = 11, \hat{r_0} = 3\,km, f_0 = 10GHz, \Delta f = \delta = 30\,kHz$

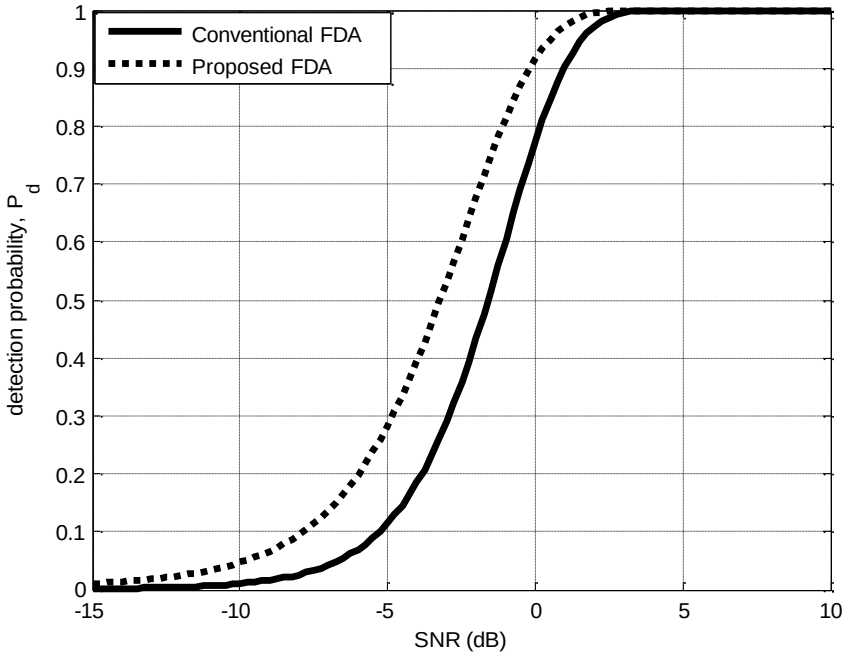

Figure- 5. 24: Comparison between the detection performance of proposed HCFDA designs and conventional FDA

For evaluation of detection performance, the probability of false alarm is kept constant i.e., $p_{fa} = 1e-4$. Fig- 5.24 shows the detection performance of proposed FDA design and compares it with conventional FDA radar detection performance. Furthermore, it can be noticed that proposed design achieves a better detection performance because a higher SNR is obtained due to a sharp transmitted power peak directed towards the target.

Fig- 5.25 (a) shows the comparison of the proposed HCFDA radar designs and conventional FDA for CRLB performance on target angle, while Fig-5.25 (b) shows CRLB performance comparison on target range. It is evident that proposed approaches gives adequate estimation performance.

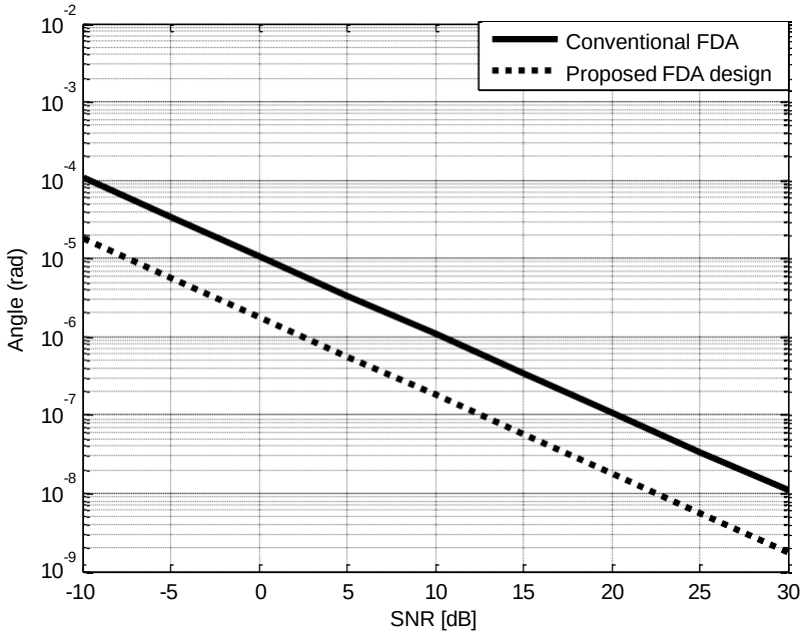

(a) CRLB on target angle

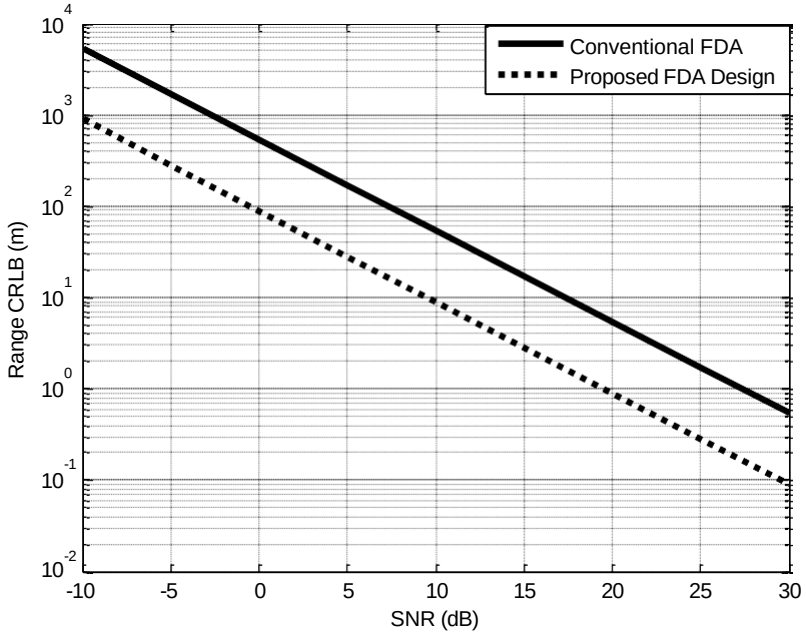

(b) CRLB on target Range

Figure- 5. 25: Comparison of CRLB estimation performance vs. SNR

5.3. Conclusion and discussion

In the nutshell, the proposed systems learn about the statistical variations of environment and in response, it makes suitable changes in the adaptive parameters for maintaining an improved performance. The cognitive properties, such as feedback, memory and application of adaptive signal processing at the receiver and transmitter have been utilized to maintain an improved performance. Consequently, the proposed radar design achieves an enhanced SINR that results in better detection performance and improved CRLB for target position estimation as compared to the conventional FDA. Likewise, the symmetrical offsets applied around the middle elements helps in generating deeper nulls in comparison to the non-symmetric designs.

CHAPTER-6

Conclusions and Future Work

6.1. Conclusions

This dissertation investigated and studied various types of hybrid radars based on linear antenna arrays. Phased array radar (PAR) is already in its mature form, while research community is focusing towards frequency diverse array (FDA) and cognitive radars (CR). Moreover, hybrid designs of CR with PAR and FDA radars promised significant performance improvement as compared to stand-alone PAR and FDAs. The performance improvement of the proposed hybrid designs is in terms of enhanced signal to interference and noise ratio (SINR), improved detection probability, better range and angle resolution, enhanced transmit energy focusing, better energy efficiency, improved tracking performance and improved Cramer Rao lower bounds (CRLB) on range and angle estimates.

To analyze the performance of hybrid cognitive phased array radar (HCPAR), a cognitive model has been proposed that avoided continuous scanning of the surveillance region. Instead, only the predicted regions based on the receiver feedback are scanned during next cycle, which resulted in saving a lot of power. Moreover, it is shown that the proposed design intelligently varied active elements of the employed phased arrays according to the requirement. Consequently, it reduced computational and hardware complexity as compared to the fixed element phased array. The more focused beam pattern towards the predicted target direction resulted in higher SINR

and improved detection probability. It has been shown that the proposed cognitive design updated the radar parameters after sensing the environment in an intelligent manner to get the improved performance.

To analyze the performance of the proposed hybrid cognitive frequency diverse array (HCFDA) radar design, a cognitive frequency offset computation scheme has been formulated. In this case, an FDA with uniform inter-element frequency offset has been assumed. Additionally, to improve the SINR and detection probability in an FDA radar paradigm, a cognitive FDA design has been proposed. The proposed design updated its parameters, intelligently, based on feedback to get improved performance. In this case, the 3-D range-angle dependent beam pattern is observed to ensure power peaks towards the predicted range and direction of the target, which resulted in improved SINR, tracking performance and detection probability. Moreover, it saved power and reduced computational complexity compared to the conventional FDA and phased array radar. The proposed design also avoided pollution of the environment from the electromagnetic radiations.

To analyze the performance of HCFDA with non-uniform frequency offset among the array elements, a cognitive FDA design has been proposed that learned the statistical variations of environment and in response, it suggested suitable changes in the adaptive parameters for maintaining an improved performance. Moreover, three new methods are introduced to compute the non-uniform frequency offsets. These offsets resulted in 3-D single maximum beam pattern, which ensured better SINR, detection probability and enhanced transmit energy focusing. Additionally, an improved CRLB for target position estimation has been achieved as compared to a conventional FDA. Moreover, a symmetrical offsets application scheme has resulted

in generating deeper nulls in comparison to the non-symmetric designs, which further improved SINR.

6.2. Future work

In future, the work presented in this dissertation may be extended in various dimensions:

- In this dissertation, we have focused only the linear arrays. For improved localization performance this work can be extended towards planer arrays as well. The planer arrays, simultaneously, localize targets in elevation and azimuth in contrast with the linear arrays, which can localize targets only in one direction. Planer PAR are in mature form but we will investigate towards cognitive planer PAR and FDA designs for achieving improved performance.
- The non-uniform frequency offset scheme for the presented cognitive FDA design achieves single maximum 3-D beam pattern, which helps to mitigate interferences efficiently. Therefore, different windowing schemes, such as Hann window, Chebyshev window, Blackman window, flattop window, cosine window etc. can be applied to a presented cognitive FDA design to achieve improved transmit focusing towards the target position.
- The neural networks (NN) utilized for cognitive radars may be applied on the presented hybrid cognitive PAR and FDA design to make them intelligent. The NN will surely help the modern radar systems to evolve into an entirely new generations of intelligent radars.

REFERENCES

[1] M. I. Skolnik, "Introduction to radar," *Radar Handb.*, vol. 2, 1962.

[2] R. W. Burns, "Radar development to 1945," 1988.

[3] M. Skolnik, "Fifty years of radar," *Proc. IEEE*, vol. 73, no. 2, pp. 182–197, 1985.

[4] K. F. Molz, "Phased array radar systems," *Radio and Electronic Engineer*, vol. 28, no. 5. pp. 331–339, 1964.

[5] M. Whorton, "Evaluating and managing Cold War era historic properties: the cultural significance of US Air Force defensive radar systems," *Matériel Cult. Archaeol. Twent. century Confl.*, pp. 216–226, 2002.

[6] J. W. Taylor Jr and G. Brunins, "Design of a new airport surveillance radar (ASR-9)," *Proc. IEEE*, vol. 73, no. 2, pp. 284–289, 1985.

[7] D. L. Collinson and J. A. Rougas, "Integrated antenna radar system for mobile and transportable air defense." Google Patents, 19-Aug-2003.

[8] S. A. Schelkunoff, "A mathematical theory of linear arrays," *Bell Syst. Tech. J.*, vol. 22, no. 1, pp. 80–107, 1943.

[9] D. R. Rhodes, "On a fundamental principle in the theory of planar antennas," *Proc. IEEE*, vol. 52, no. 9, pp. 1013–1021, 1964.

[10] H. P. Neff and J. D. Tillman, "An omnidirectional circular antenna array excited parasitically by a central driven element," *Am. Inst. Electr. Eng. Part I Commun. Electron. Trans.*, vol. 79, no. 2, pp. 190–192, 1960.

[11] K. Milne, "Phased arrays in radar," in *Phased Array Radar, IEE Tutorial Meeting on*, 1989, pp. 1–2.

[12] J. L. Allen, "The theory of array antennas (with emphasis on radar applications)," DTIC Document, 1963.

[13] D. S. Zrnic, V. M. Melnikov, R. J. Doviak, and R. Palmer, "Scanning strategy for the multifunction phased-array radar to satisfy aviation and meteorological needs," *Geosci. Remote Sens. Lett. IEEE*, vol. 12, no. 6, pp. 1204–1208, 2015.

[14] E. Yoshikawa, T. Ushio, Z. Kawasaki, S. Yoshida, T. Morimoto, F. Mizutani, and M. Wada, "MMSE beam forming on fast-scanning phased array weather radar," *Geosci. Remote Sensing, IEEE Trans.*, vol. 51, no. 5, pp. 3077–3088, 2013.

[15] Z. Spasojevic, S. Dedeo, and R. Jensen, “Dwell scheduling algorithms for phased array antenna,” *Aerosp. Electron. Syst. IEEE Trans.*, vol. 49, no. 1, pp. 42–54, 2013.

[16] M. Mouhamadou, P. Vaudon, and M. Rammal, “Smart antenna array patterns synthesis: Null steering and multi-user beamforming by phase control,” *Prog. Electromagn. Res.*, vol. 60, pp. 95–106, 2006.

[17] P. Rocca, R. L. Haupt, and A. Massa, “Interference suppression in uniform linear arrays through a dynamic thinning strategy,” *Antennas Propagation, IEEE Trans.*, vol. 59, no. 12, pp. 4525–4533, 2011.

[18] R. F. Harrington, “Sidelobe reduction by nonuniform element spacing,” *Antennas Propagation, IRE Trans.*, vol. 9, no. 2, pp. 187–192, 1961.

[19] W. H. Von Aulock, “Properties of Phased Arrays,” *Proceedings of the IRE*, vol. 48, no. 10. pp. 1715–1727, 1960.

[20] N. Fourikis, *Phased array-based systems and applications*. Wiley, 1997.

[21] C. A. Balanis, *Antenna theory: analysis and design*, vol. 1. John Wiley & Sons, 2005.

[22] H. Unz, “Linear arrays with arbitrarily distributed elements,” *IRE Trans. Antennas Propag.*, vol. 2, no. 8, pp. 222–223, 1960.

[23] D. D. King, R. F. Packard, and R. K. Thomas, “Unequally-spaced, broad-band antenna arrays,” *Antennas Propagation, IRE Trans.*, vol. 8, no. 4, pp. 380–384, 1960.

[24] R. C. Hansen, *Phased array antennas*, vol. 213. John Wiley & Sons, 2009.

[25] R. J. Mailloux, “Phased array antenna handbook,” *Boston, MA Artech House, 1994.*, 1994.

[26] D. Parker and D. C. Zimmermann, “Phased arrays-Part I: Theory and architectures,” *IEEE Trans. Microw. Theory Tech.*, vol. 50, no. 3, pp. 678–687, 2002.

[27] D. Parker and D. C. Zimmermann, “Phased arrays-part II: implementations, applications, and future trends,” *IEEE Trans. Microw. Theory Tech.*, vol. 50, no. 3, pp. 688–698, 2002.

[28] E. Brookner, “Phased-array radars,” *Sci. Am.*, vol. 252, no. 2, pp. 94–102, 1985.

[29] A. J. Fenn, D. H. Temme, W. P. Delaney, and W. E. Courtney, “The Development of Phased-Array Radar Technology,” *Physics (College. Park. Md).*, vol. 12, no. 2, pp. 321–340, 2000.

[30] H. L. Van Trees, “Optimum array processing: part IV of detection, estimation, and modulation.” Wiley, New York, 2002.

[31] H. L. Van Trees, *Detection, estimation, and modulation theory, optimum array processing*. John Wiley & Sons, 2004.

[32] B. Widrow and S. D. Stearns, “Adaptive signal processing,” *Englewood Cliffs, NJ, Prentice-Hall, Inc., 1985, 491 p.*, vol. 1, 1985.

[33] T. V Ho, J. G. McWhirter, A. Nehorai, U. Nickel, B. Ottersten, B. D. Steinberg, P. Stoica, M. Viberg, Z. Zhu, and S. Haykin, *Radar array processing*, vol. 25. Springer Science & Business Media, 2013.

[34] E. Brookner, “Major advances in phased arrays: Part I,” *Microw. J.*, vol. 40, no. 5, pp. 288–294, 1997.

[35] H. H. M. Ghouz, F. I. A. Elghany, and M. M. Qutb, “Adaptive space-time processing for interference suppression in phased array radar systems. II. Tracking radar,” *Radio Science Conference, 2000. 17th NRSC ’2000. Seventeenth National*. pp. B9/1–B9/7, 2000.

[36] B. Allen and M. Ghavami, *Adaptive array systems: fundamentals and applications*. John Wiley & Sons, 2006.

[37] R. D. Brown, R. Schneible, M. C. Wicks, H. Wang, and Y. Zhang, “STAP for clutter suppression with sum and difference beams,” *Aerosp. Electron. Syst. IEEE Trans.*, vol. 36, no. 2, pp. 634–646, 2000.

[38] R. O. Schmidt, “Multiple emitter location and signal parameter estimation,” *Antennas Propagation, IEEE Trans.*, vol. 34, no. 3, pp. 276–280, 1986.

[39] B. D. Rao and K. V. S. Hari, “Performance analysis of root-MUSIC,” *Acoust. Speech Signal Process. IEEE Trans.*, vol. 37, no. 12, pp. 1939–1949, 1989.

[40] R. Roy and T. Kailath, “ESPRIT-estimation of signal parameters via rotational invariance techniques,” *Acoust. Speech Signal Process. IEEE Trans.*, vol. 37, no. 7, pp. 984–995, 1989.

[41] G. C. Carter, “Time delay estimation for passive sonar signal processing,” *Acoust. Speech Signal Process. IEEE Trans.*, vol. 29, no. 3, pp. 463–470, 1981.

[42] A. K. Agrawal and E. L. Holzman, “Beamformer architectures for active phased-array radar antennas,” *Antennas and Propagation, IEEE Transactions on*, vol. 47, no. 3. pp. 432–442, 1999.

[43] R. E. Willey, “Space tapaering of linear and planar arrays,” *Antennas Propagation, IRE Trans.*, vol. 10, no. 4, pp. 369–377, 1962.

[44] S. U. Khan, I. M. Qureshi, F. Zaman, and A. Naveed, “Null placement and sidelobe suppression in failed array using symmetrical element failure

technique and hybrid heuristic computation," *Prog. Electromagn. Res. B*, vol. 52, pp. 165–184, 2013.

[45] R. L. Haupt, "Phase-only adaptive nulling with a genetic algorithm," *Antennas Propagation, IEEE Trans.*, vol. 45, no. 6, pp. 1009–1015, 1997.

[46] A. Akdagli, "Null steering of linear antenna arrays using a modified tabu search algorithm," *Prog. Electromagn. Res.*, vol. 33, pp. 167–182, 2001.

[47] R. E. Kalman, "A new approach to linear filtering and prediction problems," *J. Fluids Eng.*, vol. 82, no. 1, pp. 35–45, 1960.

[48] S. J. Julier and J. K. Uhlmann, "New extension of the Kalman filter to nonlinear systems," in *AeroSense'97*, 1997, pp. 182–193.

[49] E. Wan and R. Van Der Merwe, "The unscented Kalman filter for nonlinear estimation," in *Adaptive Systems for Signal Processing, Communications, and Control Symposium 2000. AS-SPCC. The IEEE 2000*, 2000, pp. 153–158.

[50] M. S. Grewal and A. P. Andrews, *Kalman filtering: Theory and Practice with MATLAB*. John Wiley & Sons, 2014.

[51] L. Zhu, W. Su, S. Wu, Y. Wang, and X. Shan, "Phased-Array Radar Beam Tracking and Predicting," *Wireless Communications, Networking and Mobile Computing, 2009. WiCom '09. 5th International Conference on*. pp. 1–4, 2009.

[52] F. E. Daum and R. J. Fitzgerald, "Decoupled Kalman filters for phased array radar tracking," *Autom. Control. IEEE Trans.*, vol. 28, no. 3, pp. 269–283, 1983.

[53] M. I. Skolnik, *Radar Handbook*. 2008.

[54] A. Ishimaru and Y.-S. Chen, "Thinning and broadbanding antenna arrays by unequal spacings," *Antennas and Propagation, IEEE Transactions on*, vol. 13, no. 1. pp. 34–42, 1965.

[55] T. F. Chun, A. Zamora, B. J. Lei, R. T. Iwami, and W. A. Shiroma, "An interleaved, interelement phase-detecting/phase-shifting retrodirective antenna array for interference reduction," *IEEE Antennas Wirel. Propag. Lett.*, no. 10, pp. 919–922, 2011.

[56] F. Tokan and F. Güneş, "Interference suppression by optimising the positions of selected elements using generalised pattern search algorithm," *IET microwaves, antennas Propag.*, vol. 5, no. 2, pp. 127–135, 2011.

[57] E. Brookner, "Phased array radars-past, present and future," *RADAR 2002*. pp. 104–113, 2002.

[58] J. H. G. Ender, H. Wilden, U. Nickel, R. Klemm, A. R. Brenner, T. Eibert, and D. Nussler, "Progress in phased-array radar applications," *Microwave Symposium Digest, 2005 IEEE MTT-S International*. p. 4 pp., 2005.

[59] D. C. Schleher, "Introduction to electronic warfare," Eaton Corp., AIL Div., Deer Park, NY, 1986.

[60] G. Schrick and R. Wiley, "Interception of LPI radar signals," in *Radar Conference, 1990., Record of the IEEE 1990 International*, 1990, pp. 108–111.

[61] K. L. Fuller, "To see and not be seen," in *IEE Proceedings F (Radar and Signal Processing)*, 1990, vol. 137, no. 1, pp. 1–9.

[62] D. E. Lawrence, "Low probability of intercept antenna array beamforming," *Antennas Propagation, IEEE Trans.*, vol. 58, no. 9, pp. 2858–2865, 2010.

[63] E. J. Carlson, "Low probability of intercept (LPI) techniques and implementations for radar systems," in *Radar Conference, 1988., Proceedings of the 1988 IEEE National*, 1988, pp. 56–60.

[64] P. E. Pace, *Detecting and classifying low probability of intercept radar*. Artech House, 2009.

[65] Y. D. Shirman, S. P. Leshchenko, and V. M. Orlenko, "Advantages and problems of wideband radar," in *Radar Conference, 2003. Proceedings of the International*, 2003, pp. 15–21.

[66] D. C. Schleher, "LPI radar: fact or fiction," *Aerosp. Electron. Syst. Mag. IEEE*, vol. 21, no. 5, pp. 3–6, 2006.

[67] M. Bouanen, F. Gagnon, G. Kaddoum, D. Couillard, and C. Thibeault, "An LPI design for secure OFDM systems," in *Military Communications Conference, 2012-Milcom 2012*, 2012, pp. 1–6.

[68] B. Qing-long, Y. Jian, Z. Yue, and C. Zeng-ping, "LPI performance of digital array radars," 2009.

[69] E. J. Baghdady, "Directional signal modulation by means of switched spaced antennas," *Commun. IEEE Trans.*, vol. 38, no. 4, pp. 399–403, 1990.

[70] H. Deng, "Waveform design for MIMO radar with low probability of intercept (LPI) property," in *2011 IEEE International Symposium on Antennas and Propagation (APSURSI)*, 2011.

[71] R. E. Mills and G. E. Prescott, "Waveform design and analysis of frequency hopping LPI networks," in *Military Communications Conference, 1995. MILCOM'95, Conference Record, IEEE*, 1995, vol. 2, pp. 778–782.

[72] J. Li, G. Liao, and H. Griffiths, “Range-dependent clutter cancellation method in bistatic MIMO-STAP radars,” in *Radar (Radar), 2011 IEEE CIE International Conference on*, 2011, vol. 1, pp. 59–62.

[73] M. M. Weiner, “Proposed Algorithm for Sequential Implementation of Adaptive Antennas and Receivers [Letters to the Editor],” *Antennas Propag. Mag. IEEE*, vol. 51, no. 5, pp. 161–162, 2009.

[74] V. Murthy, U. Pillai, and M. E. Davis, “Waveforms for Simultaneous SAR and GMTI,” in *Radar Conference (RADAR), 2012 IEEE*, 2012, pp. 51–56.

[75] G. Oliveri, F. Caramanica, and A. Massa, “Hybrid ADS-based techniques for radio astronomy array design,” *Antennas Propagation, IEEE Trans.*, vol. 59, no. 6, pp. 1817–1827, 2011.

[76] P. Antonik, M. C. Wicks, H. D. Griffiths, and C. J. Baker, “Frequency diverse array radars,” in *IEEE National Radar Conference - Proceedings*, 2006, pp. 215–217.

[77] D. K. Barton, *Frequency Agility and Diversity*, vol. 6. Artech House on Demand, 1977.

[78] P. Antonik, “An investigation of a frequency diverse array.” University College London United Kingdom, 2009.

[79] J. Huang and K.-F. Tong, “Frequency diverse array with beam scanning feature,” in *2008 IEEE Antennas and Propagation Society International Symposium*, 2008, pp. 1–4.

[80] J. Huang, K. F. Tong, and C. Baker, “Frequency diverse array: Simulation and design,” in *Antennas & Propagation Conference, 2009. LAPC 2009. Loughborough*, 2009, pp. 253–256.

[81] M. Secmen, S. Demir, A. Hizal, and T. Eker, “Frequency diverse array antenna with periodic time modulated pattern in range and angle,” in *IEEE National Radar Conference - Proceedings*, 2007, pp. 427–430.

[82] P. F. Sammartino, C. J. Baker, and H. D. Griffiths, “Frequency diverse MIMO techniques for radar,” *IEEE Trans. Aerosp. Electron. Syst.*, vol. 49, no. 1, pp. 201–222, 2013.

[83] W.-Q. Wang, H. Shao, and J. Cai, “Range-angle-dependent beamforming by frequency diverse array antenna,” *Int. J. Antennas Propag.*, vol. 2012, 2012.

[84] W.-Q. Wang and J. Cai, “MIMO SAR using chirp diverse waveform for wide-swath remote sensing,” *Aerosp. Electron. Syst. IEEE Trans.*, vol. 48, no. 4, pp. 3171–3185, 2012.

[85] A. M. Haimovich, R. S. Blum, and L. J. Cimini, “MIMO radar with widely separated antennas,” *Signal Process. Mag. IEEE*, vol. 25, no. 1, pp. 116–129, 2008.

[86] J. Li and P. Stoica, “MIMO radar with colocated antennas,” *Signal Process. Mag. IEEE*, vol. 24, no. 5, pp. 106–114, 2007.

[87] Y. Ding, J. Zhang, and V. Fusco, “Frequency diverse array OFDM transmitter for secure wireless communication,” *Electronics Letters*, vol. 51, no. 17. pp. 1374–1376, 2015.

[88] W.-Q. Wang, “Mitigating range ambiguities in high-PRF SAR with OFDM waveform diversity,” *Geosci. Remote Sens. Lett. IEEE*, vol. 10, no. 1, pp. 101–105, 2013.

[89] F. S. Johansson, L. G. Josefsson, and T. Lorentzon, “A novel frequency- scanned reflector antenna,” *Antennas Propagation, IEEE Trans.*, vol. 37, no. 8, pp. 984–989, 1989.

[90] C. Vazquez, C. Garcia, Y. Alvarez, S. Ver-Hoeye, and F. Las-Heras, “Near field characterization of an imaging system based on a frequency scanning antenna array,” *Antennas Propagation, IEEE Trans.*, vol. 61, no. 5, pp. 2874– 2879, 2013.

[91] W.-Q. Wang, “Range-angle dependent transmit beampattern synthesis for linear frequency diverse arrays,” *Antennas Propagation, IEEE Trans.*, vol. 61, no. 8, pp. 4073–4081, 2013.

[92] W. Q. Wang, “Phased-MIMO radar with frequency diversity for range-dependent beamforming,” *IEEE Sens. J.*, vol. 13, no. 4, pp. 1320–1328, 2013.

[93] P. Antonik, M. C. Wicks, H. D. Griffiths, and C. J. Baker, “Multi-mission multi-mode waveform diversity,” in *Radar, 2006 IEEE Conference on*, 2006, p. 3–pp.

[94] P. Antonik, M. C. Wicks, H. D. Griffiths, and C. J. Baker, “Range dependent beamforming using element level waveform diversity,” in *Proceedings of the International Waveform Diversity and Design Conference*, 2006, pp. 1–4.

[95] C. Yong-guang, L. Yun-tao, W. Yan-hong, and C. Hong, “Research on the linear frequency diverse array performance,” in *Signal Processing (ICSP), 2010 IEEE 10th International Conference on*, 2010, pp. 2324–2327.

[96] P. F. Sammartino, C. J. Baker, and H. D. Griffiths, “Range-angle dependent waveform,” *Radar Conference, 2010 IEEE*. pp. 511–515, 2010.

[97] H. Shao, J. Li, H. Chen, and W.-Q. Wang, “Adaptive Frequency Offset Selection in Frequency Diverse Array Radar,” *Antennas Wirel. Propag. Lett. IEEE*, vol. 13, pp. 1405–1408, 2014.

[98] W. Khan and I. M. Qureshi, “Frequency Diverse Array Radar With Time-Dependent Frequency Offset,” *Antennas Wirel. Propag. Lett. IEEE*, vol. 13, pp. 758–761, 2014.

[99] J. Shin, J.-H. Choi, J. Kim, J. Yang, W. Lee, J. So, and C. Cheon, “Full-wave simulation of frequency diverse array antenna using the FDTD method,” in *Microwave Conference Proceedings (APMC), 2013 Asia-Pacific*, 2013, pp. 1070–1072.

[100] T. Higgins and S. D. Blunt, “Analysis of range-angle coupled beamforming with frequency-diverse chirps,” in *Waveform Diversity and Design Conference, 2009 International*, 2009, pp. 140–144.

[101] P. F. Sammartino and C. J. Baker, “Developments in the Frequency Diverse Bistatic System,” *Radar Conference, 2009 IEEE*. pp. 1–5, 2009.

[102] P. F. Sammartino and C. J. Baker, “The frequency diverse bistatic system,” in *2009 International Waveform Diversity and Design Conference*, 2009.

[103] W. Q. Wang and H. C. So, “Transmit subaperturing for range and angle estimation in frequency diverse array radar,” *IEEE Trans. Signal Process.*, vol. 62, no. 8, pp. 2000–2011, 2014.

[104] W.-Q. Wang and H. Shao, “Range-angle localization of targets by a double-pulse frequency diverse array radar,” *Sel. Top. Signal Process. IEEE J.*, vol. 8, no. 1, pp. 106–114, 2014.

[105] W.-Q. Wang, H. C. So, and H. Shao, “Nonuniform frequency diverse array for range-angle imaging of targets,” *Sensors Journal, IEEE*, vol. 14, no. 8, pp. 2469–2476, 2014.

[106] P. Baizert, T. B. Hale, M. A. Temple, and M. C. Wicks, “Forward-looking radar GMTI benefits using a linear frequency diverse array,” *Electron. Lett.*, vol. 42, no. 22, pp. 1311–1312, 2006.

[107] C. Cetintepe and S. Demir, “Multipath characteristics of frequency diverse arrays over a ground plane,” *Antennas Propagation, IEEE Trans.*, vol. 62, no. 7, pp. 3567–3574, 2014.

[108] T. Eker, S. Demir, and A. Hizal, “Exploitation of linear frequency modulated continuous waveform (LFMCW) for frequency diverse arrays,” *Antennas Propagation, IEEE Trans.*, vol. 61, no. 7, pp. 3546–3553, 2013.

[109] A. M. Jones, “Frequency diverse array receiver architectures.” Wright State University, 2011.

[110] A. M. Jones and B. D. Rigling, “Planar frequency diverse array receiver architecture,” in *Radar Conference (RADAR), 2012 IEEE*, 2012, pp. 145–150.

[111] J. Farooq, M. A. Temple, and M. A. Saville, “Application of frequency diverse arrays to synthetic aperture radar imaging,” in *2007 International Conference on Electromagnetics in Advanced Applications, ICEAA’07*, 2007, pp. 447–449.

[112] J. Farooq, M. A. Temple, and M. A. Saville, “Exploiting frequency diverse array processing to improve SAR image resolution,” in *2008 IEEE Radar Conference, RADAR 2008*, 2008.

[113] M. C. Wicks and P. Antonik, “Frequency diverse array with independent modulation of frequency, amplitude, and phase.” Google Patents, 15-Jan-2008.

[114] M. C. Wicks and P. Antonik, “Method and apparatus for a frequency diverse array.” Google Patents, 31-Mar-2009.

[115] W. Khan, I. M. Qureshi, and S. Saeed, “Frequency Diverse Array Radar With Logarithmically Increasing Frequency Offset,” *Antennas Wirel. Propag. Lett. IEEE*, vol. 14, pp. 499–502, 2015.

[116] V. K. Singh and M. S. Kankanhalli, “Adversary aware surveillance systems,” *Inf. Forensics Secur. IEEE Trans.*, vol. 4, no. 3, pp. 552–563, 2009.

[117] S. Haykin, *Adaptive radar signal processing*. John Wiley & Sons, 2007.

[118] F. E. Nathanson, J. P. Reilly, and M. N. Cohen, “Radar design principles- Signal processing and the Environment,” *NASA STI/Recon Tech. Rep. A*, vol. 91, p. 46747, 1991.

[119] M. I. Skolnik, “Radar handbook,” 1970.

[120] D. F. DeLong Jr and E. M. Hofstetter, “On the design of optimum radar waveforms for clutter rejection,” *Inf. Theory, IEEE Trans.*, vol. 13, no. 3, pp. 454–463, 1967.

[121] D. F. Delong Jr and E. M. Hofstetter, “The design of clutter-resistant radar waveforms with limited dynamic range,” *Inf. Theory, IEEE Trans.*, vol. 15, no. 3, pp. 376–385, 1969.

[122] M. R. Bell, “Information theory and radar waveform design,” *Inf. Theory, IEEE Trans.*, vol. 39, no. 5, pp. 1578–1597, 1993.

[123] M. Athans and F. C. Schweppe, “Optimal waveform design via control theoretic concepts,” *Inf. Control*, vol. 10, no. 4, pp. 335–377, 1967.

[124] S. Haykin, “Cognitive radar: a way of the future,” *Signal Process. Mag. IEEE*, vol. 23, no. 1, pp. 30–40, 2006.

[125] X. Yanbo, “Cognitive Radar: Theory and Simulations.” Canada Hamilton: McMaster University, 2010.

[126] J. R. Guerci, "Cognitive radar: A knowledge-aided fully adaptive approach," *Radar Conference, 2010 IEEE*. pp. 1365–1370, 2010.

[127] S. Haykin, Y. Xue, and P. Setoodeh, "Cognitive radar: Step toward bridging the gap between neuroscience and engineering," *Proc. IEEE*, vol. 100, no. 11, pp. 3102–3130, 2012.

[128] S. Haykin and J. M. Fuster, "On cognitive dynamic systems: Cognitive neuroscience and engineering learning from each other," *Proc. IEEE*, vol. 102, no. 4, pp. 608–628, 2014.

[129] S. Haykin, "Cognitive Dynamic Systems: Radar, Control, and Radio [Point of View]," *Proceedings of the IEEE*, vol. 100, no. 7. pp. 2095–2103, 2012.

[130] S. Haykin, A. Zia, I. Arasaratnam, and Y. Xue, "Cognitive tracking radar," *Radar Conference, 2010 IEEE*. pp. 1467–1470, 2010.

[131] C. Micheloni, P. Remagnino, H.-L. Eng, and J. Geng, "Intelligent monitoring of complex environments," *Intell. Syst. IEEE*, vol. 25, no. 3, pp. 12–14, 2010.

[132] J. R. Guerci, R. M. Guerci, M. Ranagaswamy, J. S. Bergin, and M. C. Wicks, "CoFAR: Cognitive fully adaptive radar," *Radar Conference, 2014 IEEE*. pp. 984–989, 2014.

[133] P. Chavali and A. Nehorai, "Cognitive radar for target tracking in multipath scenarios," in *Waveform Diversity and Design Conference (WDD), 2010 International*, 2010, pp. 110–114.

[134] M.-O. Pun, D. R. Brown III, and H. V. Poor, "Opportunistic collaborative beamforming with one-bit feedback," *Wirel. Commun. IEEE Trans.*, vol. 8, no. 5, pp. 2629–2641, 2009.

[135] R. Mudumbai, B. Wild, U. Madhow, and K. Ramchandran, "Distributed beamforming using 1 bit feedback: from concept to realization," in *Proceedings of the 44th Allerton conference on communication, control and computation*, 2006, pp. 1020–1027.

[136] S. Song, J. S. Thompson, P.-J. Chung, and P. M. Grant, "Exploiting negative feedback information for one-bit feedback beamforming algorithm," *Wirel. Commun. IEEE Trans.*, vol. 11, no. 2, pp. 516–525, 2012.

[137] W.-Q. Wang, "Cognitive frequency diverse array radar with situational awareness," *IET Radar, Sonar Navig.*, 2015.

[138] J. R. Guerci, "CognitiveRadar, the Knowledge-aided Fully Adaptive Approach." London, UK: ArtechHouse, 2010.

[139] U. Güntürkün, "Toward the development of radar scene analyzer for cognitive radar," *Ocean. Eng. IEEE J.*, vol. 35, no. 2, pp. 303–313, 2010.

[140] P. Chavali and A. Nehorai, “Scheduling and power allocation in a cognitive radar network for multiple-target tracking,” *Signal Process. IEEE Trans.*, vol. 60, no. 2, pp. 715–729, 2012.

[141] R. Romero and N. Goodman, “Cognitive radar network: Cooperative adaptive beamsteering for integrated search-and-track application,” *Aerosp. Electron. Syst. IEEE Trans.*, vol. 49, no. 2, pp. 915–931, 2013.

[142] Y. Wei, H. Meng, Y. Liu, and X. Wang, “Extended target recognition in cognitive radar networks,” *Sensors*, vol. 10, no. 11, pp. 10181–10197, 2010.

[143] Y. Wei, H. Meng, and X. Wang, “Adaptive single-tone waveform design for target recognition in cognitive radar,” in *Radar Conference, 2009 IET International*, 2009, pp. 1–4.

[144] W. Huleihel, J. Tabrikian, and R. Shavit, “Optimal adaptive waveform design for cognitive MIMO radar,” *Signal Process. IEEE Trans.*, vol. 61, no. 20, pp. 5075–5089, 2013.

[145] M. M. Naghsh, M. Soltanalian, P. Stoica, M. Modarres-Hashemi, A. De Maio, and A. Aubry, “A Doppler robust design of transmit sequence and receive filter in the presence of signal-dependent interference,” *Signal Process. IEEE Trans.*, vol. 62, no. 4, pp. 772–785, 2014.

[146] A. Aubry, A. DeMaio, A. Farina, and M. Wicks, “Knowledge-aided (potentially cognitive) transmit signal and receive filter design in signal- dependent clutter,” *Aerosp. Electron. Syst. IEEE Trans.*, vol. 49, no. 1, pp. 93– 117, 2013.

[147] M. Inggs, “Passive coherent location as cognitive radar,” *Aerosp. Electron. Syst. Mag. IEEE*, vol. 25, no. 5, pp. 12–17, 2010.

[148] M. Inggs, “Passive Coherent Location as Cognitive Radar,” *Waveform Diversity and Design Conference, 2009 International*. pp. 229–233, 2009.

[149] S.-M. Cai and Y. Gong, “Cognitive beamforming for multiple secondary data streams with individual SNR constraints,” *Signal Process. IEEE Trans.*, vol. 61, no. 17, pp. 4189–4198, 2013.

[150] S. Haykin, “Cognitive radar networks,” in *Sensor Array and Multichannel Processing, 2006. Fourth IEEE Workshop on*, 2006, pp. 1–24.

[151] S. Haykin, “Cognitive radar networks,” *Computational Advances in Multi-Sensor Adaptive Processing, 2005 1st IEEE International Workshop on*. pp. 1–3, 2005.

[152] Y. A. Nijsure, “Cognitive radar network design and applications,” 2012.

[153] M. Srinivas and L. M. Patnaik, “Genetic algorithms: A survey,” *Computer (Long. Beach. Calif).*, vol. 27, no. 6, pp. 17–26, 1994.

[154] J. Kennedy, “Particle swarm optimization,” in *Encyclopedia of Machine Learning*, Springer, 2010, pp. 760–766.

[155] S. Okdem, “A simple and global optimization algorithm for engineering problems: differential evolution algorithm,” *Turk J Elec Engin*, vol. 12, no. 1, 2004.

[156] D. Svozil, V. Kvasnicka, and J. Pospichal, “Introduction to multi-layer feed-forward neural networks,” *Chemom. Intell. Lab. Syst.*, vol. 39, no. 1, pp. 43–62, 1997.

[157] R. Hecht-Nielsen, “Replicator neural networks for universal optimal source coding,” *Sci. YORK THEN WASHINGTON-*, p. 1860, 1995.

[158] S. S. Haykin, S. S. Haykin, S. S. Haykin, and S. S. Haykin, *Neural networks and learning machines*, vol. 3. Pearson Education Upper Saddle River, 2009.

[159] Y. Hirose, K. Yamashita, and S. Hijiya, “Back-propagation algorithm which varies the number of hidden units,” *Neural Networks*, vol. 4, no. 1, pp. 61–66, 1991.

[160] D. Dasgupta and Z. Michalewicz, *Evolutionary algorithms in engineering applications*. Springer Science & Business Media, 2013.

[161] A. E. Eiben and J. E. Smith, *Introduction to evolutionary computing*. Springer Science & Business Media, 2003.

[162] M. Gen and R. Cheng, *Genetic algorithms and engineering optimization*, vol. 7. John Wiley & Sons, 2000.

[163] F. Zaman, I. M. Qureshi, J. A. Khan, and Z. U. Khan, “An application of artificial intelligence for the joint estimation of amplitude and two-dimensional direction of arrival of far field sources using 2-L-shape array,” *Int. J. Antennas Propag.*, vol. 2013, 2013.

[164] F. Zaman, I. M. Qureshi, A. Naveed, and Z. U. Khan, “Joint estimation of amplitude, direction of arrival and range of near field sources using memetic computing,” *Prog. Electromagn. Res. C*, vol. 31, pp. 199–213, 2012.

[165] S. Vorobyov, A. B. Gershman, and K. M. Wong, “Maximum likelihood direction-of-arrival estimation in unknown noise fields using sparse sensor arrays,” *Signal Process. IEEE Trans.*, vol. 53, no. 1, pp. 34–43, 2005.

[166] J. H. Holland, “Adaptation in natural and artificial systems: An introductory analysis with applications to biology, control, and artificial intelligence.,” 1975.

[167] T. Bäck, “The Interaction of Mutation Rate, Selection, and Self-Adaptation Within a Genetic Algorithm.,” in *PPSN*, 1992, pp. 87–96.

[168] T. Bäck and H.-P. Schwefel, “An overview of evolutionary algorithms for parameter optimization,” *Evol. Comput.*, vol. 1, no. 1, pp. 1–23, 1993.

[169] R. Hooke and T. A. Jeeves, “``Direct search solution of numerical and statistical problems,” *J. ACM*, vol. 8, no. 2, pp. 212–229, 1961.

[170] V. Torczon, “On the convergence of pattern search algorithms,” *SIAM J. Optim.*, vol. 7, no. 1, pp. 1–25, 1997.

[171] E. D. Dolan, R. M. Lewis, and V. Torczon, “On the local convergence of pattern search,” *SIAM J. Optim.*, vol. 14, no. 2, pp. 567–583, 2003.

[172] P. Karamalis, A. Marousis, A. Kanatas, and P. Constantinou, “Direction of arrival estimation using genetic algorithms,” in *Vehicular Technology Conference, 2001. VTC 2001 Spring. IEEE VTS 53rd*, 2001, vol. 1, pp. 162–166.

[173] F. Zaman, S. Mehmood, J. A. Khan, I. M. Qureshi, and I. Technology, “Joint estimation of amplitude and direction of arrival for far field sources using intelligent hybrid computing,” vol. 6, no. 20, pp. 3723–3728, 2013.

[174] A. H. Quazi, “An overview on the time delay estimate in active and passive systems for target localization,” *Acoust. Speech Signal Process. IEEE Trans.*, vol. 29, no. 3, pp. 527–533, 1981.

[175] X. Huang, J. Lu, J. Zheng, J. Chuang, and J. Gu, “Reduction of peak-to- average power ratio of OFDM signals with companding transform,” *Electron. Lett.*, vol. 37, no. 8, pp. 506–507, 2001.

[176] X. Huang, J. Lu, J. Zheng, K. Ben Letaief, and J. Gu, “Companding transform for reduction in peak-to-average power ratio of OFDM signals,” *Wirel. Commun. IEEE Trans.*, vol. 3, no. 6, pp. 2030–2039, 2004.

[177] A. Vallavaraj, B. G. Stewart, and D. K. Harrison, “An evaluation of modified μ-Law companding to reduce the PAPR of OFDM systems,” *AEU- International J. Electron. Commun.*, vol. 64, no. 9, pp. 844–857, 2010.

[178] R. P. Dougherty, “Advanced time-domain beamforming techniques,” in *Proc. of*, 2004, vol. 10.

[179] M. Nofal, S. Aljahdali, and Y. Albagory, “Tapered beamforming for concentric ring arrays,” *AEU-International J. Electron. Commun.*, vol. 67, no. 1, pp. 58–63, 2013.

[180] G. Qin, D. Bao, G. Liu, and P. Li, “Cross-correlation matrix Root-MUSIC algorithm for bistatic multiple-input multiple-output radar,” *Sci. China Inf. Sci.*, vol. 58, no. 2, pp. 1–10, 2015.

[181] E. Buckley, “Ambiguity suppression in a multiple beam radar,” *RADAR 2002*. pp. 492–496, 2002.

[182] L. Osman, I. Sfar, and A. Gharsallah, “The application of high-resolution methods for DOA estimation using a linear antenna array,” *Int. J. Microw. Wirel. Technol.*, vol. 7, no. 01, pp. 87–94, 2015.

[183] Y. Wang, W.-Q. Wang, H. Chen, and H. Shao, “Optimal Frequency Diverse Subarray Design With Cramer-Rao Lower Bound Minimization,” *Antennas and Wireless Propagation Letters, IEEE*, vol. 14. pp. 1188–1191, 2015.